

AD-A145 445

INTERACTION OF ANTI-G MEASURES AND CHEST WALL MECHANICS
IN DETERMINING GAS EXCHANGE(U) VIRGINIA MASON RESEARCH
CENTER SEATTLE WA H I MODELL JUN 83 AFOSR-TR-84-0751

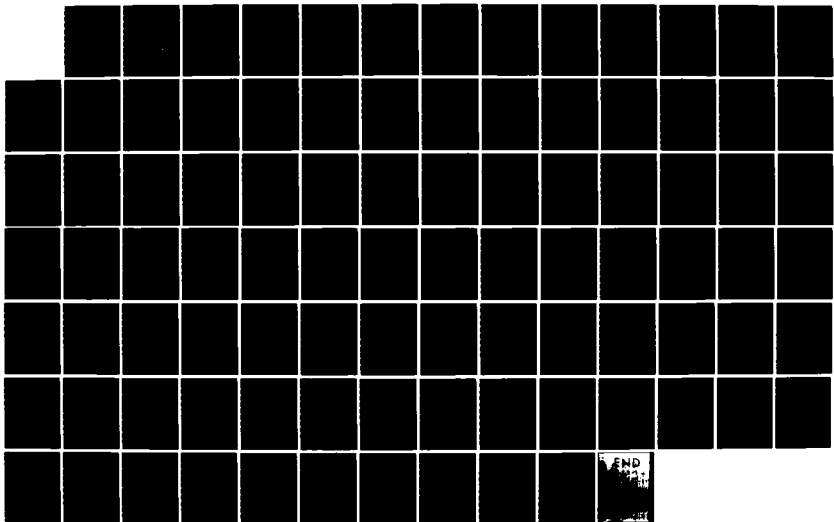
1/1

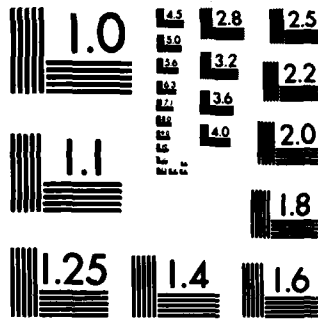
UNCLASSIFIED

F49620-81-C-0055

F/G 6/16

NL





MICROCOPY RESOLUTION TEST CHART
NATIONAL BUREAU OF STANDARDS-1963-A

UNCLASSIFIED

17

SECURITY CLASSIFICATION OF THIS PAGE (When Data Entered)

REPORT DOCUMENTATION PAGE

READ INSTRUCTIONS
BEFORE COMPLETING FORM

1. REPORT NUMBER AFOSR-TR-84-0751		2. GOVT ACCESSION NO.	3. RECIPIENT'S CATALOG NUMBER
4. TITLE (and Subtitle) Interaction of Anti-G Measures and Chest Wall Mechanics in Determining Gas Exchange		5. TYPE OF REPORT & PERIOD COVERED Final Report 1 Apr. 81 - 31 MAR 84	
7. AUTHOR(s) Harold I. Modell, Ph.D.		8. CONTRACT OR GRANT NUMBER(s) F4962C-81-C-0055	
9. PERFORMING ORGANIZATION NAME AND ADDRESS Virginia Mason Research Center 1000 Seneca Street Seattle, Washington 98101		10. PROGRAM ELEMENT, PROJECT, TASK AREA & WORK UNIT NUMBERS 2318/A1 61102C	
11. CONTROLLING OFFICE NAME AND ADDRESS USAF Office of Scientific Research/NL Bolling Air Force Base, D.C. 20332		12. REPORT DATE June 1983	
14. MONITORING AGENCY NAME & ADDRESS (if different from Controlling Office)		13. NUMBER OF PAGES 8E	
		15. SECURITY CLASS. (of this report) UNCLASSIFIED	
		15a. DECLASSIFICATION/DOWNGRADING SCHEDULE	

16. DISTRIBUTION STATEMENT (of this Report)

Approved for public release;
distribution unlimited.

17. DISTRIBUTION STATEMENT (of the abstract entered in Block 20, if different from Report)

SEP 12 1984

18. SUPPLEMENTARY NOTES

A

19. KEY WORDS (Continue on reverse side if necessary and identify by block number)

Acceleration	Intrapleural pressure
Chest Wall	Mechanical ventilation
Gas Exchange	Pulmonary circulation
G-suit	

20. ABSTRACT (Continue on reverse side if necessary and identify by block number)

This project represents an extension of an earlier project designed to examine factors influencing gas exchange during acceleration stress. Included in this report are studies dealing with the influence of the chest wall on regional intrapleural pressure during +Gz stress; influence of G-suit abdominal bladder inflation on gas exchange during +Gz stress; influence of the chest wall on gas exchange during mechanical ventilation; characterization of in vivo pressure-volume relationships of the pig's respiratory

AD-A145 445

DTIC FILE COPY

DD FORM 1 JAN 73 1473

84 08 30 028

UNCLASSIFIED

SECURITY CLASSIFICATION OF THIS PAGE (When Data Entered)

UNCLASSIFIED

SECURITY CLASSIFICATION OF THIS PAGE(When Data Entered)

20 Abstract (Continued)

system; and mechanics of the pulmonary vasculature. Results indicate that the chest wall plays a significant role in determining gas exchange parameters during +Gz stress, during application of +Gz protective measures and during mechanical ventilation.

UNCLASSIFIED

SECURITY CLASSIFICATION OF THIS PAGE(When Data Entered)

AFOSR Contract Number F49620-81C-0055
Final Report
June, 1984

INTERACTION OF ANTI-G MEASURES AND CHEST WALL
MECHANICS IN DETERMINING GAS EXCHANGE

VIRGINIA MASON RESEARCH CENTER
SEATTLE, WASHINGTON 98101

Harold I. Modell, Ph.D.

Controlling Office: USAF Office of Scientific Research/NL
Bolling Air Force Base, D.C. 20332

Accession For	
NTIS GRA&I	<input checked="" type="checkbox"/>
DTIC TAB	<input type="checkbox"/>
Unannounced	<input type="checkbox"/>
Justification	<input type="checkbox"/>
Date	
Author	
Title	
Subject	
Availability	
Notes	
A1	

ANIMAL USE STATEMENT

Care has been taken in these studies to ensure that all animal experimentation complies with all federal animal welfare regulations and the "Guide for the Care and Use of Laboratory Animals".



Classification

CONFIDENTIAL

TABLE OF CONTENTS

	page
Background	1
I. Influence of the Chest Wall on Regional Intrapleural Pressure During Acceleration (+Gz) Stress	3
H.I. Modell and F.W. Baumgardner	
II. Influence of G-Suit Abdominal Bladder Inflation on Gas Exchange During +Gz Stress18
H.I. Modell, P. Beeman and J. Mendenhall	
III. An Inexpensive Assist/Control, Volume Limited Animal Ventilator. . .	.39
H.I. Modell and J. Mendenhall	
IV. Influence of the Chest Wall on Gas Exchange During Mechanical Ventilation in Dogs.44
H.I. Modell and M.M. Graham	
V. <u>In Vivo</u> Pressure-Volume Relationships of the Pig Lung and Chest Wall.54
H.I. Modell	
VI. Adaptation of Vascular Pressure-Flow-Volume Hysteresis in Isolated Rabbit Lungs63
K.C. Beck and J. Hildebrandt	
VII. Influence of Alveolar Mechanics on the Lung Vasculature.72
H.I. Modell and J. Hildebrandt	
Publications Associated With Contract.87

BACKGROUND

High sustained gravitational stress (HSG), such as that experienced by pilots of high performance aircraft, affects cardiovascular and respiratory function adversely (3). Cardiovascular function is compromised because of changes in hydrostatic relationships caused by the increased G. Similar mechanisms influence distribution of ventilation and perfusion (2,4,7,9). In addition, the HSG may alter chest wall mechanics (5) and impair gas exchange. A number of protective measures are presently employed in an attempt to restore normal arterial blood pressure and, thus, increase pilot tolerance to high sustained gravitational forces. Some of these measures (e.g. anti-G suits) have been associated with additional detriment to pulmonary gas exchange (1,6,8), whereas others (e.g. positive pressure breathing) may enhance pulmonary gas exchange under HSG conditions. Several questions relevant to HSG tolerance must be addressed if more effective protective measures are to be developed:

1. To what extent do commonly used protective measures enhance or impair pulmonary gas exchange?
2. What is the time course of any gas exchange detriment resulting from use of protective devices (e.g. anti-G suits) during HSG?
3. Is there a cumulative effect associated with gas exchange detriment resulting from use of protective devices?
4. By what means can these measures be modified to optimize gas exchange during HSG?

This project has focused on areas related to these questions. Included in this report are studies dealing with the influence of the chest wall on regional intrapleural pressure during acceleration (+Gz)

stress in dogs and pigs (Section I); influence of G-suit abdominal bladder inflation on gas exchange during +Gz stress (Section II); influence of the chest wall on gas exchange during mechanical ventilation (Sections III and IV); characterization of the pressure-volume relationships of the pig chest wall (Section V); and mechanics of the pulmonary vasculature (Sections VI and VII).

References

1. Barr, P.-O. Hypoxemia induced by prolonged acceleration. Acta Physiol. Scand. 54: 128-137, 1962.
2. Bryan, A.C., J. Milic-Emili and D. Pengelly. Effect of gravity on the distribution of pulmonary ventilation. J. Appl. Physiol. 21: 778-784, 1966.
3. Burton, R.R., S.D. Leverett, Jr. and E.D. Michaelson. Man at high sustained +Gz acceleration: a review. Aerospace Med. 45: 1115-1136, 1974.
4. Glaister, D.H. Distribution of pulmonary blood flow and ventilation during forward (+Gx) acceleration. J. Appl. Physiol. 29: 432-439, 1970.
5. Hershgold, E.J. Roentgenographic study of human subjects during transverse accelerations. Aerospace Med. 31: 213-219, 1960.
6. Hyde, A.S., J. Pines and I. Saito. Atelectasis following acceleration: a study of causality. Aerospace Med. 34: 150-157, 1963.
7. Jones, J.G., S.W. Clarke and D.H. Glaister. Effect of acceleration on regional lung emptying. J. Appl. Physiol. 26: 827-832, 1969.
8. Nolan, A.C., H.W. Marshall, L. Cornin, W.F. Sutterer and E.H. Wood. Decreases in arterial oxygen saturation and associated changes in pressures and roentgenographic appearance of the thorax during forward (+Gx) acceleration. Aerospace Med. 34: 797-813, 1963.
9. von Nieding, G. and H. Krekeler. Effect of acceleration on distribution of lung perfusion and on respiratory gas exchange. Pflugers Arch. 342: 159-176, 1973.

SECTION I

INFLUENCE OF THE CHEST WALL ON REGIONAL INTRAPLEURAL PRESSURE DURING ACCELERATION (+Gz) STRESS

H.I. Modell and F.W. Baumgardner

The vertical intrapleural pressure gradient has been attributed to the influence of gravity acting on the lung (8,12) and to lung deformation within the chest wall (1,2). Although reports have appeared describing the distribution of intrapleural pressure along the vector of gravitational stress at 0Gz (supine) and +1Gz (head-up posture) (7,8,10), none have examined the influence of increased +Gz stress on regional intrapleural pressure. Wood et al. (13) measured intrapleural fluid pressure at various sites during +Gx (anterior to posterior) stress. However, these authors did not consider the +Gz (cranial to caudal) vector. Data with which to assess the influence of chest wall mechanics, specifically compliance and chest wall shape, on regional pressure relationships during acceleration stress are also lacking. The purpose of this study was to determine the influence of altered chest wall compliance, chest wall shape, and G-suit abdominal bladder inflation on regional intrapleural pressure during exposure to +Gz stress.

The experimental approach used in this study was chosen in an attempt to obtain data covering a spectrum of chest wall characteristics within which man may fall. It was felt that such a spectrum could be obtained by considering dogs and pigs. Hence, duplicate experiments were conducted in these experimental models.

Methods

Nine adult male dogs weighing 21.8 ± 3.2 Kg and ten Duroc-

Yorkshire pigs weighing 20.4 ± 1.3 Kg were used in this study. Anesthesia was induced with 30 mg/Kg pentobarbital sodium (dog) or with 18 mg/Kg ketamine hydrochloride and 2 mg/Kg Xylazine (pig). The animal was intubated with a cuffed endotracheal tube (dog) or with a tracheostomy tube (pig) and allowed to breathe spontaneously. An external jugular vein was cannulated for supplemental anesthesia administration (pentobarbital sodium), and a Millar catheter-tip pressure transducer was introduced through the femoral artery (dog) or carotid artery (pig) and advanced to the thoracic aorta level for arterial blood pressure monitoring. Air-filled, stainless steel cannulae were placed in two to four intercostal spaces ranging from the third to the ninth (dog) or tenth (pig) intercostal space. Each cannula, constructed from a 3 inch, 15 guage needle, was blunted and bent at a right angle 4 cm from the tip, and 24 side holes were ground along its length. Anchors were attached to the needle hub so that the cannula could be secured with suture to the skin. These "open" cannulae were used in all dog experiments. For the pig studies, the open cannulae were modified slightly to produce "balloon-tipped" cannulae. The cannulae were cut and "hinged" with a small piece of silastic tubing 2 cm from the tip, and a thin finger cot was placed over the 4 cm length and fastened at the bend.

During insertion of the cannulae, the animal was ventilated mechanically, and 10-15 cm H₂O end-expiratory pressure was imposed to insure that a pneumothorax was not created. However, a local pneumothorax was created around each open cannula (dog studies). The side holes of the cannula extended 3 cm from the tip, a distance great enough to allow communication between the intrapleural space and atmosphere during insertion. The cannulae were placed in the same

vertical plane along the ventral third of the lateral surface of the rib cage. They were directed along the intercostal space with the tips facing dorsally. Purse string sutures through at least one muscle layer and the skin were tightened around the cannulae to prevent air leakage into the intrapleural space during the experiment. Mechanical ventilation and positive end-expiratory pressure were removed, and the animal was allowed to breathe spontaneously.

When all pleural pressure monitoring sites had been established, a standard G-suit abdominal bladder (CSU-12/P) was placed around the animal's abdomen. Care was taken to ensure that the G-suit was positioned well below the level of the monitoring cannulae. The animal was placed supine on the animal end of one of two centrifuges (AMRL, Wright-Patterson AFB or USAFSAM, Brooks AFB). Imposed +Gz stress consisted of 40 second exposures to steady levels of +1 to +5Gz (onset rate = 0.1G/sec). Measurements were made with and without G-suit inflation (standard inflation scheme, 1.5 psi/G starting at approximately +2Gz) using Statham P23BB (dog) or Validyne MP-45 (pig) pressure transducers connected through air-filled tubing to the air-filled cannulae. All signals were recorded on a strip-chart recorder, an FM analog magnetic tape recorder, and, for the pig studies, in the form of digital data points sampled at rates ranging from 2 to 5 samples per second using an Apple][computer system. Between exposures, the animal's lungs were hyperinflated several times to open any atelectatic or airway closure areas.

After data had been collected at each +Gz level with and without G-suit inflation, an overdose of pentobarbital sodium was administered intravenously or the animal was sacrificed with an intravenous injection

of saturated KCl. The animal was then exposed to +4 and +5Gz as earlier. The intent of this portion of the protocol was to provide a means by which the effects of the exposure on the passive lung-chest wall system could be separated from any modifying influence of active chest wall muscular tone. These exposures were begun within 5 minutes post-KCl or pentobarbital overdose and completed within approximately 20 minutes.

At the completion of the experiment, a thoracotomy was performed to confirm the monitoring sites, to examine the lungs for any gross damage resulting from the cannulae, and, in the dog studies, to ensure that the monitoring cannulae were patent. If a cannula tip was found to be fluid filled, the data from that cannula were discarded.

To confirm that pressure measurements with the open cannulae reflected intrapleural surface pressure rather than something closer to fluid pressure changes, experiments were conducted in 2 dogs and one pig comparing pressure measurements from the two types of cannulae with the animal in the supine posture. In each experiment, cannula pairs (open, balloon-tipped) were compared at one or two intercostal space levels on each side of the animal. For example, in one experiment, one balloon-tipped cannula was placed in the right third intercostal space and one in the left seventh intercostal space. Open cannulae in this experiment were placed in the left third intercostal space and right seventh intercostal space. Pressures were recorded from all cannulae during spontaneous breathing, spontaneous breathing against increased airway resistance, spontaneous breathing with positive end-expiratory pressure, mechanical ventilation, and mechanical ventilation with positive end-expiratory pressure. Pressures ranged from approximately -12 cm H₂O to +12 cm H₂O in magnitude. Five cannula pairs were compared.

The data were then digitized using an Apple][computer system, and linear regression equations were determined for each cannula pair. The number of points per pair upon which a regression equation was determined ranged from 383 to 1068. Correlation coefficients of the five regressions ranged from 0.899 to 0.996 with the average correlation coefficient being 0.953.

Placement of a needle between the lung surface and the chest wall causes distortion of the lung around the needle which can introduce errors into pleural pressure measurements made with the needle. McMahon et al. (11), using a physical model to examine the degree of error which could be introduced by lung distortion, concluded that pressure measured with an air-filled needle would vary with, but be less than, the true intrapleural surface pressure. To estimate the degree of error introduced by distortion caused by our cannulae, we compared measured to applied pressure in the model depicted in Figure 1A. Two large pieces of dog skin with underlying fascia were moistened with saline and tacked to a piece of wood with the fascial sides apposed. A hole was made in the upper layer with a 15 gauge needle, and an air-filled pleural pressure cannula was placed between the two layers of skin as it would be placed in the animal. A weighted lucite cylinder, 7.5 cm in diameter, was placed on the skin so that the cannula was within the cylinder. The cannula was connected to a Statham P23BB transducer, and water was added to the cylinder. The measured height of the water column from 0 to 35 cm H₂O was compared to the pressure measured by the cannula-transducer system. Results, shown in Figure 1B, indicated that the cannula-transducer system provided a good estimate of the applied pressure.

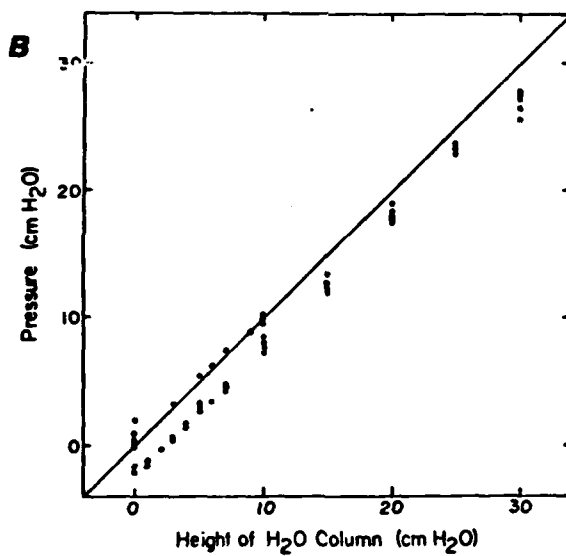
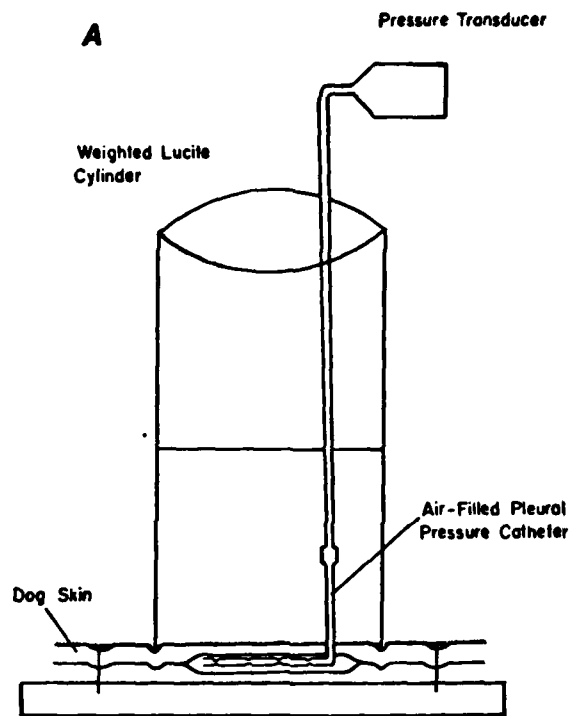


FIGURE 1. A. Model used for testing the influence of tissue distortion around the measuring cannula on pressures measured.
 B. Pressure measured with the cannula as a function of water column height in the test model cylinder (see text).

Results

Changes from intrapleural pressure measured at end-expiration (FRC) during the 0 Gz control period were determined at each +Gz level and test condition using multiple readings from strip chart recordings in dog studies and using the digitized data (2-5 samples/sec) in pig studies. Intrapleural pressure changes were determined at FRC during the 40 second exposure (at least 4 readings/exposure in dog studies) and at each G level during the slow onset phase of the exposure. Data obtained from the third and fourth, fifth and sixth, eighth and ninth (dog) and eighth and tenth (pig) intercostal spaces were pooled so that meaningful statistical analysis could be performed (Student's t-test).

The influence of G-stress on regional intrapleural pressure changes are shown in Figures 2 and 3. The change in intrapleural pressure from the 0 Gz control value at each monitoring site is plotted as a function of +Gz stress for the control state (animal spontaneously breathing and without G-suit) and after the heart had been stopped (control state minus active muscular tone, reflexes, etc.) without the G-suit. In the dog (Fig. 2), intrapleural pressure became more negative in the upper and middle thoracic regions as G-stress increased, but, in the lower thorax, the pressure increased slightly. When active chest wall muscular tone was removed, an increase in the rate of change in intrapleural pressure was seen in the upper thorax but not in the middle or lower thoracic regions. In the pig (Fig. 3), a different response was seen. At each monitoring site, intrapleural pressure became more negative as the G-stress increased. When active chest wall muscular tone was removed, the rate of change in intrapleural pressure tended to increase in all regions.

The influence of G-suit abdominal bladder inflation is also shown

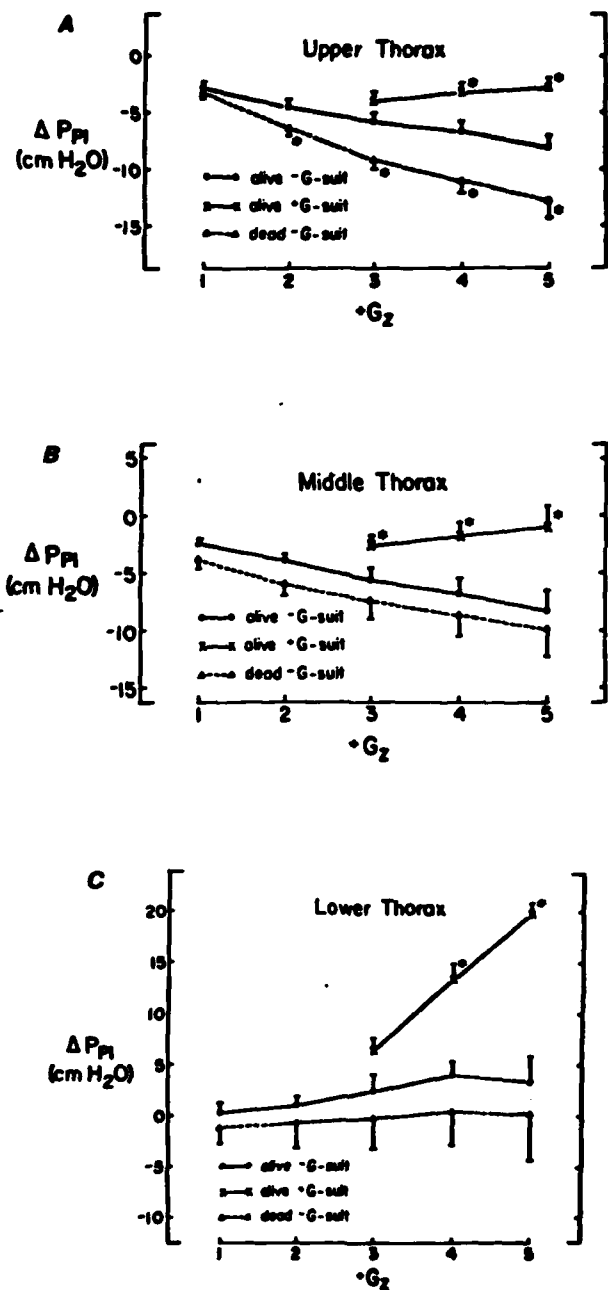


FIGURE 2. Mean intrapleural pressure changes from 0G_z measured at the third-fourth (A), fifth-sixth (B), and eighth-ninth (C) intercostal space level as a function of +G_z stress in the dog. Three conditions are shown: active muscular tone present (O), active muscular tone present with G-suit abdominal bladder inflation (X), and active muscular tone absent (Δ). Standard errors of the mean are indicated. Statistically significant differences from exposures of the live animal without G-suit (*) were determined by Student's t-test (P<0.05).

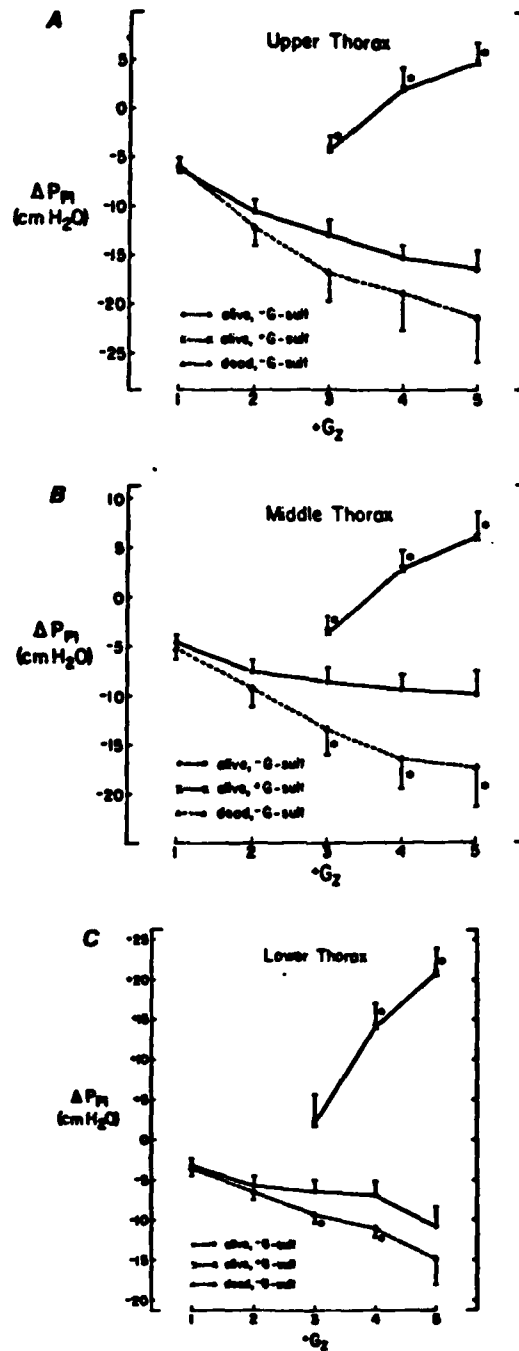


FIGURE 3. Mean intrapleural pressure changes from 0Gz measured at the third-fourth (A), fifth-sixth (B), and eighth-tenth (C) intercostal space level as a function of +Gz stress in the pig. Three conditions are shown: active muscular tone present (O), active muscular tone present with G-suit abdominal bladder inflation (X), and active muscular tone absent (Δ). Standard errors of the mean are indicated. Statistically significant differences from exposures of the live animal without G-suit (*) were determined by Student's t-test ($P < 0.05$).

in Figures 2 and 3. Only data obtained at +3Gz and above have been plotted since the bladder did not begin to inflate until approximately +2.2Gz, and data obtained at the lower G levels were essentially the same as in the control state. In both species, intrapleural pressure increased with G-suit application either approaching or becoming more positive than control levels.

Discussion

Data from the live dog studies are compared to corresponding data from the pig in Figure 4. At the level of the third-fourth intercostal space (Fig. 4A) and fifth-sixth intercostal space (Fig. 4B), the response to increased +Gz stress is qualitatively similar in the two species. It is interesting to note, however, that, at the level of the third-fourth intercostal space the magnitude of the change in intrapleural pressure appears to be greater in the pig than in the dog. Furthermore, in the non-dependent regions, the pleural pressure changes resulting from imposition of the G-suit appear larger in the pig.

Figure 4C, which shows data for the dog and pig at the eighth-ninth (dog) and eighth-tenth (pig) intercostal spaces, raises some interesting questions concerning the influence of chest wall compliance and shape on the intrapleural pressure changes occurring during +Gz stress. The most significant finding in the dog studies was that a region exists in the lower thorax where intrapleural pressure remains relatively constant. Above this region pressure becomes more negative with increasing +Gz stress (seventh intercostal space), while below this region, it becomes more positive (ninth intercostal space). A similar region located approximately 15 cm from the apex was observed by Hoppin et. al. (7) in dogs tilted from supine (0Gz) to the head-up position (+1Gz). Bryan and

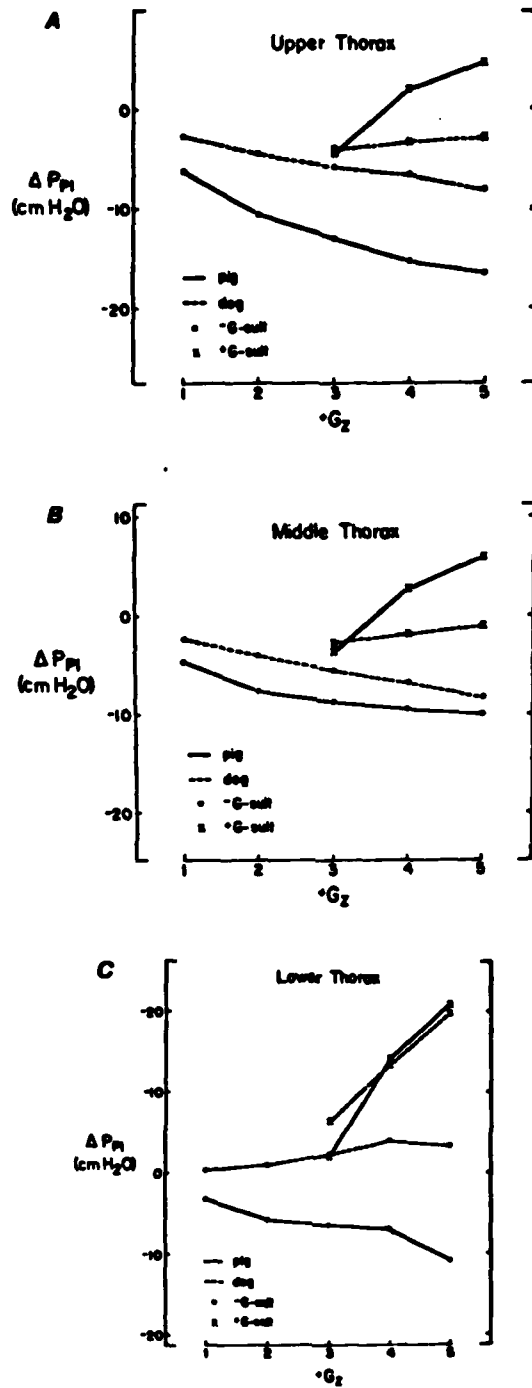


FIGURE 4. Comparison of data obtained from dog (dashed lines) and pig (solid lines). Mean intrapleural pressure changes from 0Gz measured in the upper thoracic (A), mid-thoracic (B), and lower thoracic (C) regions are shown as a function of +Gz stress. Two conditions are shown: Live animals without G-suit inflation (O) and live animals with G-suit inflation (X).

his colleagues (3) reported a similar region in humans exposed to up to +3Gz. We were unable to detect an analogous region in the pig.

This region could reflect the transition between a relatively non-compliant upper rib cage and the more compliant lower chest wall. Lupi-Herrera et al. (9) exposed dogs to negative abdominal pressure and measured the transverse diameter of the thorax at locations corresponding to about the fourth intercostal space and the eight or ninth intercostal space. They reported that the lower rib cage cross-sectional area decreased by 19% whereas the upper cross-sectional area decreased by only 5%. Data from other investigators also indicate that, in the dog, the lower chest wall is considerably more compliant than the upper chest wall regions (5,6). We postulated that, when +Gz stress is applied to the system, the lung is pulled caudally, but the upper rib cage remains relatively fixed. A more negative intrapleural pressure is created in this region, and regional lung volume increases. In the dog, the ribs below the sternum move more freely, and when the thoracic and abdominal contents are pulled in a caudal direction, the lower ribs tend to be pulled inward. The net result is a smaller "container" into which the lung displaced from the upper thorax must fit, and regional intrapleural pressure becomes more positive.

The pig's chest wall is noticeably less compliant than the dog's. Furthermore, the pig's rib cage appears to be a more rigid container than that of the dog. Hence, minimal displacement of the lower rib cage relative to that seen in the dog would be expected in the pig exposed to +Gz stress. If this is the case, the pig's chest wall should behave more like a container with rigid walls and a compliant lower limit (diaphragm). The above hypothesis would predict that, in such a system,

+Gz stress would cause the lung to be pulled caudally, but, with the exception of the lower limit, the volume of the "container" into which the lung is displaced would remain relatively fixed. Thus, the point at which regional intrapleural pressure becomes positive would reflect the degree to which the relative downward displacement of lung tissue is accommodated by an increase in "container" volume due to the downward movement of the lower boundary (i.e., the diaphragm). The data shown in Figure 3 indicating that regional intrapleural pressure in the live pig without G-suit continued to become more negative with increasing +Gz stress, even as low as the tenth intercostal space, are consistent with this prediction. If the degree of diaphragm displacement in the pig approximates the relative lung tissue displacement, a positive regional intrapleural pressure may only be seen close to the level of the diaphragm.

The data obtained in the dead pig (Fig. 3) are also consistent with this explanation. Since diaphragm displacement caudally depends to some extent on abdominal muscle tone, removal of abdominal muscle tone would permit further elongation of the lung "container", and regional intrapleural pressure would be expected to become more negative than when abdominal muscular tone was present.

The comparable increase in intrapleural pressure in dog and pig in the dependent regions (Fig. 4C) with G-suit use indicates that, in these anesthetized pigs, the straining maneuver which accompanies G-suit application in awake pigs (4) was not present. The observation that regional intrapleural pressure in non-dependent regions increases less in response to G-suit abdominal bladder inflation in the dog compared to the response in the pig (Fig. 4A,B) can be explained on the basis of chest wall compliance. As the G-suit inflates, abdominal compression

occurs, and regional intrathoracic pressure in dependent regions increases. As this pressure is transmitted to non-dependent regions in the dog, the relatively compliant chest wall can increase in volume. In the pig, however, the less compliant chest wall does not move as readily, and pressure remains high.

What are the implications of these data with respect to man exposed to high +Gz stress? The answer to this question is intimately tied to man's use of the M-1 straining maneuver. Bryan et al. (3) identified an isovolume point in man exposed to up to +3Gz. The subjects in that study did not perform straining maneuvers nor were G-suits used at the low levels of G-stress examined. This finding indicates that the human chest wall can deform in a manner similar to that seen in the dog. However, if an M-1 straining maneuver is made, the chest wall is made less compliant, and the characteristics of the lung-chest wall interaction may approach those seen in the pig. If this is the case, a successful M-1 maneuver may serve to protect the lung from increases in regional intrapleural pressure during +Gz stress and thereby reduce the degree to which airway closure may occur.

Our data (Fig. 4A,B) suggest that application of the G-suit abdominal bladder in man without an accompanying M-1 maneuver would result in a larger gas exchange detriment than that expected in the dog and less than that expected in the pig. In the presence of a straining maneuver, however, less of the pressure exerted by the abdominal bladder would be transmitted to the thorax because of increased rigidity of the abdominal wall, and any gas exchange detriment associated with the G-suit would be reduced.

References

1. Agostoni, E., E. D'Angelo. Topography of pleural surface pressure during simulation of gravity effect on abdomen. Respir. Physiol. 12: 102-109, 1971.
2. Agostoni, E., E. D'Angelo and M.V. Bonanni. The effect of the abdomen on the vertical gradient of pleural surface pressure. Respir. Physiol. 8: 332-346, 1970.
3. Bryan, A.C., J. Milic-Emili and D. Pengelly. Effect of gravity on the distribution of pulmonary ventilation. J. Appl. Physiol. 21: 778-784, 1966.
4. Burton, R.R. Positive (+Gz) acceleration tolerances of the miniature swine: application as a human analog. Aerospace Med. 44: 294-298, 1973.
5. D'Angelo, E., S. Michellini and G. Miserocchi. Local motion of the chest wall during passive and active expansion. Respir. Physiol. 19: 47-59, 1973.
6. Glazier, J.B., J.M.B. Hughes, J.E. Maloney and J.B. West. Vertical gradient of alveolar size in lungs of dogs frozen intact. J. Appl. Physiol. 23: 694-705, 1967.
7. Hoppin, F.G., Jr., I.D. Green and J. Mead. Distribution of pleural surface pressure in dogs. J. Appl. Physiol. 27: 863-873, 1969.
8. Krueger, J.J., T. Bain and J.L. Patterson, Jr. Elevation gradient of intrathoracic pressure. J. Appl. Physiol. 16: 465-468, 1961.
9. Lupi-Herrera, E., C. Prefaut, A.E. Grassino and N.R. Anthonisen. Effect of negative abdominal pressure on regional lung volumes in supine dogs. Respir. Physiol. 26: 213-221, 1976.
10. McMahon, S.M., D.F. Proctor and S. Permutt. Pleural surface pressure in dogs. J. Appl. Physiol. 27: 881-885, 1969.
11. McMahon, S.M., S. Permutt and D.F. Proctor. A model to evaluate pleural surface pressure measuring devices. J. Appl. Physiol. 27: 886-891, 1969.
12. Vawter, D.L., F.L. Matthews and J.B. West. Effect of shape and size of lung and chest wall on stresses in the lung. J. Appl. Physiol. 39: 9-17, 1975.
13. Wood, E.H., A.C. Nolan, D.E. Donald, A.C. Edmundowicz and H.W. Marshall. Technics for measurement of intrapleural and pericardial pressures in dogs studied without thoracotomy and methods for their application to study intrathoracic pressure relationships during exposure to forward acceleration (+Gx). AMRL-TDR-63-107, 1963.

SECTION II

INFLUENCE OF G-SUIT ABDOMINAL BLADDER INFLATION ON GAS EXCHANGE DURING +Gz STRESS

H. I. Modell, P. Beeman and J. Mendenhall

The influence of +Gz exposure on gas exchange in dogs has been examined by Barr, Bjurstedt and Coleridge (2), Glaister (6), and Erickson, Sandler and Stone (4). During air breathing, Barr et al. reported little change in arterial oxyhemoglobin saturation at +1.7 Gz when the abdomen was supported with counterpressure, but, when no counterpressure was provided, arterial oxyhemoglobin saturation fell.

Erickson and his colleagues (4) saw little change in arterial oxyhemoglobin saturation during exposure to +Gz levels as high as +6 Gz. However, these authors did not indicate whether abdominal counterpressure was included in the protocol.

Glaister (6) recorded arterial oxygen tension continuously during 1-2 minute exposures to +Gz levels from +2 to +5Gz. An abdominal binder was imposed on all of Glaister's animals to limit the downward diaphragm displacement accompanying +Gz stress. Between trials, these animals were subjected to +1 Gz stress. Glaister characterized his observations as a three phase phenomenon. A progressive fall in arterial oxygen tension during +Gz exposure was followed by a transient recovery upon restoration of +1Gz. A slower recovery was then seen taking up to 1.5 minutes for complete recovery to control (+1Gz) arterial oxygen tension levels. Although the results of Barr et al. suggest that abdominal restriction helps maintain arterial P_{O_2} at increased +Gz levels, Glaister's data does not.

The counterpressure applied in the above studies differed from normal application of the G-suit abdominal bladder in that active counterpressure was not supplied as +Gz stress increased. Intrapleural

pressure data measurements in dogs exposed to +Gz stress with and without a G-suit (11) indicate that continued inflation of the abdominal bladder with +Gz stress results in active lung compression suggesting that, even with air breathing, atelectasis may result.

This study was designed to examine the time course of gas exchange detriment resulting from +Gz stress in dogs, the influence of G-suit abdominal bladder inflation on the detriment, and influence of repeated +Gz stress on gas exchange.

Methods

Two series of experiments were conducted. In the first, gas exchange during single exposures to +Gz was examined. The second focused on the influence of repeated exposures. The same animal preparation was used for both studies. Seven adult mongrel dogs weighing 19.9 ± 2.6 (SD) kg were used in the first set of experiments, and five dogs (22.06 ± 1.57 kg) were used in the second set. All animals were anesthetized with 30 mg/kg pentobarbital sodium and intubated with a cuffed endotracheal tube. A Millar, catheter-tip pressure transducer was introduced through the right femoral artery and positioned in the thoracic aorta for arterial blood pressure monitoring. A 7 Fr catheter was introduced through the left femoral artery and positioned in the thoracic aorta for arterial blood sampling. A 7 Fr Swan-Ganz thermistor tip catheter was introduced through the right external jugular vein and positioned in the pulmonary artery and right atrium for thermal dilution cardiac output determinations (Series I). Because blood sampling through the distal lumen of the Swan-Ganz was not always possible at high +Gz levels, a 7 Fr catheter with multiple side-oles was also introduced through the right external jugular vein

and positioned in the right ventricle for sampling mixed venous blood. Another catheter, placed in the right femoral vein, served as an injection site for supplemental anesthesia. A standard G-suit abdominal bladder (CSU-12P) was placed around the animal, and the animal was secured to a V-board restraint in the supine position.

Remote sampling techniques were developed for blood sampling and thermal dilution cardiac output determination. An air-powered piston was used to deliver room temperature saline for thermal dilution cardiac output determinations (Figure 1-A). A 30 psi pressure source was connected to the normally closed side of a 3-way solenoid valve. One side of the solenoid was connected to the tip of a 20 cc disposable syringe. The 20 cc syringe piston and 5cc injectate syringe piston were in apposition so that when the solenoid was activated, the pressure build-up in the 20 cc syringe forced the injectate piston in, thereby injecting the bolus. A two-way solenoid valve blocked the output of the injectate syringe until the solenoid system was activated. This prevented the injectate from being drawn into the animal prematurely by the hydrostatic pressure generated by the +Gz forces.

To enable remote blood sampling, pump-syringe devices (Figure 1-B) were used that allowed collection of two samples per device. The arterial or right ventricular catheter was connected to one side of a Masterflex roller pump head. The pump outlet line passed through two miniature 3-way solenoid valves to a 20 cc syringe. Each of the 3-way valves was connected to a 10 cc sample syringe. When activated, the pump filled the 20 cc (dead space) syringe to a predetermined volume regulated by the position of a microswitch activated by the syringe piston. The microswitch activated the three-way solenoid connected to

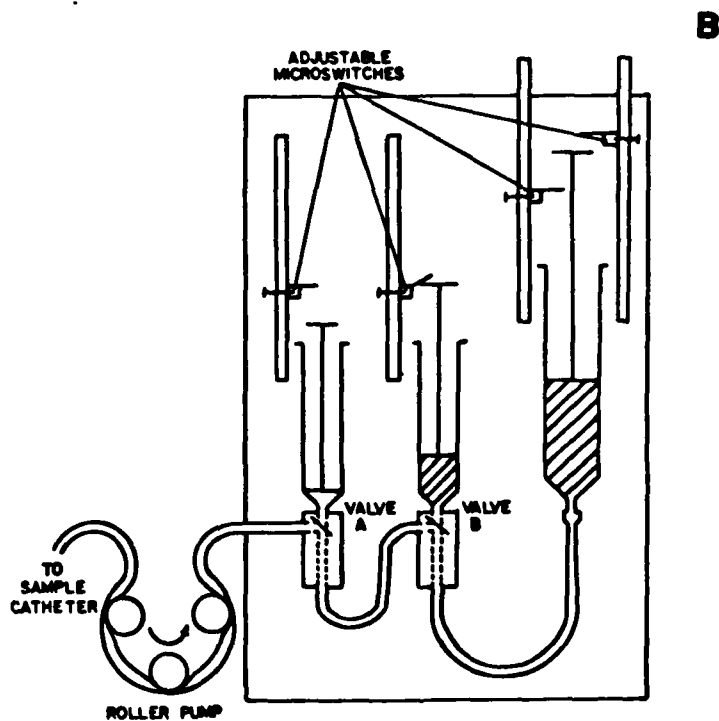
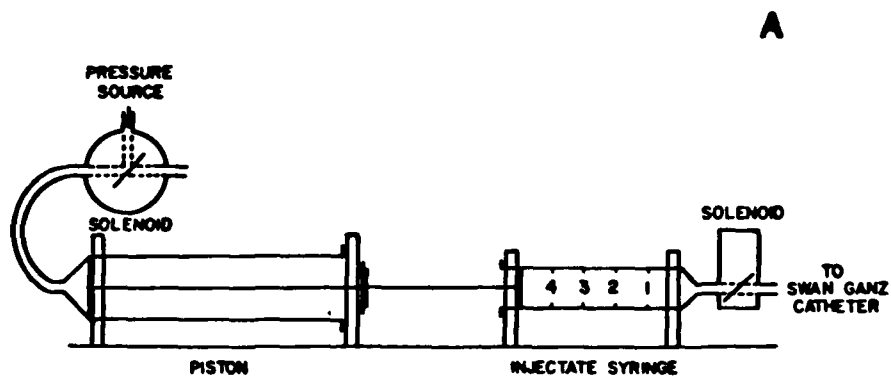


FIGURE 1. A. Schematic representation of injector used for thermal dilution cardiac output determination.
 B. Schematic representation of remote blood sampling pump-syringe device used in centrifuge studies.

the first sample syringe. This syringe then filled until the pump was turned off by activation of a microswitch by the sample syringe piston. When the pump was activated a second time, the process repeated for sample collection in the second sample syringe. Total dead space of the unit (with pump tubing) was less than 6cc.

Prior to the first +Gz exposure, the animal was heparinized with 3000 units of heparin sodium injected intravenously. Control samples of arterial and mixed venous blood were drawn for blood-gas analysis and a thermal dilution cardiac output determination was made.

Series I

Four experiments were conducted on the human centrifuge at the State University of New York at Buffalo (SUNYAB), and three animals were stressed on the animal end of the human centrifuge at the USAF School of Aerospace Medicine in San Antonio, Texas.

Each animal was exposed to +3, 4, and 5 Gz with an onset rate of 0.1 G/sec. Exposures were made with and without G-suit abdominal bladder inflation using the standard inflation scheme (1.5 psi/G beginning at +2.2 Gz).

When the desired +Gz level was reached, arterial and mixed venous blood samples were drawn. The time for blood sampling was approximately 18 seconds. Upon completion of the blood sampling, a thermal dilution cardiac output determination was made using an Edwards model 9520A cardiac output computer. The resulting curve was monitored in the centrifuge control room. At +40 seconds of the test +Gz stress, a second set of blood samples were drawn. Hence, samples to be analyzed were representative of blood-gas status at 20 and 60 seconds of exposure time.

When 0 Gz was reached at the end of the exposure, the blood samples were iced for later analysis. Three minutes after reaching 0 Gz, a third set of blood samples were drawn and iced. The animal's lungs were then inflated several times with a large volume using an Ambu bag. An additional 5-15 minutes were allowed to elapse before the next exposure.

Because the SUNYAB and USAFSAM centrifuges do not have identical capabilities, +Gz exposure schemes differed slightly at the two centrifuge sites. At the SUNYAB facility, the animal was placed on a tilt table and tilted manually to +1 Gz prior to the initiation of a test run. Time at +1 Gz averaged about 35 seconds.

At the USAFSAM facility, two schemes were used. The first simulated the SUNYAB exposures. Acceleration was initiated at an onset rate of 0.1 G/sec until +1 Gz was reached. The animal was then held at that level for 35 seconds before continuing to the desired +Gz level. In the second scheme, stress was applied at 0.1 G/sec until the desired +Gz level was reached.

Although results from the two schemes differed slightly quantitatively, they were qualitatively similar. Hence, data from both schemes were lumped with SUNYAB data for analysis.

Series II

All +Gz exposures were made using the human centrifuge at USAFSAM (3.97 M radius). Animals were exposed to +4Gz (onset rate = 0.1 G/sec) or +5Gz with G-suit inflation using the standard inflation scheme (1.5 psi/G beginning at +2.2 Gz). Acceleration levels and G-suit status were randomized within the experimental design.

The experimental procedure paralleled Series I experiments. Animals were exposed to a given Gz level for approximately 60 seconds.

After 40 seconds of the exposure, arterial and mixed venous blood samples were drawn (sampling time was approximately 18 seconds), and the animal was returned to 0Gz. When 0Gz was reached, the blood samples were iced for later analysis. After 3 minutes, the animal was exposed for a second time to the same +Gz stress, and blood samples were drawn beginning at 40 seconds of the exposure. The animal was returned to 0Gz, and the second set of blood samples were iced for later analysis. Three minutes after reaching 0Gz, a third set of blood samples were drawn and iced. The animal's lungs were then inflated several times with a large volume using an Ambu bag. At 10-15 minutes post-G stress, another set of arterial and mixed venous blood samples were drawn as 0Gz controls. The animal was then exposed to the next test condition.

After all +Gz exposures were completed, the blood samples were analyzed for PO_2 , PCO_2 , and pH using an Instrumentation Laboratories Model 113 blood gas analyzer. Instrument calibration was checked after each sample.

The commonly accepted sampling site for mixed venous blood is the pulmonary artery. However, during +Gz stress, it was not possible to obtain timed samples with our remote blood sampler from this site because the combination of the pump action and +Gz forces tended to collapse the vessel. Hence, we opted to use the right ventricle as the site for mixed venous blood samples. To ascertain whether this blood was representative of "mixed venous" blood, we performed a literature search for data relating blood gas status of right ventricular blood to pulmonary arterial blood. However, we were unable to identify any such data. We, therefore, conducted the following experiments. Nine adult mongrel dogs weighing 22.5 ± 3.70 (SD) kg were anesthetized with 30

mg/kg pentobarbital sodium and intubated with a cuffed endotracheal tube. A 7 Fr Swan-Ganz catheter was introduced through the right external jugular vein and positioned with its tip in the pulmonary artery just beyond the pulmonary valve. A second 7 Fr catheter with multiple side holes was introduced in the same way and positioned with its tip in the right ventricle. Placement of both catheters was confirmed by observing the pressure profiles measured at the catheter tips. Femoral artery and vein were cannulated for monitoring systemic arterial blood pressure and administering supplemental anesthesia.

Six animals were allowed to breathe spontaneously, and ten pairs of blood samples were drawn at five minute intervals for blood gas comparison. Each pair consisted of one 2 ml sample drawn over a 2-4 second period from the pulmonary artery and another 2 ml sample drawn over a 2-4 second period from the right ventricle. These were drawn sequentially, and the order in which they were obtained was alternated with each pair.

To extend the range of blood gas compositions, paired samples were drawn from the remaining three animals under four sets of conditions: spontaneous breathing, hypocapnia, hypoxia, and, again, spontaneous breathing. In each case, the sampling protocol was the same as in the first series. Three pairs of samples were drawn with the animal first breathing spontaneously. Mechanical ventilation was then begun using a volume limited ventilator set at a tidal volume of 15 ml/kg body weight. The respiratory frequency was adjusted to achieve hyperventilation sufficient to reduce mixed expired P_{CO_2} to approximately 10 Torr. Hyperventilation was continued at this level while three pairs of samples were obtained. The respiratory rate was then reduced, and the

animal was ventilated for three 90 second intervals with a hypoxic, hypercapnic gas mixture (16% oxygen, 3% carbon dioxide). Blood samples were drawn during the final 30 seconds of each interval. A final sample pair was obtained with the animal again breathing spontaneously.

All samples were placed immediately in an ice bath, and analyzed subsequently for P_{O_2} , P_{CO_2} and pH (Instrumentation Laboratories, Model 113). All blood gas determinations were performed in duplicate, and calibration of the instrument was checked after each sample. Hemoglobin concentration for each sample was determined using the cyanmethemoglobin method. Data were compared by paired t-test.

Figure 2 shows oxygen tensions measured from right ventricular samples compared to those measured from pulmonary artery samples. Oxygen tensions ranged from approximately 30 to 50 Torr. The overall mean P_{O_2} measured from samples drawn from the pulmonary artery was 39.2 ± 4.44 (SD) Torr, whereas the mean P_{O_2} from corresponding right ventricular samples was 38.3 ± 4.57 Torr. Although statistical analysis by paired t-test indicated that pulmonary arterial oxygen tension was significantly higher than that in the right ventricular samples ($P < .005$), the difference of 0.9 Torr would not be considered of physiological significance.

No statistical difference was found between pulmonary arterial and right ventricular blood carbon dioxide tension, pH or hemoglobin concentration. P_{CO_2} in the pulmonary arterial samples was 42.64 ± 5.48 (SD) Torr compared to 42.69 ± 5.59 Torr in the right ventricular samples. Mean values for pH and hemoglobin concentration were 7.345 ± 0.043 (SD) and 16.18 ± 1.96 g/100 ml in the pulmonary artery, and 7.343 ± 0.043 and 16.22 ± 1.57 g/100 ml in the right ventricle, respectively.

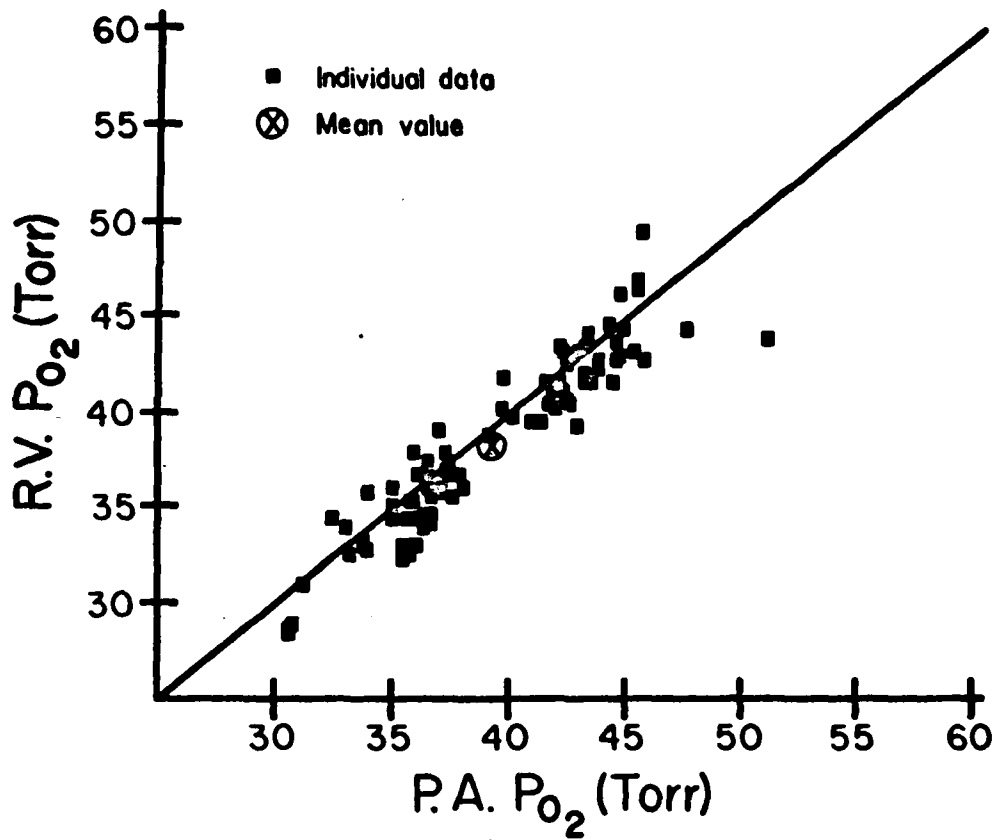


FIGURE 2. Comparison of oxygen tension measured from blood samples drawn from the right ventricle (R.V.) and pulmonary artery (P.A) of 9 dogs. Line of identity is indicated. Overall mean is indicated by the (X) .

These data confirm that the right ventricle is an adequate sampling site for mixed venous blood in the dog.

Results

Series I:

The response of arterial oxygen tension to +3, 4 and 5 Gz is shown in Figure 3. At +3 Gz, arterial P_{O_2} did not change significantly during the exposure. This was true regardless of the G-suit abdominal bladder status.

Although the pattern was similar without abdominal bladder inflation at +4 and +5 Gz, use of the standard bladder inflation scheme resulted in significant decreases in arterial P_{O_2} as the exposure continued ($P < 0.05$, Student's t-test). Furthermore, at three minutes post-exposure, the detriment was still evident with P_{O_2} remaining lower than control (0 Gz) levels ($P < 0.05$, Student's t-test).

Compared to the control value of 3.04 ± 0.99 (SD) L/min, cardiac output, measured by thermal dilution mid-exposure, fell by approximately 35% during exposure without the G-suit (1.96 ± 0.67 at +4Gz; 1.93 ± 0.93 at +5Gz) and by about 20% when the G-suit was used (2.47 ± 1.54 at +4Gz; 2.40 ± 1.19 at +5Gz) ($P < 0.05$, Student's t-test).

An indication of ventilation status early and late in the exposure may be obtained by examining the arterial CO_2 tension. Arterial P_{CO_2} data are shown in Figure 4. At +4 Gz, P_{CO_2} remained essentially constant during the exposure regardless of the G-suit status. After the exposure, however, P_{CO_2} rose ($P < .01$, Student's t-test) indicating that the alveolar ventilation decreased relative to the rate of CO_2 arrival to the alveoli.

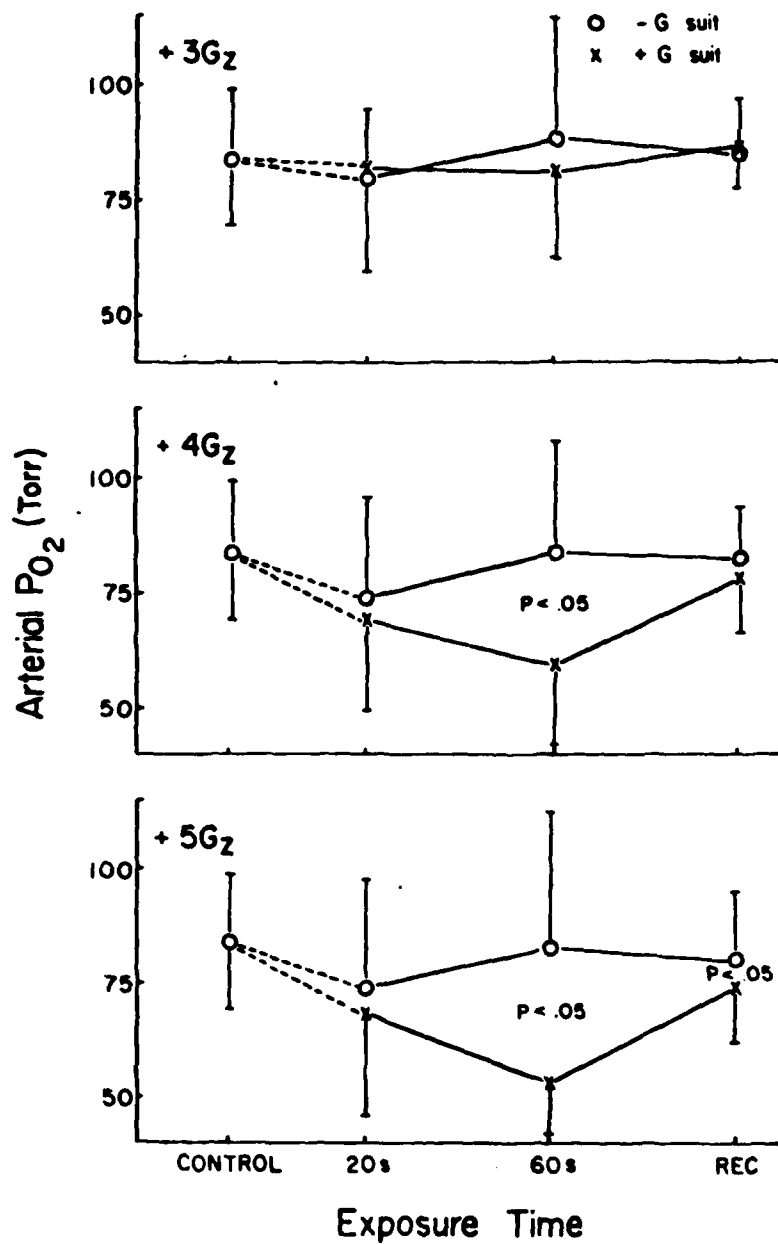


FIGURE 3. Arterial oxygen tension at +3, 4 and 5 Gz as a function of sampling time without (O) and with (X) G-suit abdominal bladder inflation. Bars indicate standard deviation. Statistical significance was determined with Student's t-test.

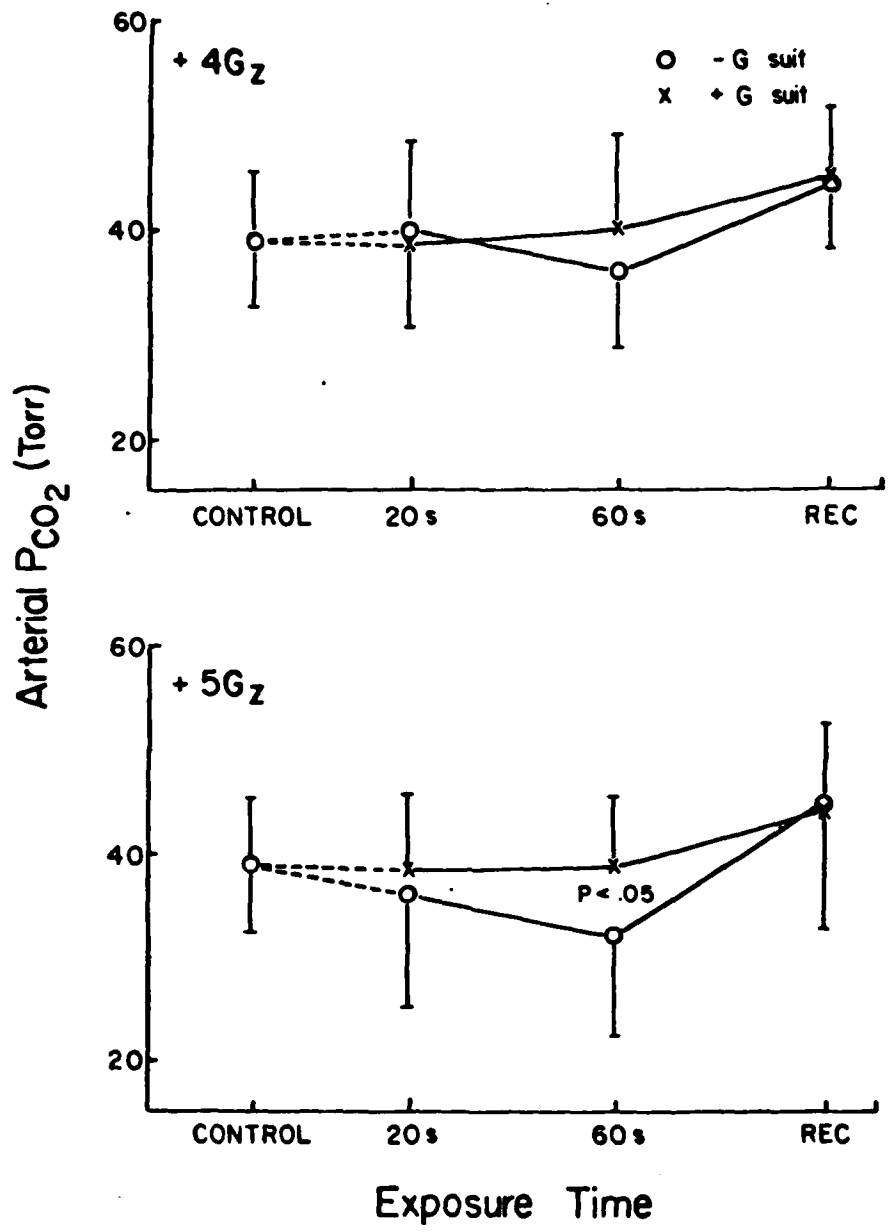


FIGURE 4. Arterial carbon dioxide tension at +4 and +5 Gz as a function of sampling time without (O) and with (X) G-suit abdominal bladder inflation. Standard deviations are indicated. Statistical significance was determined with Student's t-test.

At +5 Gz the pattern seen when the G-suit abdominal bladder was used was similar to the +4 Gz exposure. When the bladder was not inflated, the animal's alveolar ventilation increased relative to CO₂ arrival at the lung as the +Gz stress continued. This is indicated by the decreasing PaCO₂ seen during the exposure (Fig.4).

Assuming that CO₂ production remained relatively constant during the +Gz stress, an indication of cardiac output changes during the exposure may be obtained by examining the mixed venous-arterial CO₂ content differences:

$$Q = V_{CO_2} / (Cv_{CO_2} - Ca_{CO_2})$$

Mixed venous-arterial CO₂ content differences calculated from analysis of blood sampled before, during and after +4 and +5 Gz stress are shown in Figure 5. Carbon dioxide contents were calculated from blood gas tensions using the computer routines of Olszowka and Farhi (12). Carbon dioxide was used instead of oxygen because hemoglobin was estimated from the hematocrit in some experiments, and CO₂ content is less sensitive to small errors in hemoglobin determination than is oxygen content.

Figure 5 suggests that G-suit bladder inflation helped restore cardiac output even at +5 Gz. The progressive increase in mixed venous-arterial CO₂ content difference when the abdominal bladder was not inflated indicates a progressive fall in cardiac output during the +Gz stress. Further, in the case of the +4 Gz stress, more than three minutes were required for cardiac output recovery to control values (P<.025, Student's t-test).

Series II:

Data obtained from 6 +4Gz trials in 5 animals and 5 +5Gz trials in

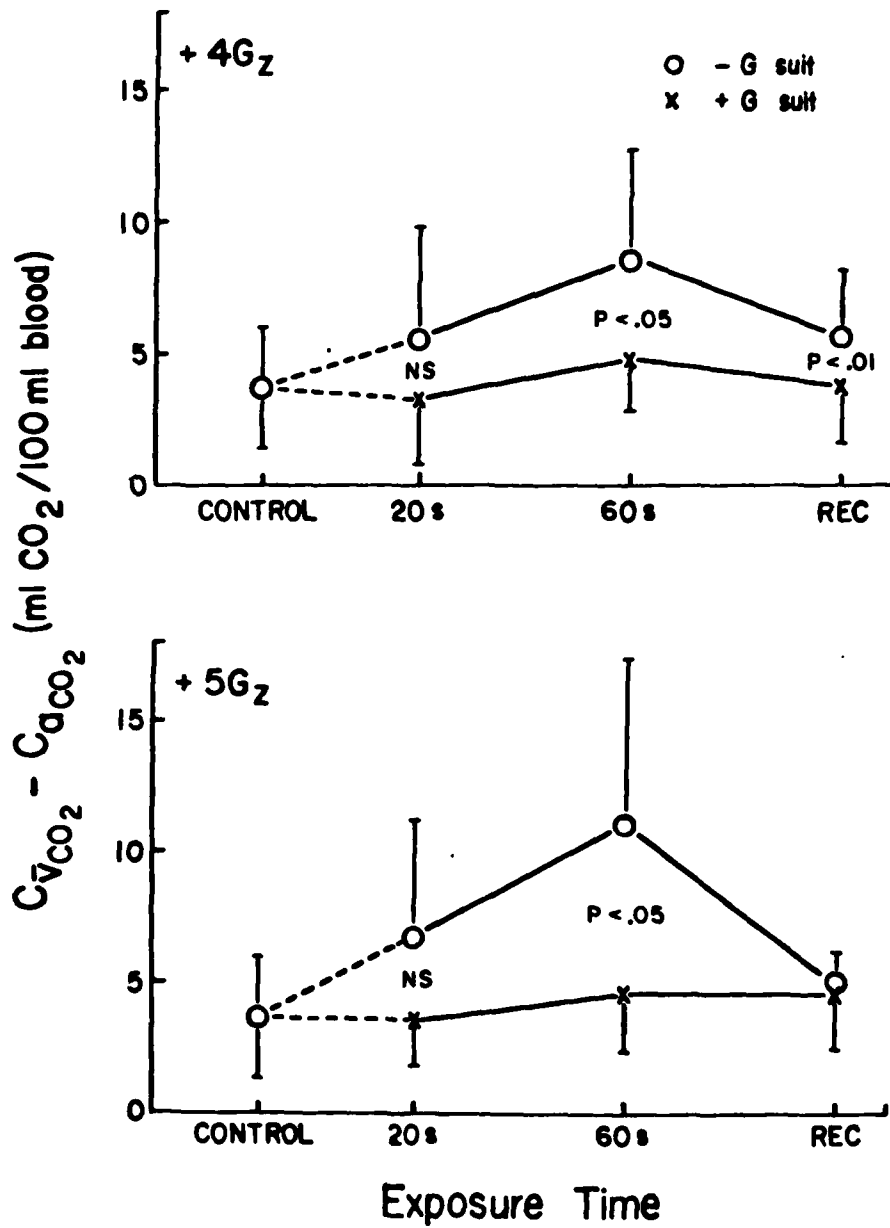


FIGURE 5. Calculated mixed venous-arterial blood carbon dioxide content as a function of sampling time without (O) and with (X) G-suit abdominal bladder inflation (see text). Statistical significance was determined with Student's t-test.

3 animals are presented in Figure 6 where the arterial P_{O_2} measured three minutes after the second +Gz exposure are compared to control values. At each acceleration level, arterial oxygen tension remained 10-15 Torr below control values ($P < .05$, Student's t-test) three minutes post-G stress. These data are consistent with Series I results (Fig. 6) in which the animal was exposed to a single period of +Gz stress.

Arterial oxygen tension in blood samples drawn during the second +4 and +5Gz exposures were essentially the same as those seen during the initial exposures. When arterial P_{CO_2} and pH were examined, no significant differences between the initial and repeated exposures were detected. These data suggest that, with repeated +Gz stress during air breathing, the same degree of gas exchange detriment accompanies G-suit abdominal bladder inflation.

Discussion

The fall in cardiac output accompanying +Gz stress in this study is comparable to that reported by other investigators (7, 10, 13). The data indicate that application of the G-suit abdominal bladder tended to restore cardiac output toward the control value. Figure 5 provides an indication of the time course of cardiac output changes when +Gz stress was applied. Early in the exposure, abdominal bladder inflation did not enhance cardiac output. However, as the exposure continued, cardiac output in trials without the G-suit became compromised to a greater extent. An additional 36% detriment occurred at +4 Gz and, at +5 Gz, an additional 39% detriment was overcome by use of the abdominal bladder.

Although the G-suit tended to maintain cardiac output, a continued fall in arterial P_{O_2} accompanied its use at the higher +Gz levels (Fig. 3). A 25-30 Torr P_{O_2} detriment was evident as the exposure

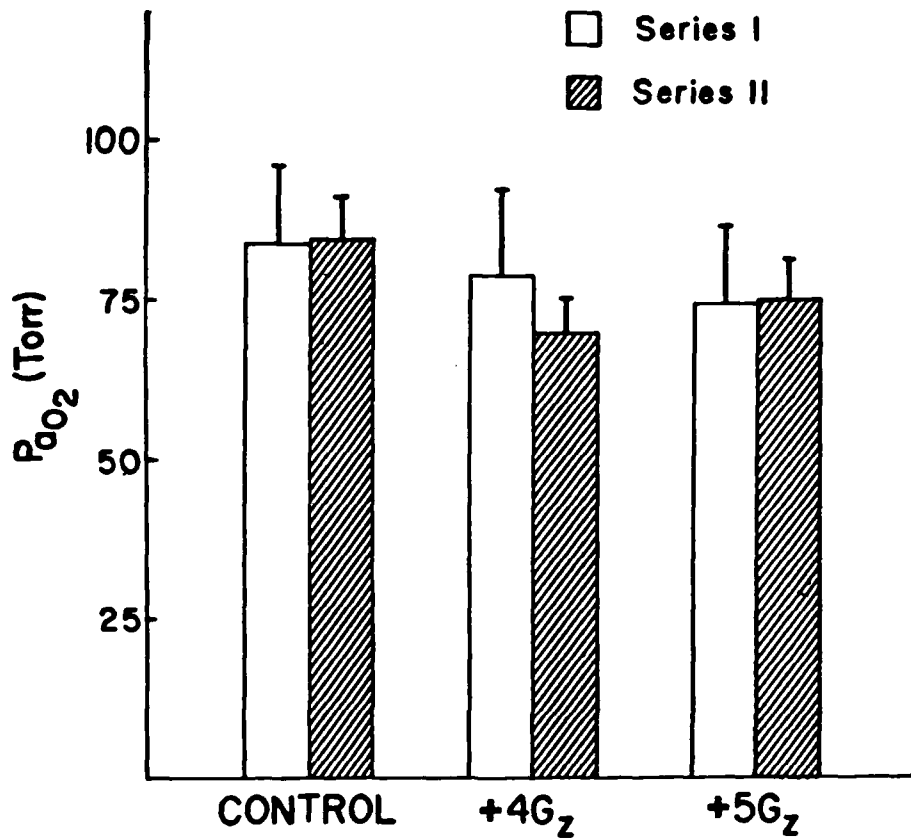


FIGURE 6. Arterial oxygen tension measured before and 3 minutes after exposure to +4 and +5 Gz with G-suit abdominal bladder inflation. Open bars indicate data from Series I experiments. Hatched bars indicated data from Series II experiments. In both series, arterial oxygen tension was significantly below control values after 3 minutes of recovery ($P < .05$, paired t-test).

continued suggesting that a larger maldistribution of ventilation-perfusion relationships was present when the G-suit was used.

Arterial CO₂ tension data (Fig. 4) indicates that alveolar ventilation relative to CO₂ arrival at the lung increased as the exposure continued without bladder inflation.

The blood gas data suggest that major changes in ventilation-perfusion maldistribution were associated with abdominal bladder inflation. Barr et al. (2) reported a slight increase in arterial Po₂ at +1.7 Gz in animals with an abdominal binder. Their data predict that maintenance of cardiac output through G-suit usage should improve the ventilation-perfusion distribution.

At higher +Gz levels, this does not appear to be the case. The continued decrease in arterial Po₂ (Fig. 3) seen with abdominal bladder inflation indicates a greater distribution of blood flow to low V_A/Q areas. This could reflect an increase in blood flow to all areas resulting from the relatively higher cardiac output. If this were the case, a greater percentage of the increased flow would be expected to be distributed to dependent lung regions thereby causing a greater shunt-like effect from areas whose ventilation-perfusion ratios are already low.

Measurements of intrapleural pressure during +Gz stress (11) in the dog indicate that G-suit bladder inflation causes positive intrapleural pressures over a significant portion of lung. These pressures are of sufficient magnitude to cause lung compression. Hence, as +Gz stress is imposed with G-suit abdominal bladder inflation, the action of the bladder may promote airway closure in a larger lung region than similar

exposures without abdominal bladder usage. The increased airway closure would lead to low V_A/Q and atelectatic areas which would be reflected by a significantly lower arterial Po_2 .

Glazier and his colleagues (8,9) examined alveolar size in dogs frozen intact while exposed to several levels of +Gz stress. At +3 Gz without an abdominal binder, a smaller alveolar volume than the +1 Gz control lung was encountered only at levels 25 cm below the lung apex. With an abdominal binder, alveoli at 10-15 cm below the apex were significantly smaller than the +1 Gz control. At the 25 cm level, alveoli were 8-9% of the volume of apical alveoli with the binder compared to 27% of the apical alveolar volume at +3 Gz without the binder.

Glaister (6) examined the lungs of a dog exposed to +1 Gz for 4.75 hr and to six one-minute exposures of up to +4 Gz. An abdominal binder was used, and the animal breathed air throughout. Glaister described the appearance of most alveoli in sections taken from the lung base as "closed off vacuoles in an otherwise solid tissue."

The abdominal binder used by Glazier et al. and Glaister did not produce increasing active counterpressure or abdominal compression as does the standard G-suit abdominal bladder. Hence, any airway closure and atelectasis seen with abdominal binders would be expected to be exacerbated by use of a continually inflating abdominal bladder.

The fact that arterial Po_2 did not return to control values after +4 Gz and +5 Gz exposure with the G-suit but did return after similar exposures without the suit (Fig. 3), and the fact that three minutes was not sufficient time for Po_2 to return to control values provide further evidence that airway closure or frank atelectasis developed as a result

of the bladder inflation.

It has been generally agreed that acceleration atelectasis occurs only when the +Gz stress is accompanied by 100% oxygen breathing and use of a G-suit. However, studies in man (1,3) indicate that exposure to high levels of +Gz stress with G-suit inflation is sufficient to cause atelectasis even though the subject breathes air. Repeated exposure to +Gz stress after atelectasis development could result in a greater gas exchange detriment than that seen during the initial exposure, since the mechanical forces would act on an altered lung-chest wall configuration. However, repeated exposure after airway closure would be expected to result in the same degree of detriment since lung-chest wall configuration and the mechanical forces generated would replicate the initial exposure. Although atelectasis development in our experiments can not be ruled out, the more likely explanation, and the one consistent with Series II results, is that the increased intrapleural pressure generated by abdominal bladder inflation creates a significant amount of airway closure yielding an increased venous admixture. This explanation is also consistent with Glaister's (5) findings. In our experiments, the anesthetized dogs most likely did not make large inspiratory efforts during the 3 minute recovery period, and, therefore, some degree of venous admixture remained at this point (Fig. 6). The detriment was easily removed by rapid reinflation with an Ambu bag, further suggesting that airway closure rather than frank atelectasis was responsible for ventilation-perfusion maldistribution.

REFERENCES

1. Barr, P-O. Hypoxemia in man induced by prolonged acceleration. Acta Physiol. Scand. 54: 128-137, 1962.
2. Barr, P-O., H. Bjurstedt and J.C.G. Coleridge. Blood gas changes in the anesthetized dog during prolonged exposure to positive radial acceleration. Acta Physiol. Scand. 47: 16-27, 1959.
3. Burton, R.R., S.D. Leverett, Jr. and E.D. Michaelson. Man at high sustained +Gz acceleration: a review. Aerospace Med. 45: 1115-1136, 1974.
4. Erickson, H.H., H. Sandler and H.L. Stone. Cardiovascular function during sustained +Gz stress. Aviat. Space Environ. Med. 47: 750-758, 1976.
5. Glaister, D.H. Acceleration atelectasis - some factors modifying its occurrence and magnitude. FPRC/Memo 220, January, 1965.
6. Glaister, D.H. Transient changes in arterial oxygen tension during positive (+Gz) acceleration in the dog. Aerospace Med. 39: 54-62, 1968.
7. Glaister, D.H. The effects of gravity and acceleration on the lung. AGARDograph 133. England: Technical Services, 1970.
8. Glazier, J.B., J.M.B. Hughes, J.E. Maloney and J.B. West. Vertical gradient of alveolar size in lungs of dogs frozen intact. J. Appl. Physiol. 23: 694-705, 1967.
9. Glazier, J.B. and J.M.B. Hughes. Effect of acceleration on alveolar size in the lungs of dogs. Aerospace Med. 39: 282-288, 1968.
10. Hershgold, E.J. and S.H. Steiner. Cardiovascular changes during acceleration stress in dogs. J. Appl. Physiol. 15: 1065-1068, 1960.
11. Modell, H.I. and F.W. Baumgardner. Influence of the chest wall on regional intrapleural pressure during acceleration (+Gz) stress. Aviat. Space and Environ. Med., (in press).
12. Olszowka, A.J. and L.E. Farhi. A system of digital computer subroutines for blood gas calculations. Respir. Physiol. 4: 270-280, 1968.
13. Peterson, D.F., V.S. Bishop and H.H. Erickson. Anti-G suit effect on cardiovascular dynamic changes due to +Gz stress. J. Appl. Physiol.: Respirat. Environ. Exercise Physiol. 43: 765-769, 1977.

SECTION III

AN INEXPENSIVE ASSIST/CONTROL, VOLUME LIMITED ANIMAL VENTILATOR

H.I. Modell and J. Mendenhall

Most commercially available volume-limited animal ventilators are piston pumps designed for use in situations in which tidal volume and frequency are controlled. Ventilators designed for clinical use, however, provide an additional mode whereby the patient may initiate a breath by creating a negative airway pressure (assist mode). The cost of such machines is prohibitive for use on a limited laboratory basis, and, in some cases, safety measures and other design features incorporated into a machine intended for clinical use may prevent use of the ventilator for specific experimental animal protocols. To circumvent these problems, we modified a field resuscitator so that it could function as a volume-limited ventilator in which animals ranging in size from approximately 5 to 45 kg body weight can be ventilated in controlled or assisted modes. The cost of the completed unit was under \$200.

A Globe Safety Products Model 3000 field resuscitator obtained from Federal Surplus Property served as the heart of the ventilator. As originally designed, this unit consists of a pneumatically driven reciprocating bellows governed by a pneumatic control circuit. In this configuration, the unit operates only in a controlled ventilation mode with tidal volume, inspiratory flow rate, expiratory time and, hence, respiratory rate at preset values.

The original pneumatic control circuit was modified to include two electronic timing circuits. A schematic diagram of the reconfigured system is shown in Figure 1. The bellows excursion is limited at the

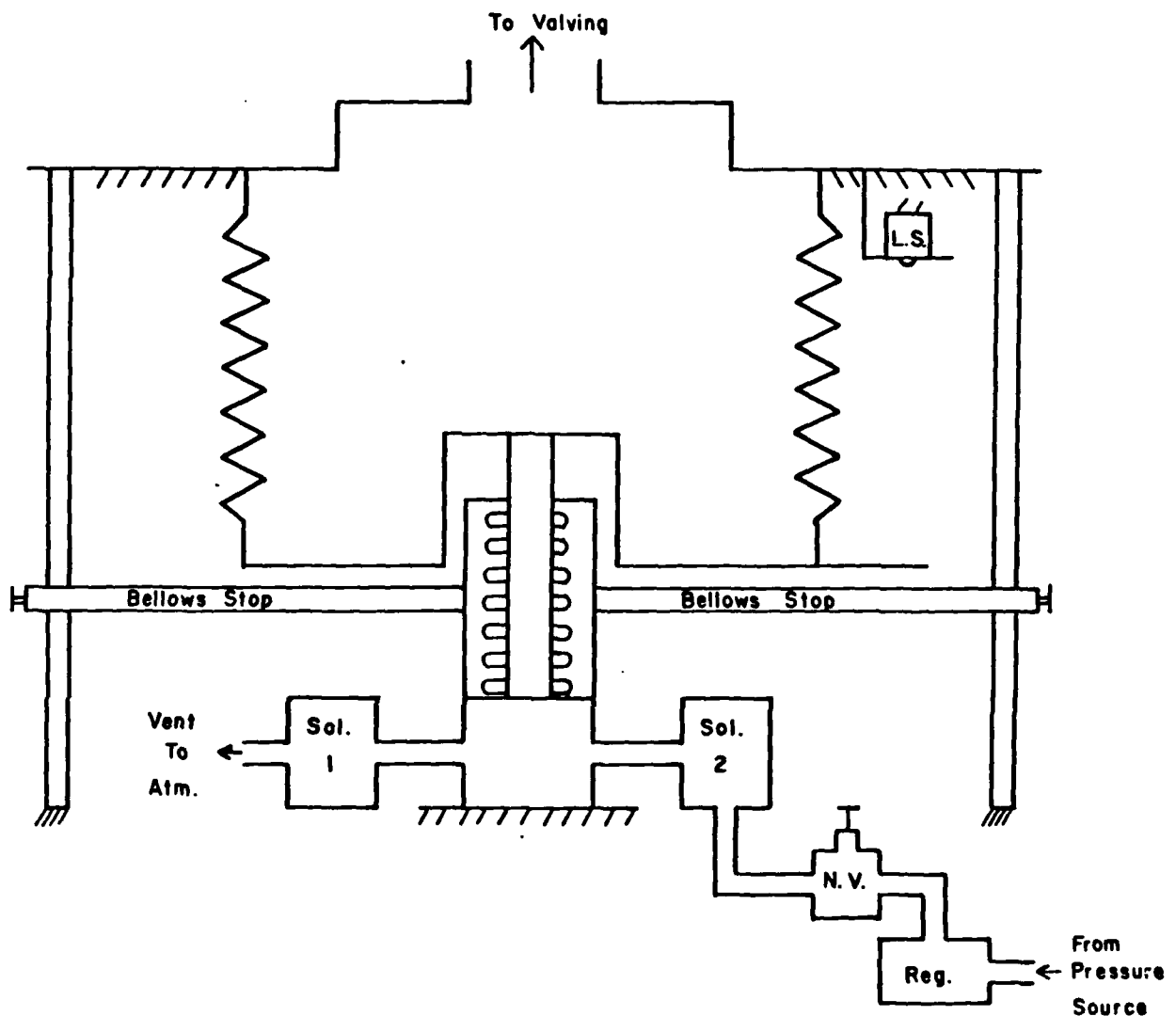


FIGURE 1. Schematic representation of reconfigured field resuscitator unit. Gas providing pressure for activating bellows movements is regulated to 28 psi (Reg.). The gas passes through a needle valve (N.V.) allowing control of inspiratory flow rate, and it is admitted to the bellows driving chamber through a solenoid (Sol. 2) activated by the electronic control circuit. The end of inspiration is marked by activation of an electronic limit switch (L.S.) which triggers the exhaust solenoid (Sol. 1) and the appropriate timing circuit (see text).

bottom by an adjustable mechanical stop, thereby allowing adjustment of tidal volume from approximately 75 to 700 ml. Bellows excursion is limited at the top by an electronic limit switch. This switch triggers a solenoid exhaust valve on the bellows driving cylinder allowing the bellows to refill from the atmosphere, and it triggers two timers, one for each mode. In the controlled ventilation mode, the governing timer determines expiratory time and is adjustable from 2 to 12 seconds. In the assisted ventilation mode, a 15 second timer is set, and a signal from a pressure transducer measuring airway pressure is fed into the timer circuit. If the signal from this transducer changes polarity, the 15 second timer is overridden ending expiration. The airway pressure at which the unit triggers is adjustable by changing the base line voltage of the amplifier to which the transducer is connected. If an inspiratory effort is not signalled, the 15 second timer marks the end of expiration. When the appropriate timer signals the end of expiration, the exhaust solenoid is closed, and the supply solenoid is opened allowing pressure (28 psi) to build up in the bellows driving cylinder. The gas generating the bellows driving pressure flows through an adjustable needle valve, thereby providing a mechanism for adjusting the rate of bellows movement and, hence, inspiratory flow rate. During expiration, the downward excursion of the bellows is enhanced by a spring mechanism present in the original design.

Driving pressure for the bellows may be supplied from any pressure source developing pressures greater than 28 psi. A pressure regulator reducing the input pressure to 28 psi is incorporated into the design prior to the needle valve.

Valving for the ventilator-patient circuit (Fig. 2) is accomplished by two passive valves and the non-rebreathing valve that is part of the

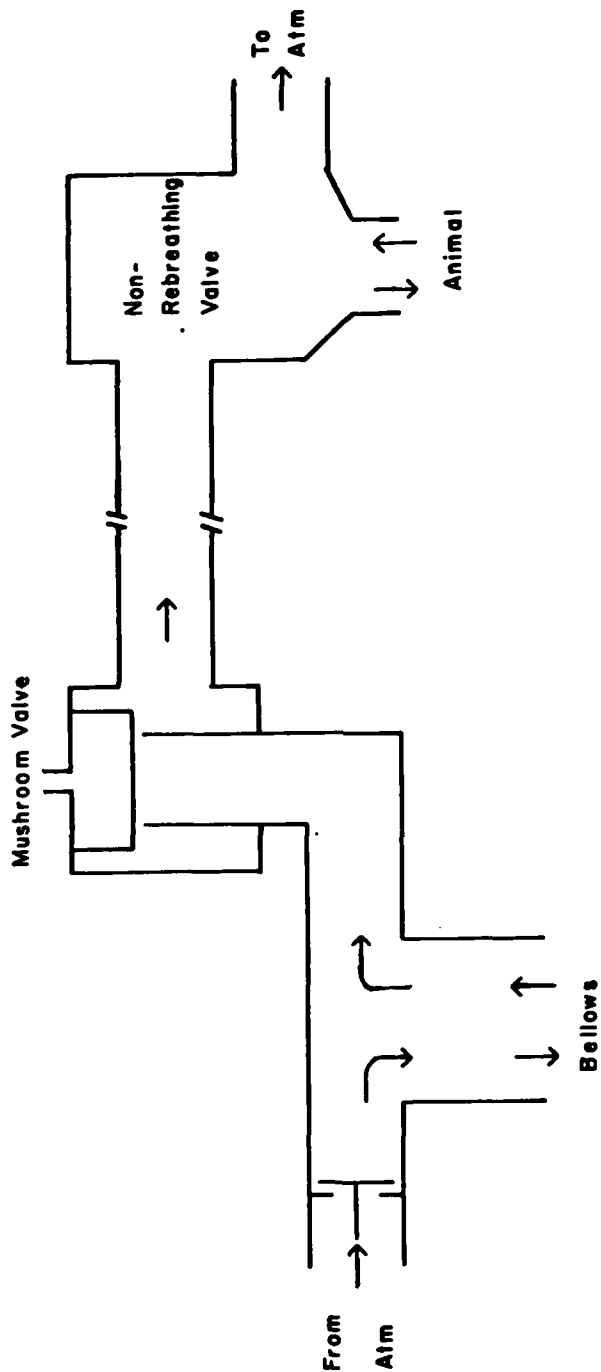


FIGURE 2. Schematic representation of the valving arrangement used with the modified ventilator (see text).

original ventilator design. A mushroom valve interposed between the bellows and the non-rebreathing valve on the inspiratory line prevents the animal from breathing "through" the ventilator, as is the case in the original design. Elimination of this clinical safety feature allows the animal to develop a negative airway pressure. The mushroom valve is operated as a passive valve taking advantage of the housing design rather than providing pressure to inflate the "mushroom" balloon to close the valve.

SECTION IV

INFLUENCE OF THE CHEST WALL ON GAS EXCHANGE DURING MECHANICAL VENTILATION IN DOGS

H.I. Modell and M.M. Graham

The influence of alterations in chest wall motion on gas exchange has not been defined clearly. Minh and his colleagues (3,4) examined the pleural pressure gradient and gas exchange in dogs during unilateral electrophrenic stimulation. These investigators successfully altered the pleural pressure gradient and observed an increase in arterial oxygen tension. Schmid et al. (8) compared chest wall motion and distribution of ventilation in anesthetized supine dogs breathing spontaneously and being mechanically ventilated after muscle paralysis. Although these investigators observed significant differences in abdominal and thoracic movement, they were unable to demonstrate significant differences in the topographical distribution of ventilation between the two states. This study was designed to determine if, during mechanical ventilation, gas exchange is influenced by a muscular effort coordinated with inspiratory flow.

Methods

Six mongrel dogs weighing 21.2 ± 4.7 Kg were anesthetized with 30 mg/kg pentobarbital sodium administered intravenously and intubated with a cuffed endotracheal tube. A 7 Fr thermal dilution Swan-Ganz catheter was introduced into the right external jugular vein and positioned so that its distal port was in the pulmonary artery and its proximal port was in the right atrium. The femoral artery and vein were cannulated for arterial blood pressure monitoring, arterial blood sampling, and administration of supplemental anesthesia.

The animal was then placed either supine or in a lateral position

(right side down), and assisted ventilation was begun with a tidal volume of 15 ml/kg using the ventilator described in Section II of this report. The ventilator triggered when the animal developed -2 cm H₂O airway pressure. After 10 minutes of ventilation, minute ventilation was determined by collecting expired gas for 1-2 minutes. Following this determination, mixed expired oxygen and carbon dioxide tensions were measured, arterial and mixed venous blood samples were drawn and iced for blood-gas determinations, and thermal dilution cardiac output determinations were made in duplicate. Another 10 minute control period was then allowed, and the process was repeated until at least two experimental runs were completed.

In three of the six animals, the orientation of the animal was changed from supine to lateral, and the protocol described above was repeated. In the remaining three animals (two supine, one lateral), at least three determinations were made in the assist mode.

After data had been collected in the assist mode, the animal was paralyzed with 20 mg/kg succinylcholine administered intramuscularly, and controlled ventilation was begun. In this mode, tidal volume and inspiratory flow rate were maintained at the levels established for the assisted ventilation mode. Expiratory time was adjusted so that respiratory rate was comparable to that set by the animal in the assist mode. Hence, all ventilator parameters established during assisted ventilation were essentially the same during controlled ventilation.

Data in the controlled mode were collected in the same manner as in the assist mode. In the three animals in which body position was changed, samples were obtained in both supine and lateral positions.

Results

No differences in any of the measured parameters were detected between the lateral and supine positions. Mean arterial blood gas values for the two modes of ventilation are shown in Figure 1. Arterial oxygen tension was higher ($P < 0.01$, paired t-test), and carbon dioxide was lower ($P < 0.01$, paired t-test) when an inspiratory muscular effort accompanied inspiration.

Calculated physiological dead space and cardiac output data are presented in Figure 2. When the animal was paralyzed and ventilated, physiological dead space increased ($P < 0.01$, paired t-test) and cardiac output decreased ($P < 0.01$, paired t-test). No differences were detected, however, between the fraction of the cardiac output calculated as representing venous admixture for each ventilation mode.

Minute ventilation measurements confirmed that this parameter was the same during assisted and controlled ventilation modes.

Discussion

An apparent controversy exists in the literature concerning the effects of chest wall motion on gas exchange. Sackner and associates (7) compared the distribution of ventilation in humans during thoracic breathing to that during diaphragmatic breathing. While differences in distribution of ventilation were detected in normal subjects, no differences were detected between the two types of breathing in patients with chronic obstructive lung disease. Schmid and co-workers (8) examined the same question in dogs during spontaneous breathing and during mechanical ventilation after muscle paralysis. Although changes in chest wall motion were detected, no differences in the distribution

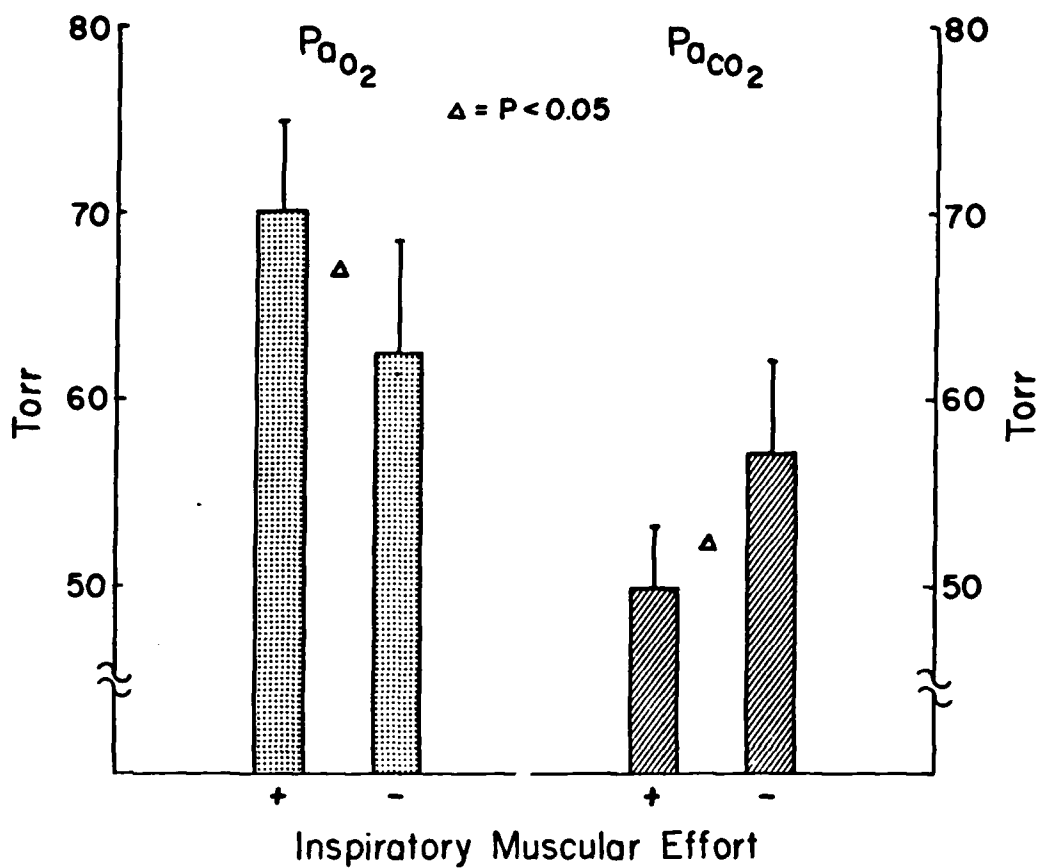


FIGURE 1. Mean arterial gas tensions obtained with a coordinated inspiratory muscular effort (assisted ventilation) and without a coordinated inspiratory muscular effort (controlled ventilation). Standard error of the mean is indicated. Statistical analysis was performed using a paired t-test.

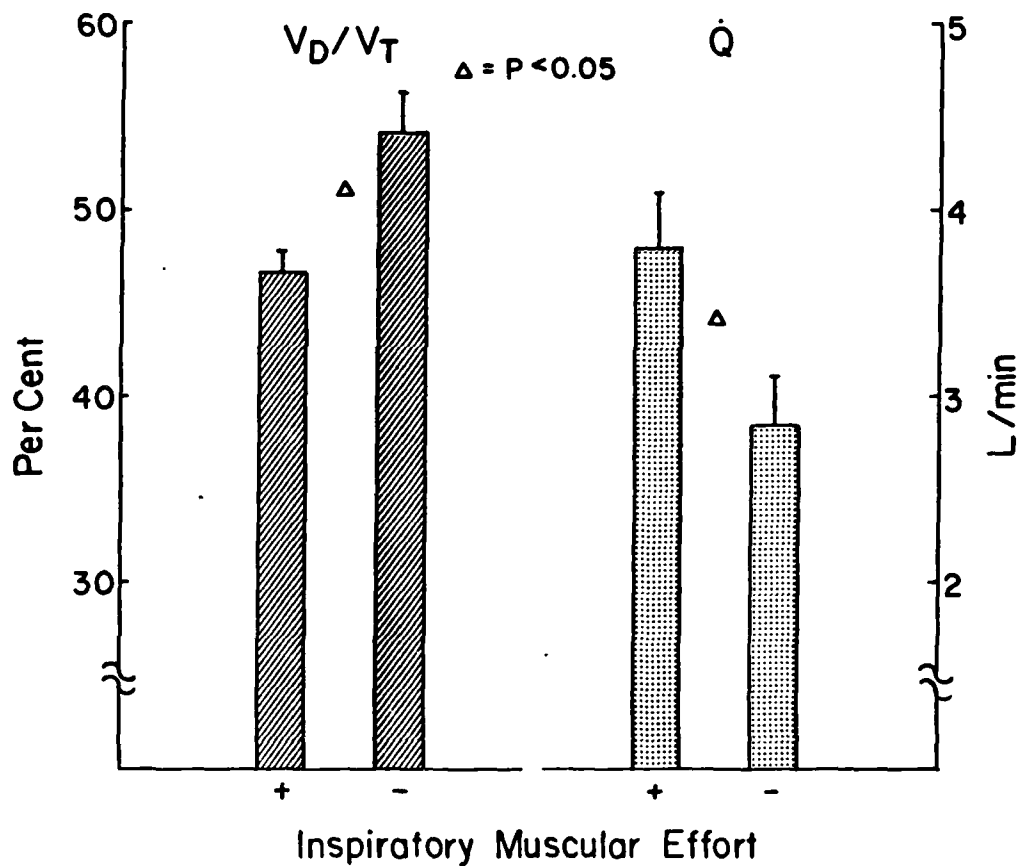


FIGURE 2. Mean physiological dead space (left panel) and cardiac output (right panel) observed with a coordinated inspiratory muscular effort (assisted ventilation) and without a coordinated inspiratory muscular effort (controlled ventilation). Standard error of the mean is indicated. Statistical analysis was performed using a paired t-test.

of regional ventilation were observed.

Hughes (1) compared thoracic to abdominal breathing in normal human subjects and concluded that gas exchange was enhanced during abdominal breathing. Minh et al. (3) noted increased arterial P_{O_2} in dogs during right electrophrenic respiration compared to spontaneous breathing.

The implication of these studies is that changes in chest wall motion may not cause significant changes in the distribution of ventilation, but they do alter ventilation-perfusion relationships. In our study, minute ventilation was kept constant, but physiological dead space increased significantly during controlled ventilation (Fig. 2). The net result of this was a decreased effective alveolar ventilation during controlled ventilation with concomitant changes in gas exchange (Fig. 1).

Was the increased dead space a result of a shift in ventilation or a shift in perfusion? Rehder et al. (6) demonstrated changes in the distribution of ventilation when human subjects previously awake, breathing spontaneously were anesthetized, paralyzed and ventilated mechanically. In dogs, however, similar changes have not been demonstrated (3,8). In two additional experiments, we ventilated animals according to the assist-control protocol with Krypton-81m in the inspire and examined the topographical distribution of ventilation with anterior view, static gamma camera imaging. In these experiments, we were unable to detect gross changes in distribution of ventilation. In a third experiment, we acquired images suitable for single photon emission computed tomography (SPECT) analysis. This analysis revealed a ventilation shift concomitant with the change in ventilation mode. The ventilation shifts are evident in the representative images shown in Figures 3 and 4.

Figure 3 shows equivalent sagittal images from the right side of the animal during assisted and controlled ventilation. During the assist mode, significant ventilation was distributed to the upper anterior lung regions. During the controlled mode, this region of high ventilation was no longer evident. Subtraction of the images, also shown in Figure 3, indicate that ventilation to the dependent lung regions was greater during controlled ventilation than during assisted ventilation.

Figure 4 shows equivalent coronal "slices" approximately 3 cm from the anterior surface of the lung. The same shift of ventilation from upper to lower lung regions is evident in these images. These data support the hypothesis that the increased dead space measured resulted from a change in distribution of ventilation.

A change in measured dead space could also occur from perfusion being shifted toward areas having lower ventilation-perfusion ratios. Such changes could occur as a result of a decreased cardiac output or alterations in mean intrathoracic pressure. To get some indication of the P_{O_2} drop expected from a cardiac output fall of the magnitude seen in our data, we analyzed a 3-compartment model of the lung (5). Assuming that oxygen consumption remained constant, only about 20% of the observed P_{O_2} drop can be explained on the basis of the cardiac output change alone. In studies aimed at determining the influence of ventilator flow pattern on gas exchange during mechanical ventilation, Modell and Cheney (4) examined two flow patterns resulting in markedly different mean intrathoracic pressures. In normal dogs, these investigators did not detect changes in gas exchange parameters associated with increased mean intrathoracic pressure. This suggests that the contribution by changes in distribution of perfusion were not



Assisted



Controlled



Assisted - Controlled



Controlled - Assisted

FIGURE 3. Sagittal SPECT "slice" images from the right lung during assisted (top, left) and controlled (top, right) ventilation modes. Differences in activity between these two images are also shown.

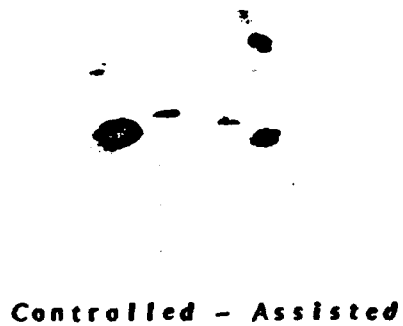


FIGURE 4. Coronal SPECT "slice" images of approximately 3 cm from the anterior surface of the lungs during assisted (top, left) and controlled (top, right) ventilation modes. Differences in activity between these two images are also shown.

large enough to account fully for the observed increase in dead space volume.

We are currently conducting additional experiments using the SPECT approach to further delineate the changes in ventilation and perfusion that occur as a result of removing a coordinated inspiratory effort.

References

1. Hughes, R.L. Does abdominal breathing affect regional gas exchange? Chest 76: 288-293, 1979.
2. Minh, V.-D., N. Kurihara, P.J. Friedman and K.M. Moser. Reversal of the pleural pressure gradient during electrophrenic stimulation. J. Appl. Physiol. 37: 496-504, 1974.
3. Minh, V.-D., P.J. Friedman, N. Kurihara and K.M. Moser. Ipsilateral transpulmonary pressures during unilateral electrophrenic respiration. J. Appl. Physiol. 37: 505-509, 1974.
4. Modell, H.I. and F.W. Cheney. Effects of inspiratory flow pattern on gas exchange in normal and abnormal lungs. J. Appl. Physiol 46: 1103-1107, 1979.
5. Modell, H.I., A.J. Olszowka, R.A. Klocke and L.E. Farhi. Normal and abnormal lung function, a program for independent study, The American Thoracic Society, New York, 1975.
6. Rehder, K., A.D. Sessler and J.R. Rodarte. Regional intrapulmonary gas distribution in awake and anesthetized-paralyzed man. J. Appl. Physiol. 42: 391-402, 1977.
7. Sackner, M.A., G. Silva, J.M. Banks, D.D. Watson and W.M. Smoak. Distribution of ventilation during diaphragmatic breathing in obstructive lung disease. Am. Rev. Resp. Dis. 109: 331-337, 1974.
8. Schmid, E.R., K. Rehder, T.J. Knopp and R.E. Hyatt. Chest wall motion and distribution of inspired gas in anesthetized supine dogs. J. Appl. Physiol.: Respirat. Environ. Exercise Physiol. 49: 279-286, 1980.

SECTION V

IN VIVO PRESSURE-VOLUME RELATIONSHIPS OF THE PIG LUNG AND CHEST WALL

H.I. Modell

Results of our pleural pressure studies (4) indicate that the chest wall plays an important role in determining regional intrapleural pressure during acceleration stress. The pig has been proposed as a model for studying the response to acceleration stress because its chest wall characteristics appear to resemble human chest wall characteristics in some respects. However, little information is available in the literature describing the mechanical properties of the pig's lung and chest wall. Additional data concerning these properties are necessary to interpret intrapleural pressure and gas exchange data in pigs exposed to acceleration stress (+Gz). The purpose of this study was to provide information concerning the static properties of the pig respiratory system.

Methods

Six Yorkshire pigs weighing 20.1 ± 3.05 Kg were anesthetized with 18 mg/Kg ketamine hydrochloride and 2 mg/Kg xylazine administered intramuscularly. An external jugular vein was cannulated for supplemental anesthesia administration (Pentobarbital sodium), a tracheostomy was performed, and a carotid artery was cannulated for arterial pressure monitoring. A pleural pressure monitoring cannula (4) was introduced into the fourth or fifth intercostal space on each side of the animal. We have verified that these cannulae reflect changes in pressure accurately (4). However, it is not clear whether this type of cannula measures the absolute value of the intrapleural pressure correctly (3). Therefore, the recorded pressures were adjusted

initially to approximately -5 cm H_2O to ensure equal starting points for later pressure analysis. In the analysis, only pressure changes were considered. The animal was then ventilated mechanically at a tidal volume of 15 ml/Kg and a rate sufficient to lower the monitored mixed expired P_{CO_2} to approximately 10 Torr. This level is below the pig's apneic threshold, and when removed from the ventilator, time of apnea was greater than one minute.

To ensure a constant lung volume history prior to a test run, mechanical ventilation was removed, the animal's lungs were then inflated to 30 cm H_2O airway pressure (P_{aw}), and the animal's lungs were allowed to deflate passively. This maneuver resulted in pre-run recorded intrapleural pressure (P_{pl}) reflecting a control P_{pl} at the animal's functional residual capacity (FRC).

During each experimental run, the lungs were inflated with a predetermined volume of air sufficient raise P_{aw} to approximately 30 cm H_2O (600 ml to 1 L) using a 1 L syringe. The lungs were then deflated in 100 or 200 ml steps until the pre-run FRC was reached. An additional 50-100 ml was then removed to obtain data below FRC. Each volume step was held for 3-5 seconds to allow P_{aw} and P_{pl} to reach a plateau.

All pressure signals were recorded on FM magnetic tape as well as on a strip-chart recorder. The signals were then digitized at a rate of 5 samples/second using an Apple][+ computer system. Computer analysis of the digitized data included averaging 5 to 15 points at each plateau and calculating changes in P_{aw} and P_{pl} from the pre-run FRC pressures at each volume step.

Results and Discussion

To obtain pressure-volume curves of the respiratory system, chest wall and lungs, it is necessary to know the pressure distending the structure (i.e., the difference between pressure inside and pressure outside) at a series of volumes. In our experiments, we assumed that hyperventilating the animal to below its apneic threshold would result in relaxation of the respiratory muscles. Under these conditions, the pressure on the outside of the elastic component of the chest wall is atmospheric pressure. Thus, for the entire respiratory system, the distending pressure is the alveolar pressure; for the chest wall, it is the intrapleural pressure; and for the lungs, it is the difference between alveolar and intrapleural pressures. In our experimental protocol, we adjusted the reading of the pleural pressure cannulae at the beginning of the experiment. Because of this, we were unable to obtain data concerning the absolute magnitude of intrapleural pressure, but accurate relative pressure measurements were assured.

Average pressure-volume curves obtained from the six animals are shown in Figures 1, 2 and 3. In these plots, distending pressure is expressed relative to the initial pressure (pre-run FRC value). Because absolute lung volume determinations were not made in these experiments, volume is also expressed relative to the pre-run FRC. Pressure-volume curves of the respiratory system are shown in Figure 1. Since no air flow occurred during each volume step, it was assumed that airway pressure was equal to alveolar pressure at each step. These curves are analogous to the classic relaxation curves obtained by Rahn et al. (5) in humans. The primary difference between the shapes of these curves and those obtained in man is that these curves appear to flatten, indicating decreased compliance, near FRC rather than well below it.

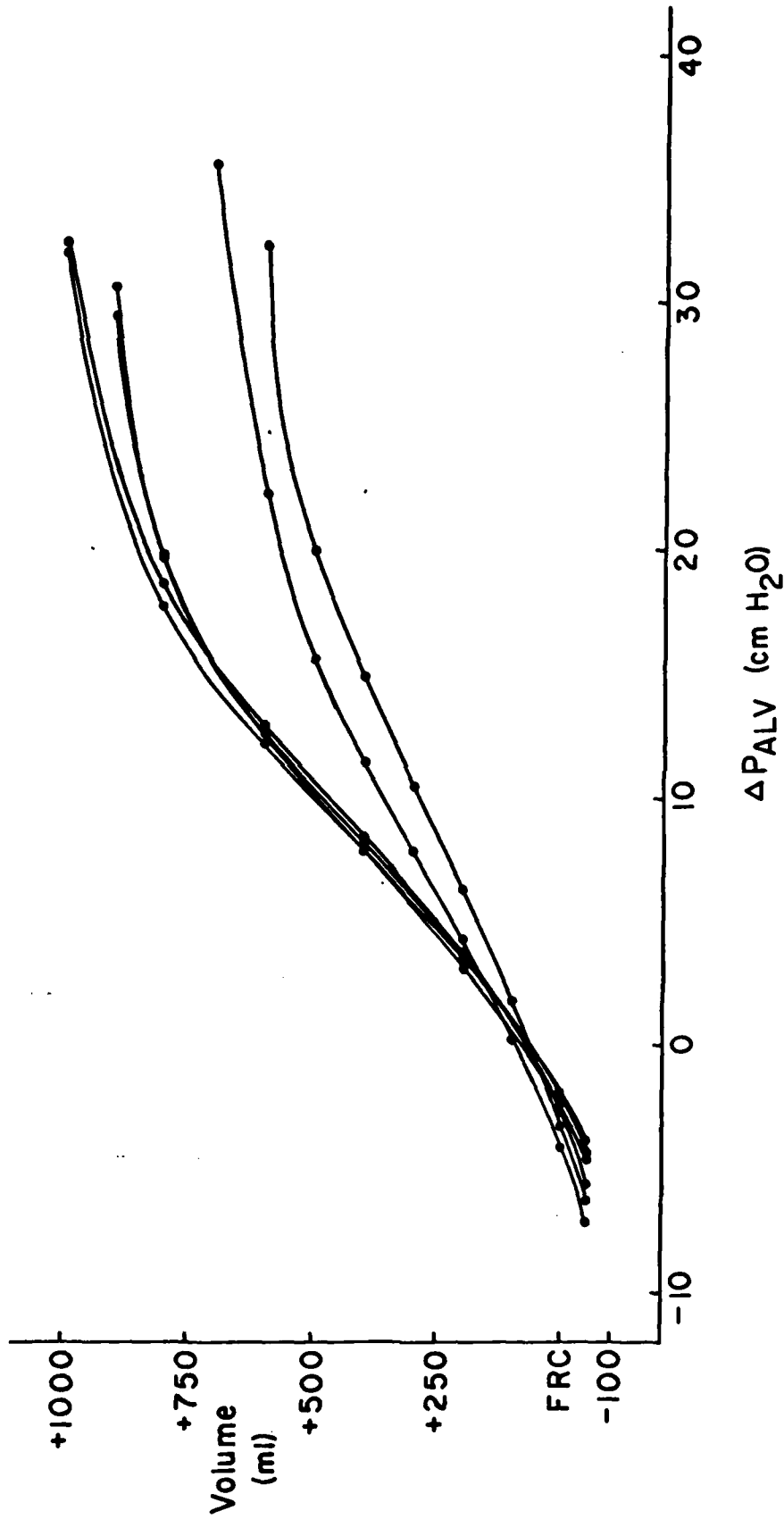


FIGURE 1. Mean pressure-volume curves from 6 pigs. Mean data are shown. Curves have been fit by eye.

In vivo pressure-volume curves of the chest wall are presented in Figure 2. These curves suggest that the upper elastic limit of the pig's chest wall is within the "vital capacity" range. Thus, in the pig, the chest wall acts in consort with the lung to determine the upper limit of the respiratory system.

Pressure-volume curves of the lungs (Figure 3) were obtained by subtracting the chest wall curves from the total system curves. The shape of the lung curves are consistent with similar curves obtained from man (5) and other mammals (6,7).

The mean compliances of the lung, chest wall and total respiratory system calculated over the volume range examined are plotted in Figure 4. Attinger and Cahill (1) measured lung compliance in pigs ranging in weight from 9 to 45 Kg. Their reported value (57 ml/cm H₂O) is similar to the value we obtained in the FRC range. As Figure 4 indicates, we found a large variation in lung compliance over the volume range examined. Although lung and chest wall compliances were similar around FRC, they diverged at larger lung volumes with the lungs being significantly more compliant at mid-range. These data suggest that the contribution of the chest wall to total respiratory system static properties is greater in the pig than in man.

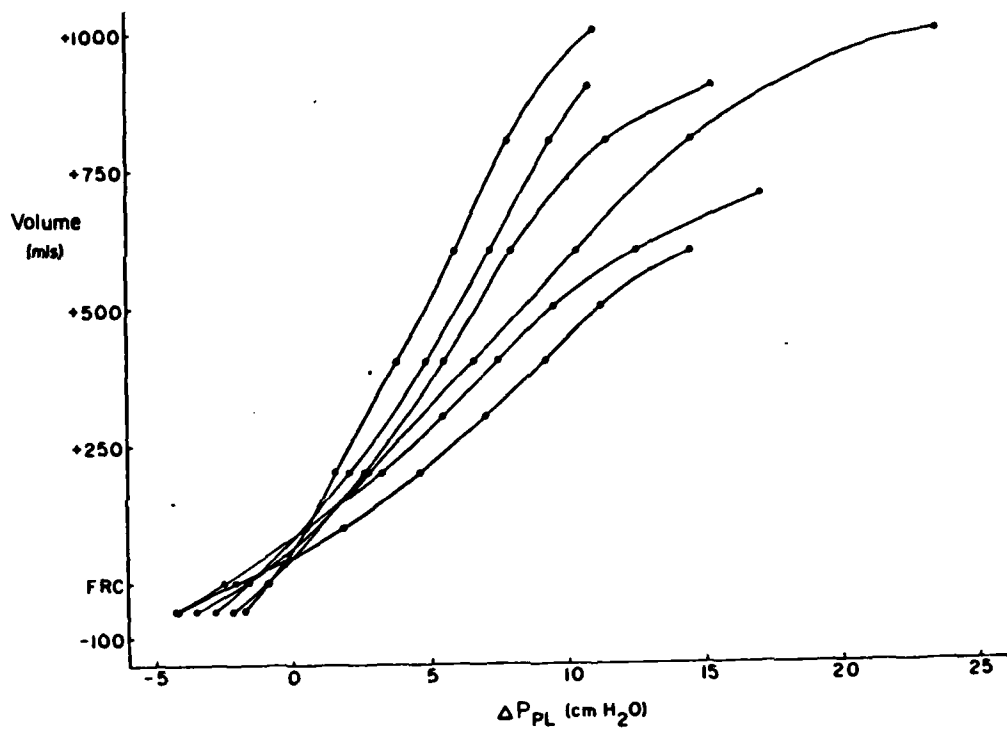


FIGURE 2. Mean chest wall curves from 6 pigs. Mean data are shown. Curves have been fit by eye.

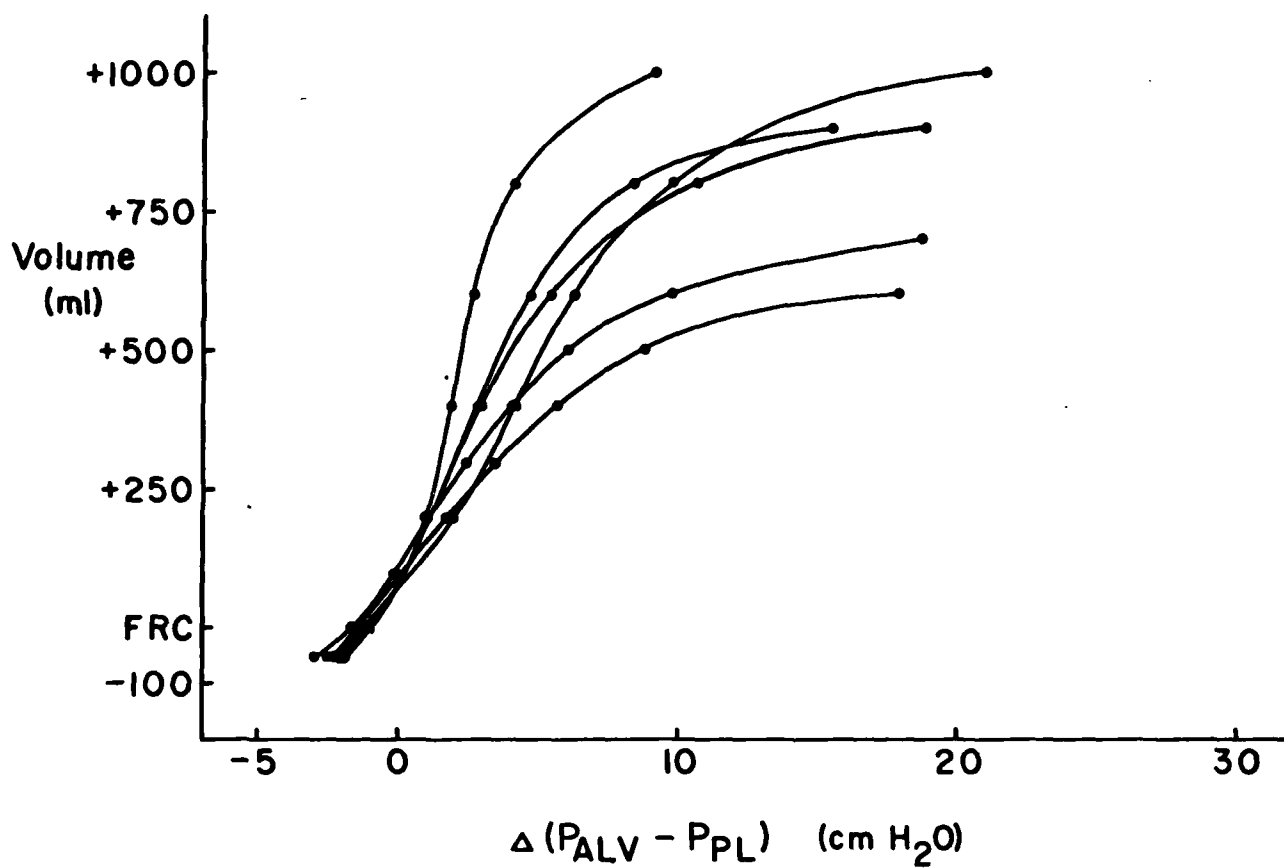


FIGURE 3. Mean lung curves from 6 pigs. Mean data are shown. Curves have been fit by eye.

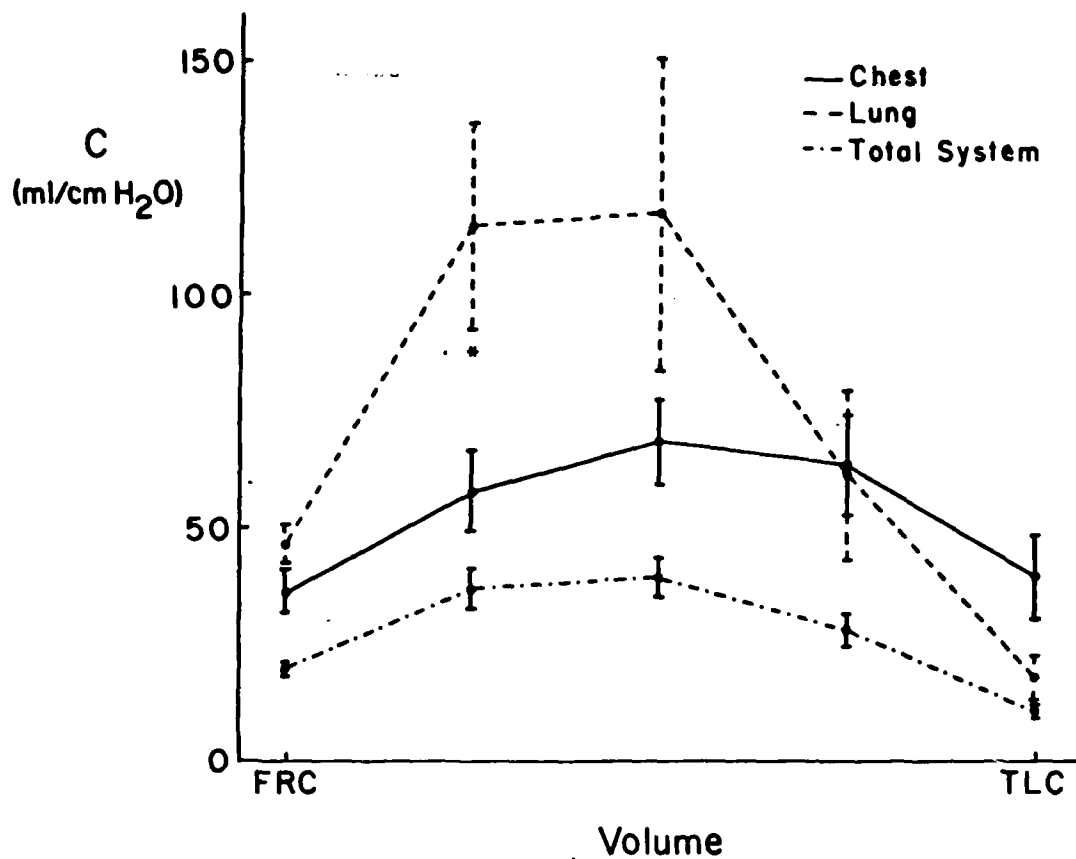


FIGURE 4. Mean compliances of the lung, chest wall and total respiratory system calculated over the volume range examined. Standard errors of the mean are indicated. Statistically significant differences ($P < .05$, paired t-test) between lung and chest wall compliances are also indicated (*).

References

1. Attinger, E.O. and J.M. Cahill. Cardiopulmonary mechanics in anesthetized pigs and dogs. Am. J. Physiol. 198: 346-348, 1960.
2. Faridy, E.E., S. Permutt and R.L. Riley. Effect of ventilation on surface forces in excised dogs' lungs. J. Appl. Physiol. 21: 1453-1462, 1966.
3. McMahon, S.M., S. Permutt and D.F. Proctor. A model to evaluate pleural surface pressure measuring devices. J. Appl. Physiol. 27: 886-891, 1969.
4. Modell, H.I. and F.W. Baumgardner. Influence of the chest wall on regional intrapleural pressure during acceleration (+Gz) stress. Aviat. Space Environ. Med. (in press)
5. Rahn, H., A.B. Otis, L.E. Chadwick and W.O. Fenn. The pressure-volume diagram of the thorax and lung. Am. J. Physiol. 146: 161-178, 1946.
6. Schroter, R.C. Quantitative comparisons of mammalian lung pressure volume curves. Respir. Physiol. 42: 101-107, 1980.
7. Wohl, M.E.B., J. Turner and J. Mead. Static volume-pressure curves of dog lungs - in vivo and in vitro. J. Appl. Physiol. 24: 348-354, 1968.

Adaptation of vascular pressure-flow-volume hysteresis in isolated rabbit lungs

KENNETH C. BECK AND JACK HILDEBRANDT

*Department of Physiology and Biophysics, University of Washington, 98195;
and Virginia Mason Research Center, Seattle, Washington 98101*

BECK, KENNETH C., AND JACK HILDEBRANDT. *Adaptation of vascular pressure-flow-volume hysteresis in isolated rabbit lungs.* J. Appl. Physiol.: Respirat. Environ. Exercise Physiol. 54(3): 671-679, 1983.—Hysteresis within two pairs of variables describing the state of the lung vascular system [pulmonary arterial pressure (Ppa) and flow (Q) and Ppa and change in vascular volume (ΔV_{vasc})] was investigated in isolated plasma-perfused rabbit lungs. Q was increased and decreased stepwise, in series of five cycles each, while pulmonary venous pressure (Ppv) and lung volume were held constant. Changes in V_{vasc} were estimated from changes in fluid volume of the venous reservoir. The relationships within pairs of variables over each complete cycle were described by loops whose areas and widths were used to quantify the hysteresis. In successive cycles, these parameters decreased toward constant values (limit cycles), most of the change occurring by the second cycle. Areas of Ppa- ΔV_{vasc} loops correlated closely with areas of Ppa-Q loops over all five cycles of a series. For Ppa-Q loops, the ratio of average pressure-width to total pressure excursion decreased from 0.15 initially to around 0.05 in the fifth cycle. It was concluded that the relationships between Ppa and Q and Ppa and ΔV_{vasc} are markedly sensitive to vascular pressure or flow history.

pulmonary vasculature; pulmonary vascular resistance; viscoelasticity; adaptation

AS IN OTHER BEDS, pulmonary vascular resistance depends on smooth muscle tone in resistance vessels, but, in addition, it is a function of lung volume and transpulmonary pressure (13, 33), and depends on "waterfall" effects (33). Some investigators have indicated that pressure-flow history may also be a factor (2, 3, 6, 17). Despite these earlier reports of vascular pressure-flow hysteresis, little has been done to document the phenomenon more fully (5). All soft tissues, particularly those containing smooth muscle, have length-tension or pressure-volume relationships that depend on stress history; in other words, they exhibit hysteresis (8). One might therefore expect an intact vascular bed to show pressure-flow and pressure-volume hysteresis; e.g., vascular resistance should be lower and vessel diameters larger if vessel wall stress has just decreased from a high value than if increased from a low value. Furthermore, since continuous cycling of strips from various tissues has been shown to result in decreased length-tension hysteresis (11, 23, 32) and pressure-volume hysteresis (31), one should also expect to find a progressive approach to a pressure-flow limit cycle in a perfused organ.

The present study was undertaken to document pressure-flow hysteresis in isolated perfused lungs in a quantitative way by investigating the approach to the limit cycle between inflow pressure and flow (at constant outflow pressure) and to correlate this hysteresis with vascular pressure-volume hysteresis. In addition, a correspondence was sought between previously published reports of hysteresis in isolated vessels on the one hand and whole-organ pressure-flow and pressure-volume hysteresis on the other.

METHODS

Equipment. Various fixed rates of flow were generated by a roller pump (either Sarns or Masterflex model 7545-00) in series with a bubble trap containing 4-15 ml air to damp flow pulsations (Fig. 1). An electromagnetic flow probe in series with the pulmonary bed and a length of large-bore tubing (9 mm ID) completed the circuit to the venous reservoir, whose height was used to control the venous outflow pressure. The stainless steel vascular cannulas (3.4 mm ID) were fitted with side pressure ports 5 mm from their ends to measure vascular pressure relative to the base of the lungs.

In some experiments, the fluid volume of the circuit (including lungs) was monitored continuously by measuring the small pressure difference between the bottom of the reservoir and the bottom of a reference column of saline beside the reservoir. This system was calibrated by adding measured volumes of perfusate to the reservoir. A sensitive differential transducer (Validyne MP45, ± 2 cmH₂O) detected volume changes within the range ± 20 ml (reservoir ID 38 mm). Volume changes due to the compliance of the perfusion system (tubing and bubble trap) were subtracted from the recorded reservoir volume signal. Thus corrected, reservoir volume changes included both interstitial and vascular volume changes of the lungs.

In seven experiments a heat exchanger was substituted for the bubble trap to maintain the perfusate temperature at 37°C measured in the reservoir. In these experiments the lung preparation was also heated by placing it in a warmed plastic tent. By use of these two devices, perfusate and lung temperature could be regulated within $\pm 1^\circ\text{C}$. All other studies were carried out at room temperature (21-25°C).

The perfusion circuit was primed with 150-200 ml horse plasma that had been frozen for storage and thawed

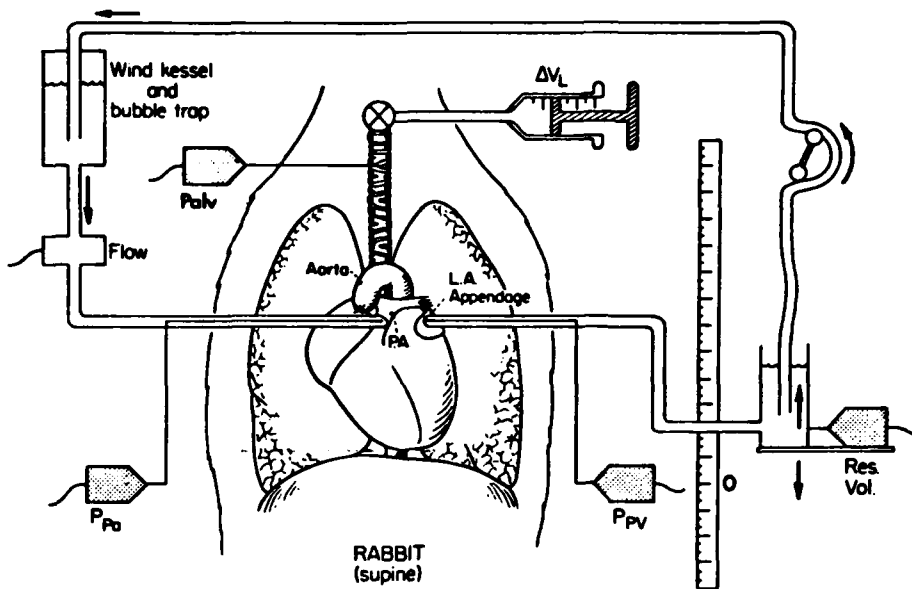


FIG. 1. Perfusion and measurement apparatus. Lungs remained in widely opened chest cavity of supine animal. Transducers were zeroed 1 cm above table, estimated to be level with base of lungs. Constant flows were generated with roller pump. ΔV_L , change in lung volume; Palv, alveolar pressure; LA, left atrium; PA, pulmonary artery; Ppa, pulmonary arterial pressure; Ppv, pulmonary venous pressure.

immediately prior to use. Occasionally the perfusate was expanded by adding a solution of 6% dextran (60,000 daltons, Sigma, industrial) in Ringer solution. Tracheal pressure was measured with an air-filled transducer (Valdine, MP45, ± 50 cm H₂O), and lung volume (VL) changes were made using a graduated 50-ml syringe. Pressures in the pulmonary artery (Ppa), left atrium (Ppv), and trachea (Palv), and perfusate flow (\dot{Q}) were recorded continuously. Reservoir volume changes (ΔV_{vasc}) were also recorded in some experiments. Each signal was recorded on an ink-writing eight-channel recorder (Beckman model R 611) and simultaneously on magnetic tape at a rate of 7–12 samples/s after digitization using a laboratory minicomputer (15). Data obtained from the strip chart and computer were compared from time to time and were never found to differ significantly. Pressure-flow and pressure-volume hysteresis of the perfusion system itself was checked by replacing the lungs by a short piece of Tygon tubing and was found to be negligible.

Animal preparation. Experiments were performed using 18 New Zealand white rabbits of either sex weighing 2.51 ± 0.20 (SD) kg. They were anesthetized with pentobarbital sodium (Nembutal) by injecting the drug in an ear vein in doses of 12–25 mg over a period of 30–45 min. Total dose was usually about 100 mg. After subcutaneous infiltration with lidocaine along the sternum, a long incision was made from the xiphoid process to the larynx and a cannula was installed in the trachea. The animal was killed by 50–100 mg of pentobarbital, and its chest was opened by splitting the entire length of the sternum. The ribs were tied back, thymus gland and pericardium were removed, and ties were placed around the aorta and the heart at the atrioventricular groove. The perfusion cannulas were inserted and tied into the pulmonary artery and left atrial appendage, and flow was begun at 50 ml/min for 1 min to flush blood from the lungs. The lungs were inflated with 5–10 large breaths to a peak Palv of 25–30 cmH₂O using 2.5% CO₂-16% O₂-81.5% N₂. VL was left fixed by closing the stopcock connected to

the trachea at a point on a deflation limb where Palv was 4–5 cmH₂O, about 60% of total lung capacity. Flow was then turned on to the first flow step of the first hysteresis loop. To remove fluttering, (Fig. 2) slight adjustments of the positions of the cannulas were usually required to produce smooth Ppv traces. Any cycles in which such fluttering occurred and the first few cycles obtained immediately after surgery were not included in the data analysis.

The protocol for measuring hysteresis consisted of making changes in \dot{Q} and recording Ppa and, in some animals, both Ppa and ΔV_{vasc} , while holding Ppv and VL constant (Fig. 2). The pump speed was raised in five successive increments and decreased by the same decrements to produce a flow cycle (Fig. 2). Timing and adjustments were all done by hand; each step change required less than 2 s for completion and the duration of each step was 8–10 s from onset. In preliminary experiments, we determined that increasing the duration of the flow steps to 30 s made no difference in the results. We therefore used short flow steps to keep the experiments short to avoid problems with tissue deterioration. The minimum flow was 50 ml/min and peak flow was 400 ml/min, a near normal cardiac output for rabbits of this size [estimates in the literature range from 89 ml·min⁻¹·kg⁻¹ in pentobarbital-anesthetized rabbits (27) to 220 ml·min⁻¹·kg⁻¹ in awake restrained rabbits (20)]. Series consisting of 5–10 successive flow cycles were done in which the last step for one cycle was the first for the following. After each series, lungs were subjected to the same inflation history as described above; a maximum of 10 series was obtained from any one animal.

Two protocols were followed in two groups of animals for preparing the tissue for the above hysteresis determination. The first protocol involved keeping perfusion, lung volume, and venous pressure constant for a period of at least 2 min before beginning the cycling of flow. This was done to study the effects of flow cycling beginning from a steady state. Flow was 50 ml/min, the minimum value for each flow cycle. Twelve animals in

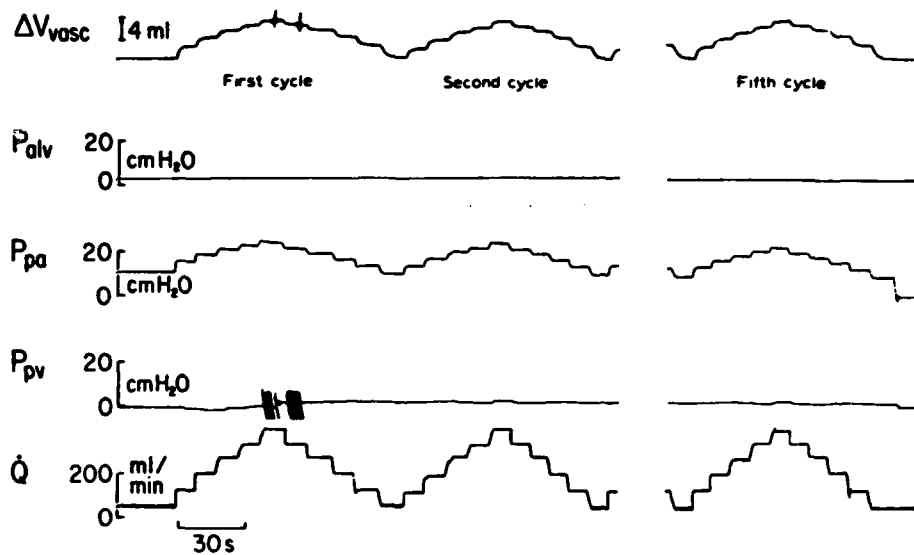


FIG. 2. Sample data from series of 5 flow cycles. With pulmonary venous pressure (P_{pv}) and lung volume fixed, flow (\dot{Q}) was varied between 50 and 400 ml/min in 5 steps while pulmonary arterial pressure (P_{pa}) and changes in vascular volume (ΔV_{vasc}) were measured. An example of P_{pv} fluttering appears in 1st cycle. P_{alv} , alveolar pressure.

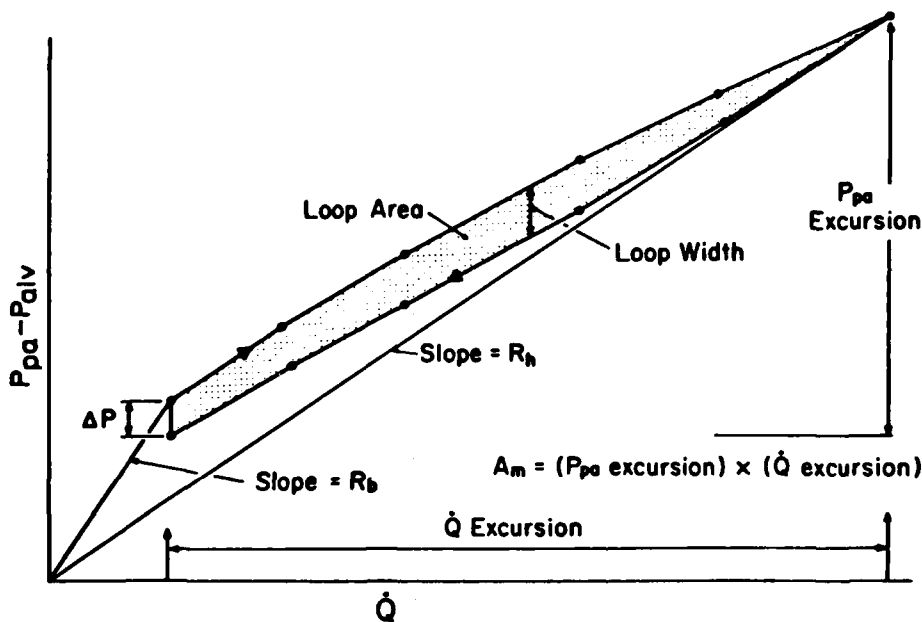


FIG. 3. Schematic representation of pressure-flow hysteresis. Loop is formed by connecting data points (filled circles) obtained at end of each step of flow cycle. See text for abbreviations.

this group were studied at room temperature (21°C), and an additional three were studied at 37°C. In the group studied at room temperature, four were studied before and after addition of papaverine (0.13 mg/ml perfusate, final concentration), and one was studied only after papaverine was added. Hysteresis between P_{pa} and \dot{Q} was analyzed using this protocol. The second protocol was designed to test the effect of varying times allowed to reach a steady state and differed from the first in that flow was turned off completely between series of flow cycles, for time intervals ranging from 30 s to 10 min. Changes in vascular volume (ΔV_{vasc}) were also measured simultaneously with P_{pa} during \dot{Q} cycling. All six of these animals were studied at 37°C with no added vasodilators. At most four different time periods were studied in a given animal, and the order of the periods was randomized.

Data processing. Values for all variables (\dot{Q} , P_{pa} , P_{pv} ,

P_{alv} , and, when measured, ΔV_{vasc}) were measured at the end of each step of a cycle of \dot{Q} . Loops representing hysteresis between P_{pa} and \dot{Q} ($P_{pa}-\dot{Q}$) and, in the second protocol, between P_{pa} and ΔV_{vasc} ($P_{pa}-\Delta V_{vasc}$) were obtained by plotting P_{pa} vs. \dot{Q} and ΔV_{vasc} vs. P_{pa} . Parameters used to describe the loops were (Fig. 3): 1) loop areas (A), 2) maximum area (A_{max}), 3) resistances at the beginning of a cycle of flow (R_b) and at the highest flow level (R_h), 4) the differences in P_{pa} (ΔP) or in the lung fluid volume (ΔV) from the beginning to the end of a cycle, and 5) loop widths parallel to the pressure axis.

A was calculated by computer using the formula

$$A = \frac{1}{2} \sum_{i=2}^n (Y_i + Y_{i-1})(X_i - X_{i-1}) + \frac{1}{2} (Y_1 + Y_n)(X_1 - X_n)$$

where Y_i is either P_{pa} or ΔV_{vasc} , and X_i is \dot{Q} or P_{pa} at the end of the i th step of flow. Each calculated area represented the area bounded by the closed loop, the

beginning point (X_1, Y_1) being connected to the end point (X_n, Y_n) if these did not overlap. The units of area were $\text{cmH}_2\text{O} \cdot \text{ml} \cdot \text{min}^{-1}$ for Ppa- \dot{Q} loops and $\text{ml} \cdot \text{cmH}_2\text{O}$ for Ppa- ΔV_{vasc} loops. Ppa- \dot{Q} area does not represent energy loss over a cycle as in pressure-volume or length-tension studies. Ppa- ΔV_{vasc} areas include some contribution from fluid filtration during a cycle, resulting in slightly open loops, though in lungs with stable fluid balance (closed loops) most of the area represents actual energy loss (see DISCUSSION).

A_{max} was considered to be the area of the bounding rectangle defined by the extremes of a loop. The ratio, A/A_{max} , is equal to the ratio of average loop width to maximum Ppa excursion (Ppa $_{\text{exc}}$ Fig. 2) by the following reasoning. If a loop of total breadth, \dot{Q}_{exc} , is divided into an arbitrarily large number, n , of very thin vertical slices of breadth $\Delta\dot{Q}_i$ and width ΔP_{pa_i} , then the total area of the loop is the sum of the areas of all slices. Since $A_{\text{max}} = \text{Ppa}_{\text{exc}} \cdot \dot{Q}_{\text{exc}}$, then

$$A/A_{\text{max}} = \sum_{i=1}^n \frac{\Delta P_{\text{pa}_i} \cdot \Delta\dot{Q}_i}{\text{Ppa}_{\text{exc}} \cdot \dot{Q}_{\text{exc}}}$$

If all the slices have equal breadths, $\Delta\dot{Q}_i = \dot{Q}_{\text{exc}}/n = \Delta\dot{Q}$, then

$$A/A_{\text{max}} = \sum_{i=1}^n \frac{\Delta P_{\text{pa}_i} \cdot \Delta\dot{Q}}{\text{Ppa}_{\text{exc}} \cdot (n \cdot \Delta\dot{Q})} = \frac{1}{n} \sum_{i=1}^n \frac{\Delta P_{\text{pa}_i}}{\text{Ppa}_{\text{exc}}} = \frac{\overline{\Delta P_{\text{pa}}}}{\text{Ppa}_{\text{exc}}}$$

The ratio A/A_{max} is therefore an indicator of loop "fatness" and was used to compare loops obtained under different perfusion conditions.

Vascular resistances upstream from the vascular waterfall of zone 2 (43) were calculated using the relation $R = (\text{Ppa} - \text{Palv})/\dot{Q}$. All lungs in this study were in zone 2 conditions. The openness of the ends of Ppa- \dot{Q} loops (ΔP , Fig. 3) was measured by taking the difference between the values of Ppa measured at the ends of the first and last flow steps of each cycle. The corresponding parameter (ΔV , Fig. 4) for Ppa- ΔV_{vasc} loops was calculated in a similar way. Positive values were usually obtained for ΔP , i.e., pressure was less at the end of the cycle compared with the beginning, but ΔV was usually negative, volume being larger at the end than at the beginning. Of all the loop parameters the ratio A/A_{max} is probably the best single indicator of hysteresis behavior, since it gives a quantitative estimate of the loop widths expected for a given overall pressure excursion. The other parameters were used to document loop position and shape changes.

Loop widths were measured in a few representative cycles as the vertical distance between ascending and descending limbs at the midflow point. Differences between parameters were tested using either paired or unpaired t tests (as appropriate) and were considered significant wherever $P < 0.05$.

RESULTS

When \dot{Q} was cycled as described, we always encountered hysteresis between Ppa and \dot{Q} and between ΔV_{vasc} and Ppa. A typical chart record for both loop determinations is shown in Fig. 2 and examples of the two types of hysteresis are shown in Fig. 4.

Effects of continuous cycling. Seven complete series of

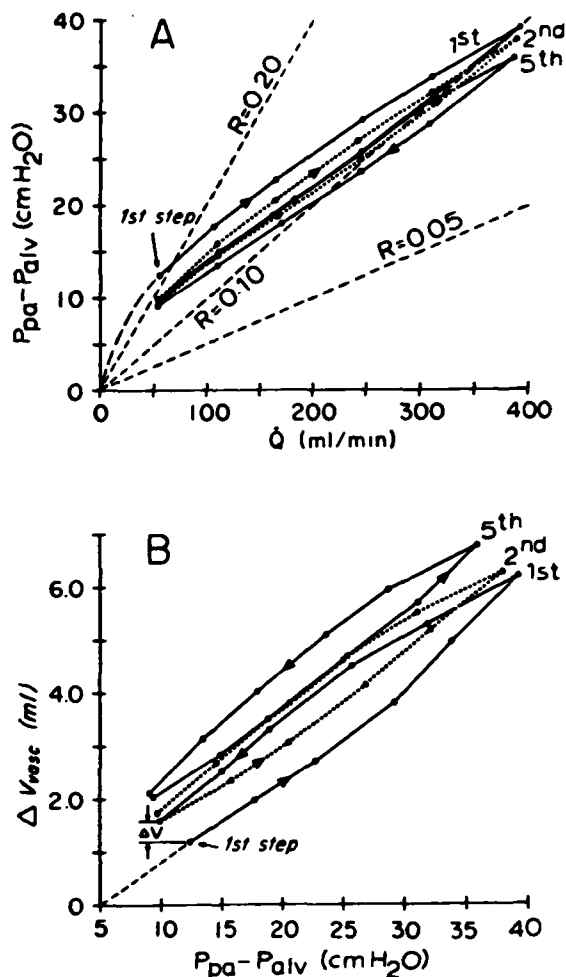


FIG. 4. Examples of 1st, 2nd, and 5th Ppa- \dot{Q} loops (A), and Ppa- ΔV_{vasc} loops (B), in same series of \dot{Q} cycles. Direction is indicated by arrows, and loops from 2nd cycle are indicated by broken line. Straight dashed lines in (A) represent lines of constant vascular resistance (R), and weight gain/cycle, ΔV , is shown for 1st cycle in B. See text for other abbreviations.

Ppa- \dot{Q} loops were obtained in seven lungs using the first protocol. Plots of the changes in loop parameters over five consecutive \dot{Q} cycles are shown in Fig. 5 (x---x). A paired t test was used to test significance of the differences in loop parameters between consecutive cycles. Significant decreases were seen in A , A/A_{max} , R_b , and ΔP between the first and second cycles, but no change occurred in R_n . No statistically significant changes were seen beyond the second cycle, indicating that a "limit cycle" had essentially been reached. In two additional animals, 10 consecutive loops were obtained whose parameters are represented in Fig. 6. It can be seen that again no physiologically significant changes occurred after the second cycle in a series. Therefore, all loops after the third in a series were considered to be limit cycles in runs such as these where flow was maintained between series.

To assess the contribution of smooth muscle tone to the changes occurring with consecutive cycles, seven series were obtained in five experiments in which papaverine was added to the perfusate in high enough concen-

tration to produce a maximal decrease in vascular resistance. As can be seen from Fig. 5 (x...x), the patterns are similar to corresponding prepapaverine data (x---x), indicating that activated smooth muscle is not necessary to produce either hysteresis or changes in hysteresis with continuous cycling. However, both area and resistance were significantly less in each of the five cycles after papaverine, though A/A_{max} and ΔP were not. Maximum pressure width at midflow ranged from 1.8 to 4.0 cmH₂O in first loops of series before papaverine and from 0.7 to 2.0 cmH₂O in limit cycles. After papaverine, widths ranged from 0.9 to 1.9 cmH₂O in first cycles and from 0.7 to 1.0 cmH₂O in limit cycles.

To rule out the possibility that greater tissue viscosity at room temperature caused a hysteresis to develop that was not present at body temperature, four series of loops were obtained at 37-38°C in a separate group of three animals. Hysteresis was still present in all cycles (Fig. 5, Δ --- Δ) and the patterns of change with consecutive cycling were similar to those at room temperature. There were no statistically significant differences in any loop parameters for any cycle compared with the series obtained at room temperature.

Adaptation parameters are likely to be dependent on the protocol followed during a particular adaptation experiment. Our first and second protocols differed in that

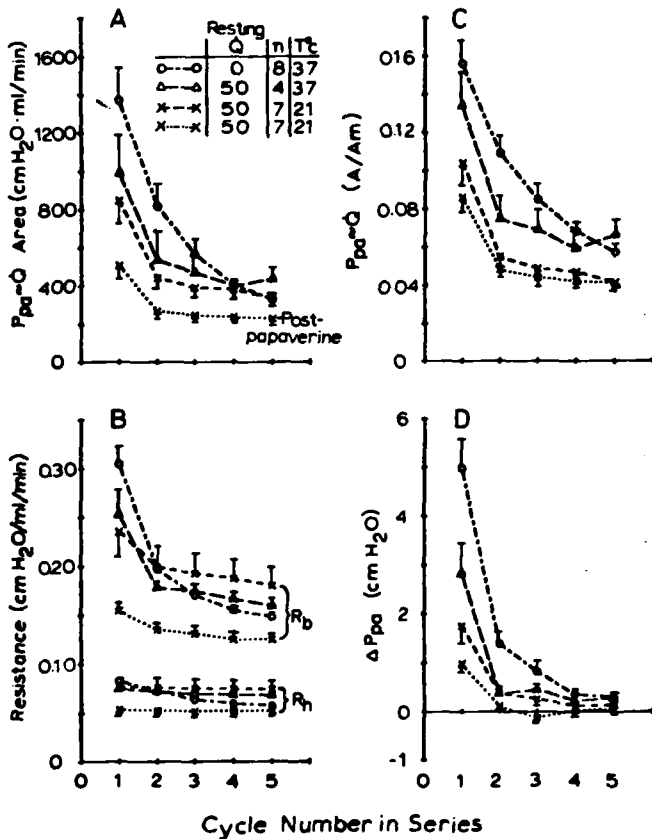


FIG. 5. Changes in loop parameters during continuous Q cycling, (with SE bars) for various conditions of resting Q, temperature, and vasodilation. Resting Q refers to level of flow maintained between series, and n refers to number of series included in average represented by each symbol. See text for abbreviations and explanation of symbols.

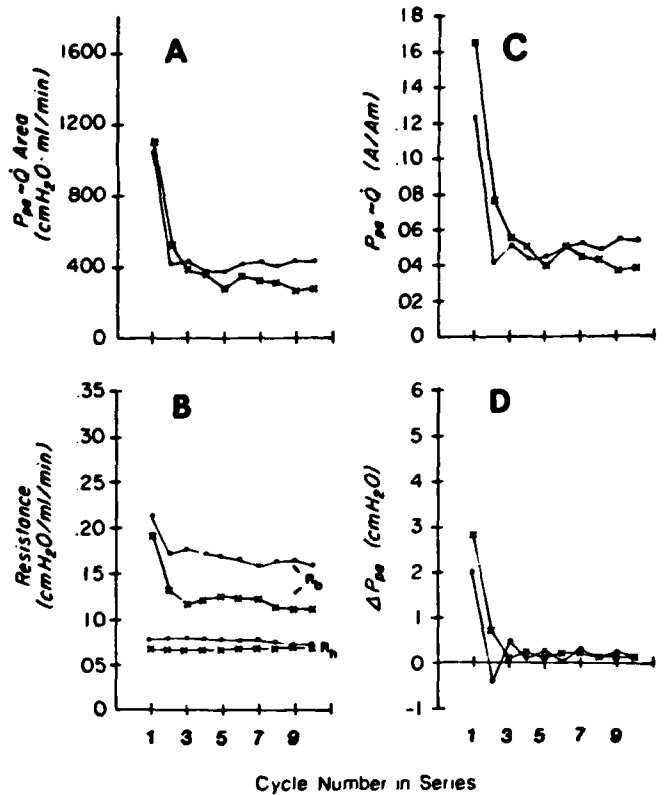


FIG. 6. Parameters obtained from 2 series of 10 cycles from 2 animals (● and x). See text for abbreviations.

flow was maintained between series in *protocol 1*, whereas flow was turned off completely between series using *protocol 2*. To compare these two protocols, the results for the six animals studied using *protocol 2* (see below) from only those series preceded by zero-flow rest times equal to or greater than 2 min are plotted in Fig. 5 (circles). These can be compared with results obtained using *protocol 1* at 37°C, in which the low-flow rest periods between series were also greater than or equal to 2 min (triangles, Fig. 5). When flow was off between series of *protocol 2*, the parameters A, A/A_{max} , R_b , and R_h all continuously decreased even between the fourth and fifth cycles, indicating more cycles would be necessary before a limit cycle could be reached, as compared with data obtained using *protocol 1* at 37°C.

Effects of rest periods with zero Q. Six animals were studied at 37°C to examine the effects of various complete rest periods between successive series (*protocol 2*). The rest period began immediately on completion of the last step of the preceding series. Generally, time at zero Q did not result in an increase in vascular resistance or ΔV measured in the fourth and fifth cycles of series, indicating that neither vasoconstriction nor microvascular injury occurred during the rest periods. We analyzed data only from those series in which vascular resistance in the fourth or fifth cycle was nearly the same (within 10%) as in the same cycles of immediately preceding series.

The differences between loop parameters from the first and fifth cycles were plotted against the time spent at

zero flow immediately preceding the series (Fig. 7). Although hysteresis decreased with continuous cycling (Fig. 5), Fig. 7 shows it recovered during rest periods. The process of recovery appears quasi-exponential with a half time on the order of 2 min. The phenomenon does not depend on a change in smooth muscle activity during the rest period, since the analysis was restricted to those series in which vascular resistance in later cycles did not increase.

Ppa- ΔV_{vasc} areas. In experiments performed at 37°C, the reservoir volume signal was used to estimate ΔV_{vasc} at each 8- to 10-s flow step. At the same Ppa, ΔV_{vasc} was always larger on descending flow limbs compared with ascending limbs. This corresponded with larger \dot{Q} on descending limbs consistent with larger vessel diameters or vascular recruitment or both. The areas of Ppa- ΔV_{vasc} loops were clearly related to Ppa- \dot{Q} areas as shown in Fig. 8, where lines connect data points for individual loops in a given series. Both Ppa- ΔV_{vasc} and Ppa- \dot{Q} areas decrease progressively with continuous flow cycling until limit cycles are reached. Included in Fig. 8 are seven series from lungs that gained large amounts of edema fluid in each cycle. The dashed lines indicate those series in which ΔV of the fourth and fifth cycles showed an overall reservoir volume change/cycle of greater than 0.3 ml, whereas the solid lines connect cycles in series in which fluid gain of limit cycles was less than 0.3 ml [mean $0.12 \text{ ml} \pm 0.074 \text{ (SD), } n = 21$]. In two series the Ppa- \dot{Q} areas of the first loops were considerably less than expected from the Ppa- ΔV_{vasc} areas (circles, Fig. 8). The cycles from which these areas were calculated were technically sound, but both were first loops following a 10 min period of zero flow. However, two other series following 10 min of zero flow (squares, Fig. 8)

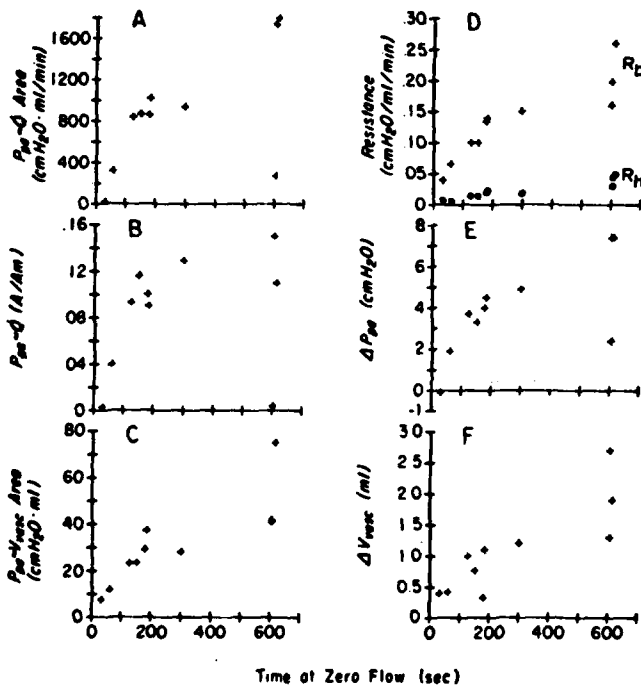


FIG. 7. Differences between loop parameters of 1st and 5th cycles in series plotted as function of length of rest period (time at zero flow). See text for abbreviations.

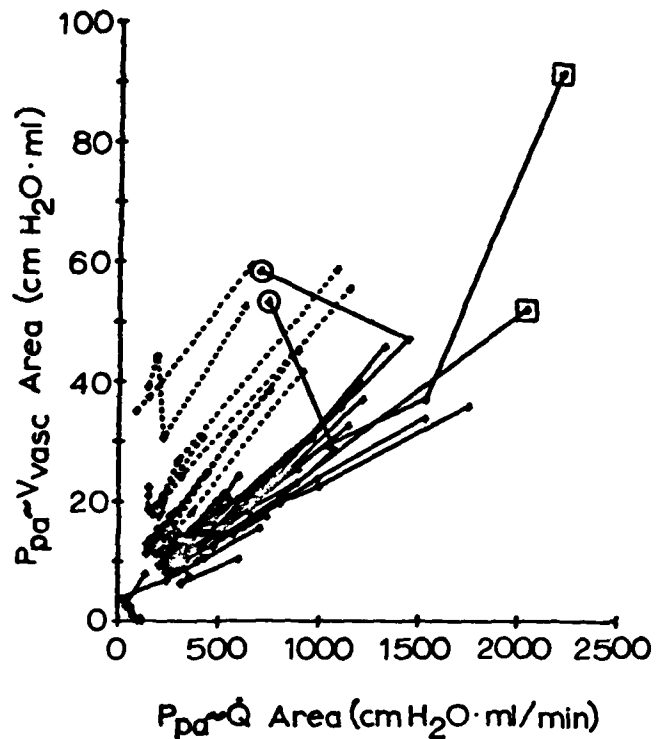


FIG. 8. Areas of simultaneously measured Ppa- \dot{Q} and Ppa- ΔV_{vasc} loops are compared in all series obtained at 37°C. Data from consecutive cycles of same series are connected. Dashed lines indicate those series in which edema formation (ΔV) was more rapid (see text). Highlighted data points are discussed in text.

follow the pattern that was most often seen. Most of the lines when extrapolated to the vertical axis have positive intercepts, suggesting the existence of a contribution to Ppa- ΔV_{vasc} area from fluid filtration. The mean of the extrapolated intercepts of the solid lines in Fig. 8 was only $2.6 \pm 3.5 \text{ (SD, } n = 21) \text{ cm H}_2\text{O}\cdot\text{ml}$ though this is significantly different from zero.

DISCUSSION

The animal model used here was similar to the perfused rabbit lung preparation developed by Nicolaysen (21). The use of horse plasma eliminates the non-Newtonian viscous behavior of whole blood and has been shown to be nearly as effective as rabbit plasma or whole blood in delaying the onset of edema in perfused rabbit lungs (21). There was an increased susceptibility of the lungs to edema at 37°C, in agreement with Nicolaysen (21). Papaverine relaxed the vascular smooth muscle of our isolated lungs, though the amount of relaxation was highly variable among preparations mostly due to the large variation in initial prepapaverine vascular resistances. Though most lungs required less than 40 cmH₂O perfusion pressure at a \dot{Q} of 400 ml/min, in some the resistance before papaverine was so high that initial pressures of up to 90 cmH₂O were required in zone 2 conditions to perfuse at 400 ml/min. Nevertheless, fluid filtration at this Ppa remained low, suggesting that the constriction was precapillary. After papaverine, Ppa at 400 ml/min was always less than 30 cmH₂O and often

less than 20 cmH₂O, indicating a near normal vascular resistance. However, if blood had been used to perfuse, vascular resistance would undoubtedly have been somewhat higher than normal at maximum flows. The cause of the initial vasoconstriction was not determined. Once perfusion was begun, vascular resistance was reasonably stable, though in one animal long rest periods at zero \dot{Q} were followed by a large vasoconstriction (data not included).

The relationships between Ppa and \dot{Q} and Ppa and ΔV_{vasc} (Fig. 4) appear nearly linear over the flow range 50–400 ml/min, consistent with several earlier reports (2, 28, 33). The Ppa- \dot{Q} relationship is nonlinear as zero \dot{Q} is approached (Refs. 28 and 33 and curved dashed line, Fig. 4), though we did not study hysteresis in the range of very low flows. The size of the vascular Ppa- ΔV_{vasc} hysteresis in limit cycles is comparable to that seen in other nonconstricted lung tissue (1). The size of the Ppa- \dot{Q} hysteresis clearly correlates with the Ppa- ΔV_{vasc} hysteresis (Fig. 8), but it is difficult to draw firm conclusions about quantitative relationships, at a given Ppa, between the degrees of overall volumetric and flow irreversibilities. The latter could arise from small diameter changes occurring mainly in the major resistance vessels, whereas volume hysteresis could receive a large component from low-resistance segments.

Effects of continuous cycling. Hysteresis in Ppa- \dot{Q} loops was dependent on cycle number in a series, a dependence that was seen both before and after treatment with papaverine and especially in those studies preceded by rest periods in which flow was turned off (Fig. 5). In all series there were no significant changes in R_h in consecutive cycles, though all other parameters decreased, mostly between the first and second cycle (Fig. 5). Thus most of the tissue changes occur on the increasing \dot{Q} limb of the first cycle, with smaller additional loop narrowing developing in later cycles. These features are not in general unlike the pressure-volume hysteresis of whole lungs or length-tension hysteresis of other tissues. Since hysteresis was also present (and dependent on cycle number) after papaverine it may be concluded that smooth muscle activity is not a prerequisite for hysteresis, in agreement with studies on soft tissues that have little or no smooth muscle (8, 11, 32).

These properties of Ppa- \dot{Q} hysteresis have parallels in the mechanics of vessel walls. The diminution of hysteresis area during cycling is a notable feature of soft tissue mechanics whether the tissue is from blood vessels (11, 23, 30) or other tissue (8, 14, 26, 32). Length-tension hysteresis loops are wide in the first stretch-release cycle, becoming narrower in subsequent cycles. A limit cycle is usually reached after two to three cycles (8, 11) though as many as a dozen or more may sometimes be needed (22). If the specimen is allowed to rest for varying lengths of time, the wide first-loop area recovers, decaying again in subsequent cycles (11, 23, 26). Smooth muscle activity increases the viscous behavior of tissue, increasing both hysteresis loop areas (11, 26) and stress relaxation (29). Conversely, we found the absolute Ppa- \dot{Q} hysteresis area to be diminished by papaverine, although A/A_{max} was not significantly altered (Fig. 5). Both extremes of the LT loops of strips of isolated vessel drift to lower tensions

at a given length during repeated cycling (8, 11). However, the vascular resistances measured at the extremes of Ppa- \dot{Q} loops decreased significantly only at the low-flow end (Fig. 5). This observation is surprising, since one would expect vascular wall creep to be longer at higher intravascular pressures (and therefore wall tension), if creep is approximately proportional to stress, as has been suggested by Fung (8). However, the observation could be explained if flow resistance is determined by an inverse power function of radius, such as in the Poiseuille equation or Fung's sheet flow model in capillaries (9). For a given change in radius, the change in resistance would be inversely related to the starting radius. Thus, even if vascular wall creep was larger at the high-flow ends of loops, changes in resistance could be less than changes seen at low-flow ends, where radii are much smaller.

Effects of rest periods with zero \dot{Q} . In series preceded by periods during which \dot{Q} was turned off, limit cycles were not attained within five cycles. The lower intravascular pressures and vessel wall stresses present during a period of no flow (zone 1 conditions) compared with rest periods of constant low flow (zone 2 conditions) favor stress recovery and more extensive derecruitment of vessels. Thus, during the first few cycles after a period at no flow, both vessel wall stress adaptation and vessel recruitment should be larger than following periods of maintained flow, which could explain the more marked decay of most loop parameters. From these data it is not possible to separate the relative contributions of recruitment versus viscoelasticity to the pressure adaptation. The magnitude of the pressure-flow hysteresis obtained in the first cycle following 3–10 min of no flow was similar to that found in the first cycles obtained after surgery (data not shown).

The recovery of vascular Ppa- \dot{Q} hysteresis with time spent at zero \dot{Q} is consistent with the findings of Barer and Nusser (3), who observed an increase in pulmonary vascular resistance in intact cats following periods of low vascular pressure. The recovery is also consistent with the properties of isolated vessels or vessel wall strips (11, 23) and other soft tissues (26, 41). When flow is turned on following a rest, the pressure history of the vessels then includes also the series that preceded that rest. No rest is equivalent to continuous limit cycling (Fig. 6), whereas increased rest times provide longer periods during which the vessel walls are less strained, allowing stress recovery toward the initial state, erasing recent "memory". The recovery process, whatever it is, may not be completed even after 10 min of rest (Fig. 7). This is consistent with the findings of Goto and Kimoto (11), who found incomplete recovery of length-tension hysteresis even after 20 min and with reported stress-relaxation curves of soft tissues, which must include very long time constants for a complete description (8, 12, 19, 34, 35).

Ppa- ΔV_{vasc} areas. Vascular pressure-volume hysteresis was estimated using changes in fluid level of the venous reservoir. These changes included fluid filtration from capillaries as well as vascular volume changes (16). If, however, analysis is restricted to those preparations that gained less than 0.3 ml of fluid over a limit cycle then a striking parallel exists between vascular Ppa- ΔV_{vasc} and Ppa- \dot{Q} loops, even in prelimit cycles (Fig. 8).

Vascular pressure-volume hysteresis was documented by Sarnoff and Berglund (25), who used an isolated perfused dog lung preparation in which vascular pressure-volume loops were determined during perfusion. They felt that most of the hysteresis was due to stress relaxation of vessel walls, though some could also have been attributed to fluid fluxes from capillaries. In addition, Frank et al. (7) and Smith and Mitzner (31) measured vascular pressure-volume curves in air-filled vessels of excised dog lungs, eliminating the fluid filtration component of the volume changes but adding an unknown component from movable menisci. Both groups found significant pressure-volume hysteresis, and Smith and Mitzner (31) noted that the hysteresis reached a limit cycle after about three cycles. This is consistent with our finding of vascular pressure-volume hysteresis, and with our finding that pressure-flow and pressure-volume hysteresis loops become nearly constant after the first few cycles. On the other hand, Rosenzweig et al. (24), using a fluid-filled vasculature where vascular volume changes were measured from changes in lung weight, reported no significant vascular pressure-volume hysteresis. Maseri et al. (18) were also unable to find significant pressure-volume hysteresis in the pulmonary vascular bed of dogs, using an indicator-dilution technique to measure vascular volume changes. Likewise Caro and Saffman (4) were unable to document pressure-diameter hysteresis of intact intraparenchymal vessels using X rays to measure vessel size. It is possible that the methods used in the latter three studies were not sufficiently sensitive to detect the relatively small pressure-volume hysteresis that does occur.

Although lung pressure-flow or pressure-volume hysteresis have previously been documented, quantitative descriptions of the adaptation process, particularly in the same preparation have been lacking. We found that lung vascular resistance and volume can depend markedly on previous pressure-flow history and that hysteresis effects should therefore be borne in mind in studies documenting changes in vascular resistance or volume. As in lung inflation studies, it would be inadvisable to rely on the first increase in flow to measure vascular pressure-flow or pressure-volume relations in isolated lungs or, presumably, intact animals. However, preconditioning by varying flow at least once between expected maximum and minimum levels renders pressure-flow hysteresis relatively unimportant. The loop parameter, A/A_{\max} , de-

creased from initial highs of between 0.08 and 0.16 to about 0.05 in limit cycles, indicating that final ("conditioned") average loop widths are about 5% of the maximal pressure excursion. We further found that the protocol used prior to obtaining limit cycles can importantly influence the time necessary to attain reproducible loops.

The hysteresis we documented is consistent with the viscoelastic properties of smooth muscle, though vascular wall creep may not be the only mechanism responsible for the hysteresis. If, for instance, the capillaries that are recruited as vascular pressures are raised in isolated lungs (10) do not close at the same pressures as they open, recruitment hysteresis could contribute to overall pressure-flow hysteresis. In addition, the support that larger blood vessels receive from surrounding lung parenchyma may also contribute to vascular pressure-diameter irreversibility. Edema fluid accumulation around large vessels could, potentially, be a factor, though its effect was not evident in these experiments. Vascular hysteresis was still present and not noticeably different in lungs that were rapidly gaining edema fluid. In spite of this, we did not analyze data, except as indicated in Fig. 8, from grossly edematous preparations.

Though we have documented that hysteresis may be important, particularly in a lung that has not been preconditioned, we did not investigate many interventions that could have an effect on vascular hysteresis. Factors such as changes in pulmonary venous pressure, lung volume, increased lung tissue recoil, edema, use of different protocols for studying pressure-flow or pressure-volume relationships, or maximally contracted arterial smooth muscle may affect hysteresis in both unconditioned and conditioned lungs.

The assistance and advice of Harold Modell and John Butler are gratefully acknowledged. We are indebted also to the Florence Packing Co. of Stanwood, WA for making horse blood available. Support was obtained from the University of Washington graduate school research fund, National Heart, Lung, and Blood Institute Program Project Grant HL-24163, Air Force Grant AFOSR F49620-78-C-0058 and a predoctoral training grant from Virginia Mason Research Center.

This work is based in part on a doctoral dissertation submitted by K. Beck to the University of Washington.

Address reprint requests to K. C. Beck, S-3 Plummer Bldg., Mayo Clinic, Rochester, MN 55905.

Received 26 July 1982; accepted in final form 27 September 1982.

REFERENCES

1. BACHOFEN, H., AND J. HILDEBRANDT. Area analysis of pressure-volume hysteresis in mammalian lungs. *J. Appl. Physiol.* 30: 493-497, 1971.
2. BANISTER, J., AND R. W. TORRANCE. The effects of tracheal pressure upon flow: pressure relations in the vascular bed of isolated lungs. *Q. J. Exp. Physiol.* 45: 352-367, 1960.
3. BARER, G. R., AND E. NUSSE. Pulmonary blood flow in the cat. The effect of positive pressure respiration. *J. Physiol. London* 138: 103-118, 1957.
4. CARO, C. G., AND P. G. SAFFMAN. Extensibility of blood vessels in isolated rabbit lungs. *J. Physiol. London* 178: 193-210, 1965.
5. CULVER, B. H., AND J. BUTLER. Mechanical influences on the pulmonary microcirculation. *Annu. Rev. Physiol.* 42: 187-198, 1980.
6. DALY, M. DEB., AND P. G. WRIGHT. The effects of anticholinesterases upon pulmonary vascular resistance in the dog. *J. Physiol. London* 139: 273-293, 1957.
7. FRANK, N. R., E. P. RADFORD, JR., AND J. L. WHITTENBERGER. Static volume-pressure interrelations of the lungs and pulmonary vessels in excised cats' lungs. *J. Appl. Physiol.* 14: 167-173, 1959.
8. FUNG, Y. C. B. Stress-strain-history relations of soft tissues in simple elongation. In: *Biomechanics, Its Foundations and Objectives*, edited by Y. C. B. Fung. Englewood Cliffs, NJ: Prentice-Hall, 1972, p. 181-208.
9. FUNG, Y. C., AND S. S. SOBIN. Theory of sheet flow in lung alveoli. *J. Appl. Physiol.* 26: 472-488, 1969.
10. GLAZIER, J. B., J. M. B. HUGHES, J. E. MALONEY, AND J. B. WEST. Measurements of capillary dimensions and blood volume in rapidly frozen lungs. *J. Appl. Physiol.* 26: 65-76, 1969.
11. GOTO, M., AND Y. KIMOTO. Hysteresis and stress relaxation of the blood vessels studied by a universal tensile testing instrument. *Jpn. J. Physiol.* 15: 169-184, 1966.
12. HILDEBRANDT, J. Pressure-volume data of cat lung interpreted by

- a plastoelastic, linear viscoelastic model. *J. Appl. Physiol.* 28: 365-372, 1970.
13. HILDEBRANDT, J. Lung. Surfactant mechanics: some unresolved problems. In: *Regulation of Ventilation and Gas Exchange*, edited by J. B. West. New York: Academic, 1978, p. 261-297.
 14. HILL, A. V. The viscous elastic properties of smooth muscle. *Proc. R. Soc. London Ser. B* 100: 108-115, 1926.
 15. KEHL, T. H., C. MOSS, AND L. DUNKEL. LM²—a logic machine mini-computer. *Computer* November, p. 12-22, 1975.
 16. LUNDE, P. K. M., AND B. A. WAALER. Transvascular fluid balance in the lung. *J. Physiol. London* 205: 1-18, 1978.
 17. MALONEY, J. E., D. H. BERGEL, J. B. GLAZIER, J. M. B. HUGHES, AND J. B. WEST. Transmission of pulsatile pressure and flow through the isolated lung. *Circ. Res.* 23:11-24, 1968.
 18. MASERI, A., P. CALDINI, P. HARWARD, R. C. JOSHI, S. PERMUTT, AND K. L. ZIERLER. Determinants of pulmonary vascular volume. *Circ. Res.* 31: 218-228, 1972.
 19. MIKAMI, T., AND E. O. ATTINGER. Stress relaxation of blood vessel walls. *Angiologica* 5: 281-292, 1968.
 20. NEUTZE, J. M., F. WYLER, AND A. M. RUDOLPH. Changes in the distribution of cardiac output after hemorrhage in rabbits. *Am. J. Physiol.* 215: 856-864, 1968.
 21. NICOLAYSEN, G. Perfusate qualities and spontaneous edema formation in an isolated perfused lung preparation. *Acta Physiol. Scand.* 83: 563-570, 1971.
 22. REMINGTON, J. W. Hysteresis loop behavior of the aorta and other extensible tissues. *Am. J. Physiol.* 180: 83-95, 1955.
 23. REMINGTON, J. W. Extensibility behavior and hysteresis phenomena in smooth muscle tissue. In: *Tissue Elasticity*, edited by J. W. Remington. Washington, DC: Am. Physiol. Soc., 1957, p. 138-153.
 24. ROSENZWEIG, D. Y., J. M. B. HUGHES, AND J. B. GLAZIER. Effects of transpulmonary and vascular pressures on pulmonary blood volume in isolated lungs. *J. Appl. Physiol.* 28: 553-560, 1970.
 25. SARNOFF, S. J., AND E. BERGLUND. Pressure-volume characteristics and stress relaxation in pulmonary vascular bed of the dog. *Am. J. Physiol.* 171: 238-244, 1952.
 26. SASAKI, H., AND F. G. HOPPIN, JR. Hysteresis of contracted airway smooth muscle. *J. Appl. Physiol.: Respirat. Environ. Exercise Physiol.* 47: 1251-1262, 1979.
 27. SEARS, M. R., AND H. K. FISHER. Natural human fibrinopeptides: failure to affect respiration and circulation in rabbits and monkeys. *Am. Rev. Respir. Dis.* 110: 616-622, 1974.
 28. SHOUKAS, A. A. Pressure-flow and pressure-volume relations in the entire pulmonary vascular bed of the dog determined by two-part analysis. *Circ. Res.* 37: 809-818, 1975.
 29. SIEGMAN, M. J., T. M. BUTLER, S. U. MOERS, AND R. E. DAVIES. Calcium-dependent resistance to stretch and stress relaxation in resting smooth muscles. *Am. J. Physiol.* 231: 1501-1508, 1976.
 30. SIPKEMA, P. Low-frequency viscoelastic properties of canine femoral arteries in vivo. *Am. J. Physiol.* 236 (*Heart Circ. Physiol.* 5): H720-H724, 1979.
 31. SMITH, J. C., AND W. MITZNER. Analysis of pulmonary vascular interdependence in excised dog lobes. *J. Appl. Physiol.: Respirat. Environ. Exercise Physiol.* 48: 450-467, 1980.
 32. SUGIHARA, T., J. HILDEBRANDT, AND C. J. MARTIN. Viscoelastic properties of alveolar wall. *J. Appl. Physiol.* 33: 93-98, 1972.
 33. WEST, J. B., AND C. T. DOLLERY. Distribution of blood flow and the pressure-flow relations of the whole lung. *J. Appl. Physiol.* 20: 175-183, 1965.
 34. WESTERHOF, N., AND A. NOORDERGRAAF. Arterial viscoelasticity: a generalized model. *J. Biomech.* 3: 357-379, 1970.
 35. ZATZMAN, M., R. W. STACY, J. RANDALL, AND A. EBERSTEIN. Time course of stress relaxation in isolated arterial segments. *Am. J. Physiol.* 177: 299-302, 1954.

SECTION VII

INFLUENCE OF ALVEOLAR MECHANICS ON THE LUNG VASCULATURE

H.I. Modell and J. Hildebrandt

A common pressure-flow model of the pulmonary vascular bed is that of a collection of Starling resistors arranged in parallel (3,20,22). Under "zone 2" conditions, the driving pressure for flow is considered to be the difference between pulmonary arterial and alveolar pressures. In "zone 3", the driving pressure is the difference between pulmonary arterial and venous pressure. A key assumption in this analysis is that alveolar pressure represents the effective pressure to which the alveolar vessel bed is exposed. However, some data suggest that this is not the case (5,12,13,18). Alveolar surface forces may, in fact, influence the degree to which alveolar pressure is transmitted to these vessels. It is reasonable to assume that the pulmonary vasculature is also subject to mechanical forces within the interstitium and alveolar walls (10,11,14,19). Hence, the pressure-flow characteristics of this bed should be related to stresses associated with mechanics of both the interstitium and alveolar wall.

The sum total of forces acting on alveolar walls reflects the interaction between forces within the wall's structural framework and forces generated by the presence of an air-liquid (surfactant) interface. This interaction is reflected in the pressure-volume (P-V) curve of the lung. The volume achieved by application of a pressure across the lung depends upon volume history, and the observed hysteresis depends mainly on surface phenomena. The surface and the tissue exhibit stress-adaptation (9), so that these forces change when lung volume is static. Thus, to gain an accurate indication of how pressure-flow

characteristics of the alveolar vessel bed are influenced by in vivo, it is necessary to determine these relationships during dynamic lung volume changes using blood flows that reflect in vivo rates. To date, most studies focusing on these issues have not provided these conditions (5,12,15,16,18,21,23).

Studies purporting to examine the role of interfacial surface tension in determining pressure-flow relationships filled the lungs with fluid (saline, 6% dextran in saline, or plasma) to eliminate the air-liquid interface (5,21). These fluids, however, are capable of moving across the alveolar epithelium and causing interstitial edema. Hence, the results of these studies may, in fact, reflect the influence of combined alveolar flooding and interstitial edema. Experiments separating these two factors have not been reported. Ventilating perfused lungs whose surface tension properties have been altered without fluid filling (1,4) or by filling with fluid that does not cross alveolar epithelium (2,8) should provide a means of separating the surface force effects from alveolar structure effects. Such information would contribute greatly to our understanding of pulmonary hemodynamics during a variety of environmental stresses, including acceleration stress, which alter mechanical forces on alveolar walls. We have recently begun studies aimed at elucidating these relationships using isolated, perfused cat lungs.

Cats have been chosen as the primary experimental animal for these studies on the basis of cost and lung size. The general techniques involved in perfusing isolated cat lungs are well established (6,7,17). It was necessary, however, to establish a data acquisition system and computer analysis techniques with which to obtain and analyze data from

the proposed experiments. Preliminary studies have been conducted to ascertain whether our data acquisition and analysis schemes are feasible for examining alveolar wall-capillary wall mechanical interactions.

Methods

Cats weighing approximately 3 Kg were anesthetized with ketamine and pentobarbital sodium. A tracheostomy was performed, an external jugular vein was cannulated for administration of supplemental anesthesia, and a catheter was placed in the carotid artery. A thoracotomy was performed, and ties placed around the pulmonary artery and aortic arch. The animal was then heparinized and sacrificed (exsanguination), the aorta was tied, and the heart and lungs were removed. The lungs were connected to the perfusion system by cannulae placed in the pulmonary artery and left atrial appendage, and a tie was placed around the A-V groove to prevent leakage from the left atrium into the left ventricle.

The perfusion and monitoring system are shown schematically in Figure 1. The system allows for monitoring of pressures at the tips of the pulmonary artery and pulmonary vein and pressure at the airway. Provision is also made for monitoring the volume of perfusate in the venous reservoir, the perfusion flow, the volume change in the plexiglass box, and the temperature change in the plexiglass box. All pertinent signals are recorded on a strip chart recorder and on an FM analog tape recorder.

After all cannulae were in place, the lung was placed in the plexiglass box-spirometer system and inflated to 30 cm H₂O transpulmonary pressure to determine an upper limit for added volume. The lungs were allowed to deflate to 5 cm H₂O and ventilated at a rate

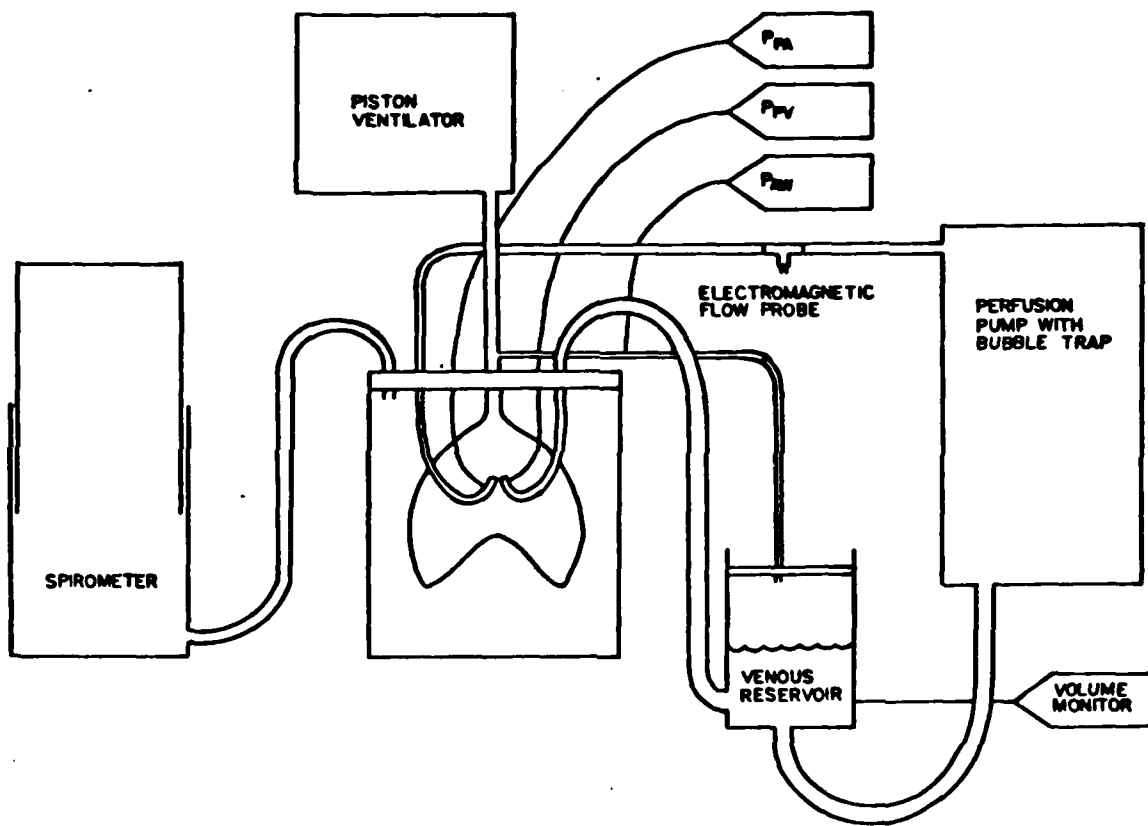


FIGURE 1. Schematic representation of the perfusion and monitoring system. The lungs are placed in a lucite box. Volume changes in the box are monitored with a spirometer. The lungs are ventilated with a closed system, piston ventilator. A venous reservoir serves as a perfusate source for the pump system. This reservoir may be constantly exposed to airway pressure to keep the relationship between alveolar and pulmonary venous pressures constant. Pulmonary artery, pulmonary vein and airway pressure are monitored continuously along with the volume in the perfusion reservoir.

of 5 breaths/min with a tidal volume of 50 ml using a closed system. Perfusion was then instituted using a constant flow at the first of three test levels. Five percent dextran in lactated ringers solution or a mixture of the animal's blood and ringers (1:6) was used as the perfusate. A vasodilator (Papavarine) was added to the perfusate to eliminate active vascular tone. Vascular pressures were referenced to the level of the left atrium. To ensure zone 2 conditions, pulmonary venous pressure was set below the lung. After steady state conditions were achieved, monitored pressures and volumes were recorded on the FM analog recorder for a 5 consecutive breath run. The lung-ventilator volume was then increased by 50 ml, thereby increasing end-expiratory volume, and the process was repeated. This procedure was repeated until end-inspiration occurred near Total lung capacity after which end-expiratory volume was decreased in steps of 50 ml. By altering end-expiratory volume in steps to a volume near Total lung capacity, data were obtained at normal tidal volume excursions along the inflation and deflation limbs of the lung pressure-volume (P-V) curve. Upon completion of the P-V curve at the first test flow, the experiment was repeated using one or two more flows. The order of testing flows were randomized among experiments.

An example of the raw data tracing from one run is shown in Figure 2. These data were digitized at a rate of 5 samples/sec from the FM analog recordings and analyzed using an Apple][+ computer system. For the purposes of the pilot studies, two or more consecutive tidal volume cycles from each 5 breath run were chosen for analysis, and respective points in the cycle were averaged to yield a mean cycle for each experimental run. The mean cycle was then divided into ten equidistant

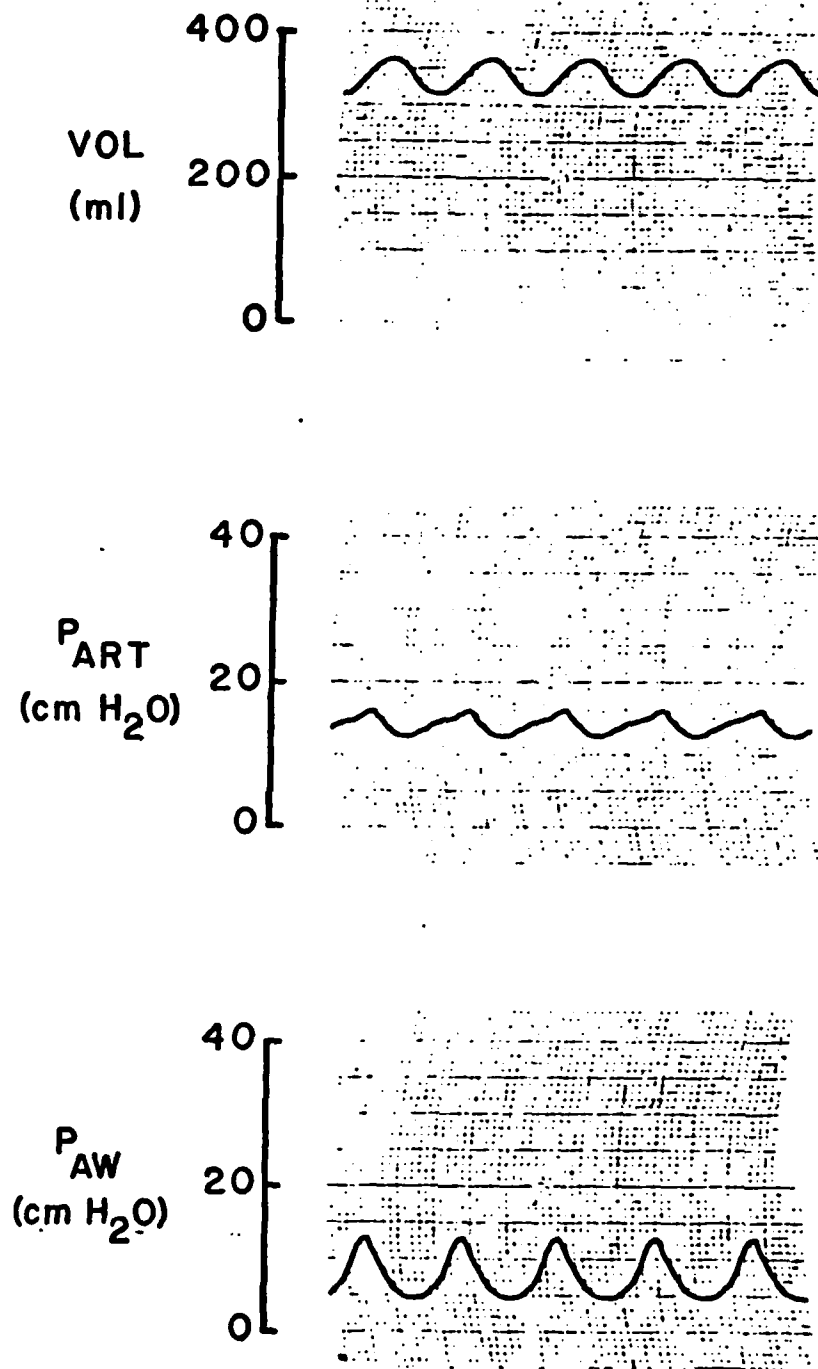


FIGURE 2. Raw data as recorded on a strip chart recorder for one experimental run. Top trace is volume change in the lucite box, middle channel is pulmonary arterial pressure, and the lower trace is airway pressure.

points, and calculations were made using these points for each parameter measured. In actual experiments, all 5 cycles/run will be used, and the cycle will be divided into 25 equidistant points. The data were then plotted to yield lung P-V relationships and indicators of perfusion pressure-flow relationships. Perfusion driving pressure (arterial pressure - alveolar pressure) as a function of lung volume and perfusion driving pressure as a function of transpulmonary pressure were plotted for each flow condition.

The analysis is illustrated in Figure 3 which shows a P-V curve for an air-filled lung. The characteristics of this curve reflect elastic forces generated in lung tissue and forces generated as a result of the air-liquid interface (21). By using the hysteresis properties of the air-filled lung P-V curve, we can obtain information regarding the influence of the air-liquid interface on the vasculature. It may be assumed that tissue forces are nearly the same at points taken at the same volume on the inflation and deflation limbs of the P-V curve (e.g. points A and B of Fig. 3). Hence, transpulmonary pressure difference between inflation and deflation limbs reflect forces acting at the air-liquid interface. By examining families of such points (i.e., same volume, different transpulmonary pressures) obtained from multiple runs, the pressure-flow characteristics of the bed can be related to influence of interfacial forces reflected as transpulmonary pressure. Under constant flow conditions, this relationship becomes a plot of perfusion driving pressure expressed as a function of transpulmonary pressure.

Representative plots of the P-V relationships and perfusion pressure expressed as a function of transpulmonary pressure from one set of lungs are shown in Figures 4 and 5. Pressure-volume curves obtained

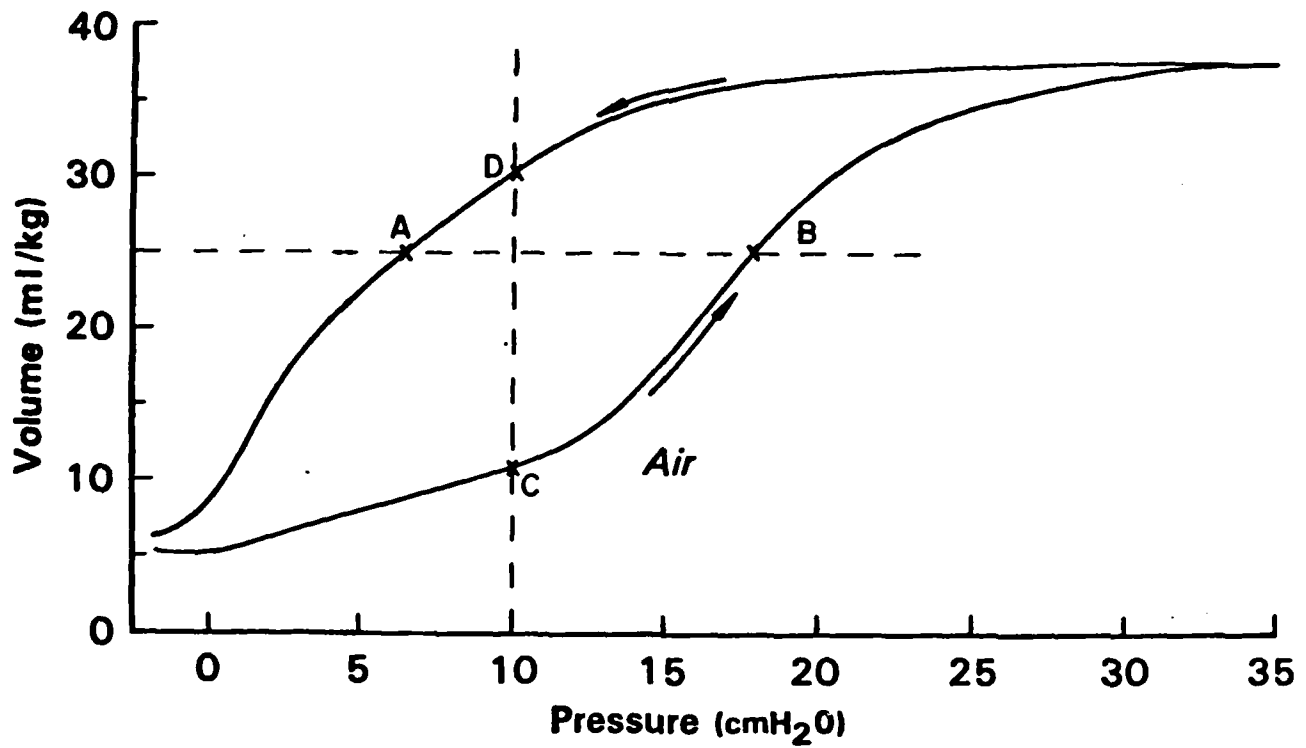


FIGURE 3. Standard pressure-volume curve of an air-filled lung. A and B represent isovolume points. C and D represent isopressure points (see text).

are presented in Figure 4. Loops indicate mean tidal volume excursions on the inflation and deflation limbs of the overall lung P-V curve. These curves are consistent with curves presented by Hoppin and Hildebrandt (9) for non-perfused cat lungs undergoing similar maneuvers.

Figure 5 shows perfusion driving pressure expressed as a function of transpulmonary pressure for a flow of 50 ml/min (low flow). Families of isovolume points were taken from the curves in Figure 4 to obtain this plot. It is evident from this plot that interfacial forces have a marked influence on the pulmonary microvasculature under these conditions. In fact, a linear regression performed on these data yields a line having a correlation coefficient of 0.89. These data are consistent with those of Pain and West (18) who found lower vascular resistance during inflation limbs than during deflation limbs of isolated dog lungs.

Thus far, the analysis has dealt with examining points having the same lung volume but different transpulmonary pressures. If families of points having the same transpulmonary pressures but different lung volumes are considered (e.g. points C and D, Fig. 3), additional information may be obtained. Forces acting at these points reflect a contribution from tissue and interfacial surface forces. Hence, by examining the isoflow perfusion pressure versus volume plot at these points, an indication of the interaction of tissue and surface forces on the vasculature may be inferred. Several possibilities exist for this interaction: 1) tissue forces may predominate, 2) tissue and surface forces interact equally, or 3) surface forces predominate. In addition, the tissue forces may work in concert with surface forces, or they may oppose the action of surface forces on the vasculature.

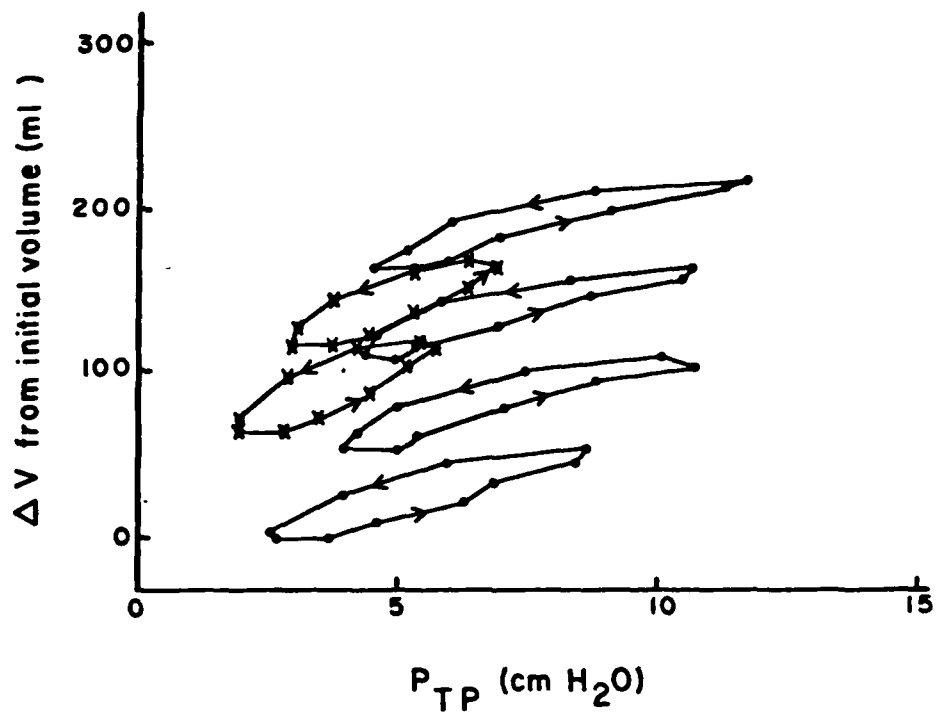


FIGURE 4. Examples of pressure-volume loops of tidal breaths obtained at various points on the inflation limb (●-●) and deflation limb (X-X) of the overall pressure-volume curve.

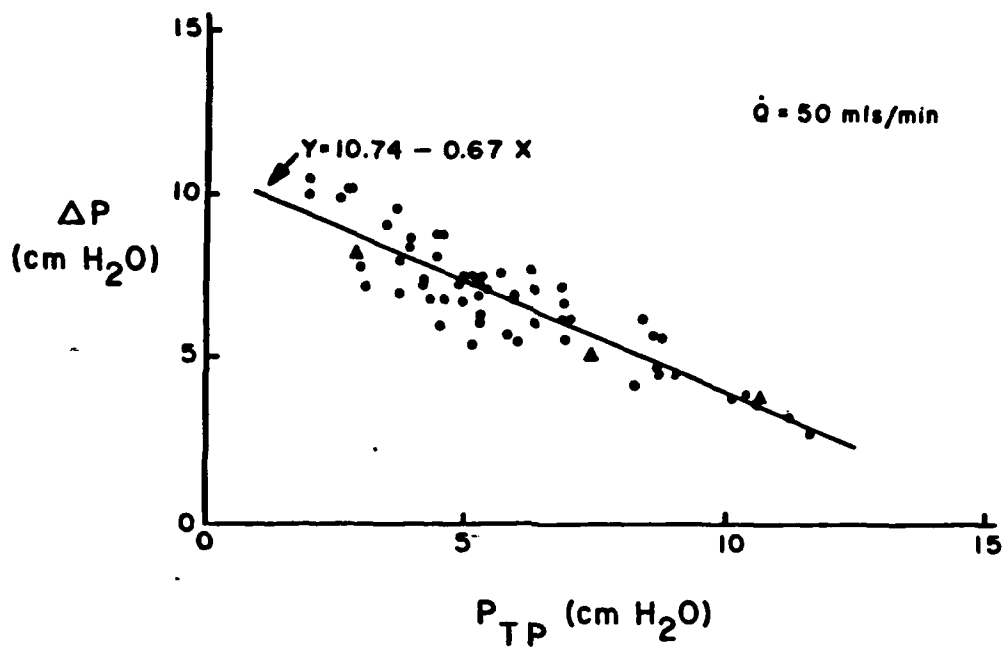


FIGURE 5. Perfusion driving pressure plotted as a function of transpulmonary pressure. The plot represents families of isovolume points. One family of isovolume points is indicated (▲).

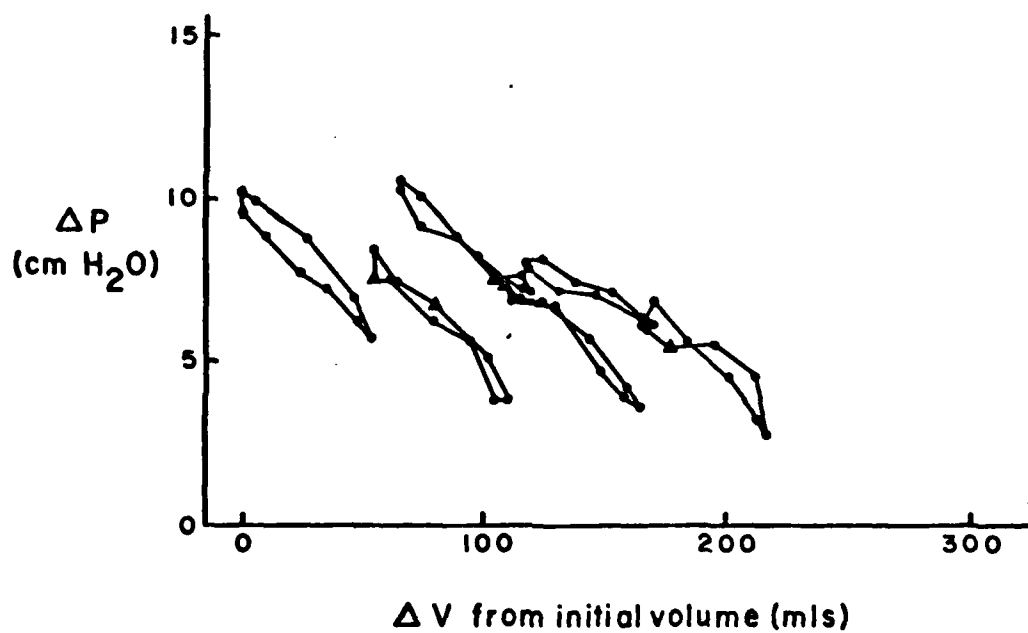


FIGURE 6. Perfusion driving pressure plotted as a function of lung volume. The plot represents families of isopressure points. One family of isopressure points is indicated (▲).

Figure 6 shows perfusion driving pressure expressed as a function of lung volume for the same flow conditions as Figure 5. Tidal volume loops for each run are indicated. In these lungs, and at the low flow of 50 ml/min, there does not appear to be a correlation between driving pressure and lung volume. This suggests that, in these lungs, 1) volume changes at the same transpulmonary pressure reflect alterations in the tissue component, and this component has little effect on the vasculature; or 2) that the surface component is significant, but tissue forces act to oppose the surface effects on the vasculature.

The possible explanations for these data, however, are not as simple as the analysis suggests. Because the intent of these experiments was to establish data acquisition and analysis schemes, experiments were continued even if the test lung became edematous. Data presented in Figures 4, 5 and 6 are from edematous lungs. Under these complex conditions of low flow and edema in portions of the lungs, it is difficult to draw conclusions regarding the contributions of the various forces.

The 50 ml/min flow represents approximately 10% of the in vivo cardiac output for these lungs. Hence, it is likely that only a small portion of the vascular bed was open during these runs. In zone 2 lungs, the driving pressure measured as arterial minus alveolar pressure reflects a pressure drop across two resistances, the extra-alveolar bed on the arterial side and that portion of the alveolar bed upstream to the Starling resistor effect (waterfall). It may very well be that under low flow conditions and in the presence of edema, the primary site of resistance represents extra-alveolar vessels and vessels that course through atelectatic or low compliant (edematous) areas of the lung. If

this is the case, these vessels would be exposed primarily to retractile forces acting on surrounding tissues, but the normal relationships of these tissue forces may have been altered by the presence of edema. Data from Hida and Hildebrandt (8) indicate that the retractile forces acting on vessels would decrease during interstitial edema. If this is the case, one would predict that the increased surface forces at higher transpulmonary pressures would put more tension on lung parenchyma tending to "tether" low resistance vessels. The increased tethering forces would result in larger vessel diameters and decreased resistance. Figures 5 and 6 are consistent with this hypothesis.

The lungs in this experiment represent one point on a spectrum ranging from non-edematous lungs to lungs with complete alveolar flooding and interstitial edema. Data related to both ends of this spectrum are necessary to understand mechanisms within it. The experiments in progress are designed to provide data at the extremes as well as within this spectrum.

Another variable complicating the picture in this experiment is the low perfusion flow rate used. This flow was consistent with other studies in the literature (5) but represents a level well below normal values. At higher flows, more of the vascular bed would be recruited, and the influence of alveolar mechanics on the vasculature would increase. Data related to this "perfusion spectrum" is not available at the present time.

References

1. Albert, R.K., S. Lakshminarayan, J. Hildebrandt, W. Kirk and J. Butler. Increased surface tension favors pulmonary edema formation in anesthetized dogs' lungs. J. Clin. Invest 63: 1015-1018, 1979.
2. Bachofen, H., J. Hildebrandt and M. Bachofen. Pressure-volume curves of air- and liquid-filled excised lungs -- surface tension in situ. J. Appl. Physiol. 29: 422-431, 1970.
3. Banister, J. and R.W. Torrance. The effects of the tracheal pressure upon flow: pressure relations in the vascular bed of isolated lungs. Quart. J. Exptl. Physiol. 45: 352-367, 1960.
4. Berend, N., K.L. Christopher and N.F. Voelkel. Breathing He-O₂ shifts the lung pressure-volume curve of the dog. J. Appl. Physiol.: Respirat. Environ. Exercise Physiol. 54: 576-581, 1983.
5. Bruderman, I., K. Somers, W.K. Hamilton, W.H. Tooley and J. Butler. Effect of surface tension on circulation in the excised lungs of dogs. J. Appl. Physiol. 19: 707-712, 1964.
6. Dawson, C.A., R.L. Jones, and L.H. Hamilton. Hemodynamic responses of isolated cat lungs during forward and retrograde perfusion. J. Appl. Physiol. 35: 95-102.
7. Frank, N.R., E.P. Radford, Jr., and J.L. Whittenberger. Static volume-pressure interrelations of the lungs and pulmonary blood vessels in excised cats' lungs. J. Appl. Physiol. 14: 167-173, 1959.
8. Hida, W. and J. Hildebrandt. Alveolar surface tension, lung inflation and hydration affect interstitial pressure P_x(f). J. Appl. Physiol. (in press)
9. Hoppin, G.G., Jr. and J. Hildebrandt. Mechanical properties of the lung. pp 83-162, IN: Bioengineering Aspects of the Lung Vol. 3, ed. John West, New York: Marcel Dekker, Inc., 1977.
10. Howell, J.B.L., S. Permutt, D.F. Proctor and R.L. Riley. Effect of inflation of the lung on different parts of pulmonary vascular bed. J. Appl. Physiol. 16: 71-76, 1961.
11. Liebow, A.A. Pulmonary emphysema with special reference to vascular changes. Amer. Rev. Resp. Dis. 80: 67-91, 1959.
12. Lloyd, T.C., Jr. and G.W. Wright. Pulmonary vascular resistance and vascular transmural gradient. J. Appl. Physiol 15: 241-245, 1960.

13. Lopez-Muniz, R., N.L. Stephens, B. Bromberger-Barnea, S. Permutt and R.L. Riley. Critical closure of pulmonary vessels analyzed in terms of Starling resistor model. J. Appl. Physiol 24: 625-635, 1968.
14. Macklin, C.C. Evidences of increase in the capacity of the pulmonary arteries and veins of dogs, cats, and rabbits during inflation of the freshly excised lung. Rev. Can. Biol. 5: 199-232, 1946.
15. Maloney, J.E., J. Cannata and B.C. Ritchie. The influence of transpulmonary pressure on the diameter of small arterial blood vessels in the lung. Microvasc. Res. 11: 57-66, 1976.
16. Murray, J.F. Effects of lung inflation on pulmonary arterial pressure in dogs with pulmonary edema. J. Appl. Physiol.: Respirat. Environ. Exercise Physiol. 45: 442-450, 1978.
17. Nisell, O. The influence of blood gases on the pulmonary vessels of the cat. Acta Physiol. Scand. 23: 85-90, 1950.
18. Pain, M.C.F. and J.B. West. Effect of the volume history of the isolated lung on distribution of blood flow. J. Appl. Physiol. 21: 1545-1550, 1966.
19. Permutt, S. Effect of interstitial pressure of the lung on pulmonary circulation. Med. Thorac. 22: 118-131, 1965.
20. Permutt, S., B. Bromberger-Barnea and H.N. Bane. Alveolar pressure, pulmonary venous pressure, and the vascular waterfall. Med. Thorac. 19: 239-260, 1962.
21. Radford, E.P., Jr. Static mechanical properties of mammalian lungs. pp. 429-449, IN: Handbook of Physiology, Sec. 3, Respiration, Vol. 1. ed. W.O. Fenn and H. Rahn, Washington, D.C.: American Physiological Society, 1964.
22. Thomas, L.J., Jr., A. Roos and Z.J. Griffo. Relation between alveolar surface tension and pulmonary vascular resistance. J. Appl. Physiol. 16: 457-462, 1961.
23. West, J.B., C.T. Dollery and A. Naimark. Distribution of blood flow in isolated lung; relation to vascular and alveolar pressure. J. Appl. Physiol. 19: 713-724, 1964.
24. Whittenberger, J.L., M. McGregor, E. Berglund and G. Borst. Influence of state of inflation of the lung on pulmonary vascular resistance. J. Appl. Physiol. 15: 878-882, 1960.

PUBLICATIONS ASSOCIATED WITH CONTRACT

Manuscripts published or in press:

- Modell, H.I. and M.M. Graham. Limitations of Kr-81m for quantitation of ventilation scans. J. Nucl. Med 23:301-305, 1982.
- Beck, K.C. and J. Hildebrandt. Adaptation of vascular pressure-flow-volume hysteresis in isolated rabbit lungs. J. Appl. Physiol.: Respirat. Environ. Exercise Physiol. 54: 671-679, 1983.
- Modell, H.I. and F.W. Baumgardner. Influence of the chest wall on regional intrapleural pressure during acceleration (+Gz) stress. Aviat. Space and Environ. Med. (in press).

Abstracts and Symposia (Presentations at scientific meetings):

- Graham, M.M. and H.I. Modell. Limitations of Krypton-81m use for ventilation scans. J. Nucl. Med. 22: P92, 1981.
- Modell, H.I. Effects of acceleration (+Gz) on the intrapleural pressure gradient. The Physiologist 24: 96, 1981.
- Modell, H.I. Influence of abdominal restriction on gas exchange during +Gz stress in dogs. The Physiologist 25: 213, 1982.
- Modell, H.I. Influence of abdominal restriction on gas exchange during +Gz stress in dogs. The Physiologist 25:S95-S96, 1982 (Symposium)
- Beeman, P.F. and H.I. Modell. Sampling site for "mixed venous" blood in dogs -- pulmonary artery or right ventricle? The Physiologist 25: 269, 1982.
- Modell, H.I. Influence of the chest wall (CW) on gas exchange during mechanical ventilation (MV). The Physiologist 26: A-69, 1983.
- Modell, H.I. Influence of the chest wall (CW) on regional intrapleural pressure (Ppl) during acceleration (+Gz) stress. Fed. Proc. 43: 897, 1984.

Manuscripts submitted or in preparation:

- Modell, H.I., P. Beeman and J. Mendenhall. Influence of G-suit abdominal bladder inflation on gas exchange during +Gz stress. submitted to the Journal of Applied Physiology, 23 April 1984.
- Modell, H.I. and M.M. Graham. Influence of the chest wall on gas exchange during mechanical ventilation in dogs. In preparation for submission to the Journal of Applied Physiology or Anesthesiology.
- Modell, H.I. In vivo pressure-volume relationships of the pig lung and chest wall. In preparation for submission to the Journal of Applied Physiology.

PROFESSIONAL PERSONNEL ASSOCIATED WITH CONTRACT

Harold I. Modell, Assistant Member, Virginia Mason Research Center.

Michael M. Graham, Assistant Professor, Division of Nuclear Medicine, University of Washington.

Jack Hildebrandt, Member, Virginia Mason Research Center.

Kenneth C. Beck, Graduate student, Department of Physiology and Biophysics, University of Washington. Current Address: Department of Anesthesiology, Mayo Clinic, Rochester, Minnesota.

END

FILMED

10-84

DTIC